8-2019

Targeted EDTA Chelation Therapy with Albumin Nanoparticles to Reverse Arterial Calcification and Restore Vascular Health in Chronic Kidney Disease

Saketh Ram Karamched
Clemson University, sakethram.k@gmail.com

TARGETED EDTA CHELATION THERAPY WITH ALBUMIN NANOPARTICLES TO REVERSE ARTERIAL CALCIFICATION AND RESTORE VASCULAR HEALTH IN CHRONIC KIDNEY DISEASE

A Dissertation
Presented to
the Graduate School of
Clemson University

In Partial Fulfillment
of the Requirements for the Degree
Doctor of Philosophy
Bioengineering

---

by
Saketh Ram Karamched
August 2019

Accepted by:
Dr. Narendra Vyavahare, Ph.D., Committee Chair
Dr. Agneta Simionescu, Ph.D.
Dr. Alexey Vertegel, Ph.D.
Dr. Christopher G. Carsten, III, M.D.

ABSTRACT

Cardiovascular diseases (CVDs) are the leading cause of death globally. An estimated 17.9 million people died from CVDs in 2016, with ~840,000 of them in the United States alone. Traditional risk factors, such as smoking, hypertension, and diabetes, are well discussed. In recent years, chronic kidney disease (CKD) has emerged as a risk factor of equal importance. Patients with mild-to-moderate CKD are much more likely to develop and die from CVDs than progress to end-stage renal failure. Vascular calcification (VC), typical in aging, several genetic and metabolic disorders, is now recognized as a strong and independent predictor of cardiovascular events and mortality, not only in diabetic and CKD patients, even in the general population. VC is classified into two distinct types based on location in the vessel wall; intimal and medial. Elastin-associated medial arterial calcification (CKD) is more specific to CKD and contributes significantly to cardiovascular mortality in these patients. It is responsible for loss of vessel elasticity, increased arterial stiffness, increased pulse pressures and systolic blood pressure, and left ventricular hypertrophy ultimately causing arrhythmias and heart failure.

Current clinical practice is mostly focused on prevention and retardation of VC progression. Unfortunately, most patients with CKD remain underdiagnosed, and those diagnosed have already heavily calcified vessels. As such, they are undertreated since preventative strategies no longer work at this stage. Unfortunately, there is no FDA-approved treatment available that reverses calcification in countless CKD patients. A treatment strategy which promotes resorption of calcified lesions, while simultaneously

avoiding demineralization from normally calcified tissues (i.e., bones and teeth) remains an urgent health care need. Chelating agents bind to metal cations, can dissolve and "wash away" calcium deposits if delivered in close proximity to the calcification sites.

This work was undertaken to see if we can develop targeted therapies to deliver chelating agents to vascular calcification sites. Amongst chelating agents known for their affinity to Calcium ions (Ca^{2+}), we found that EDTA chelates Ca^{2+} from hydroxyapatite better than others. In our laboratory, we have developed a unique targeting mechanism by using nanoparticles to deliver chelating agents and other drugs to degraded elastin, a characteristic feature of VC. We take this approach forward in clinically relevant animal models of CKD.

First, we tested the targeted nanoparticle-based EDTA chelation therapy in a rat model of adenine-induced renal failure. The targeted nanoparticles delivered EDTA at the sites of vascular calcification and reversed mineral deposition without any side effects. Furthermore, we validated the adenine-CKD model in mice to monitor MAC *in vivo* and explore the phenotypic and functional alterations associated with it. We were able to target our nanoparticles to calcified arteries in these mice. The mouse model will help us to test whether our EDTA chelation therapy tangibly improves arterial function by restoring vascular health. Lastly, we investigated the possibility of using an *ex vivo* organ culture model of VC as a simpler, and relatively easier model to assess if EDTA chelation therapy promotes vessel homeostasis. The work presented here represents another major step forward towards the development of targeted EDTA chelation therapy as an

unconventional therapeutic approach to reverse pathological calcifications in CKD patients.

DEDICATION

In memory of my late father, Sri K. Srinivas, for teaching me compassion, patience, inquisitiveness, and for being an example of the man I want to grow up to be.

I would like to dedicate this work to my mother, Dr. Karamched Radha, who has always put my life, comfort, and happiness before hers and has been an immovable rock supporting me in every step of my life. If not for her love and support, I would not be where I am today.

To my ageless and timeless grandmother, Smt. K. Chudamani Devi for raising me, bestowing me with the gift of talking, and inspiring me with her wisdom and love for reading.

To Dr. K.M. Cherian, Late Dr. K.K. Haridas, Dr. K. Shiva Prakash, Dr. C. Narasimhan, Dr. Daljeet Kaur Saggu, and all the nurses and hospital staff at Vijaya Heart Foundation Chennai, Amrita Institute of Medical Sciences and Research Center Kochi, and Care Hospitals Hyderabad for taking care of me and doing what is best for my health and wellbeing.

ACKNOWLEDGMENTS

First and foremost, I would like to express my sincere gratitude and immense respect to my advisor, Dr. Narendra Vyavahare, for his continued support, guidance, patience, criticism, and mentorship throughout my journey as his graduate student. It has been an honor and privilege to be his student. His critical thinking, thirst for innovation, and passion for making a difference will continue to inspire me in my journey forward as a researcher.

I would like to extend my gratitude to my committee members Dr. Agneta Simionescu, Dr. Alexey Vertegel, and Dr. Christopher G. Carsten, III for their valuable insights, ideas, and advice throughout the length of this project.

I acknowledge my fellow lab members, past and present: Dr. Vaideesh Parasaram, Dr. Nasim Nosoudi, Dr. Hobey Tam, Xiaoying Wang, Tyler Gibson, Hannah Moreland, Hannah Gore, and Aniqa Chowdhury. Some of the work in this dissertation would not have been possible without their inputs, guidance, and motivation. I thank Dr. Agnes Nagy-Mehesz for all her help and advice with Western Blots and Immunohistochemistry.

I would like to thank Dr. Martine LaBerge and the Clemson Bioengineering family for taking me in as a young graduate student and providing me a home for the last six and a half years. Thank you, Maria Torres, for always being there for me whenever I needed her during my time as a graduate student. I am thankful to all the administrative staff for their cooperation and timely help. I would also like to thank my fellow graduate students

and friends within and outside Clemson Bioengineering for making my stay at Clemson memorable. Special thanks to Daniel Odenwelder for his friendship, and motivation.

This work would not have been possible without the staff at Godley Snell Research Center: Dr. John Parrish, Tina Duncan-Parker, Travis Pruitt, Jesse Privett, and Cynthia Smoak. Their help with animal maintenance and conducting animal studies has been invaluable.

I am especially thankful to my family and friends for always believing in me. I would like to express my gratitude to my brother and sister-in-law, Dr. Phani Shashanka Karamched and Dr. Madhuri Dutta, my cousins Dr. Ravi Kumar Komanduri and Dr. Suneetha Komanduri, for their love and motivation. A huge thank you to all the friends that have been part of my life in the United States so far. I would have been a lost soul here without Achyuth Bukkapattanam, Sindhura Reddy Gade, Bharadwaj Ginakunta, Haneesh Kotha, and the rest of the gang. Thank you all for your friendship and support. Special thanks to Achyuth for his care, kindness, and reminding me that I could handle anything that comes my way. I am grateful to Orient XI, for enriching my life with their friendship and constant support.

Lastly, I would like to acknowledge the financial supported provided to this project by the National Institutes of Health and Hunter Endowment awarded to Dr. Vyavahare.

TABLE OF CONTENTS

Page

LIST OF TABLES

LIST OF FIGURES

LIST OF ABBREVIATIONS

AAAs	Abdominal aortic aneurysms
ACA	Aortic calcification area
ACEi	Angiotensin-converting enzyme inhibitors
ADMA	Assymtric dimethyl arginine
AGEs	Advanced glycation end products
Ahsg	α2-Heremans-Schmid glycoprotein
ALP	Alkaline phosphatase
AMP	Adenine monophosphate
ApoE	Apolipoprotein E
APRT	Adenine phosphoribosyl transferase
ARBs	Angiotensin receptor blockers
aSMA	Alpha smooth muscle actin
BAL	British anti-lewisite
BAPTA	1,2-bis(o-aminophenoxy) ethane-*N,N,N′,N′*-tetraacetic acid
BMP	Bone morphogenic protein
BSA	Bovine serum albumin
CAC	Coronary artery calcium
$CaCl_2$	Calcium chloride
CASRs	Calcium sensing receptors
CCBs	Calcium channel blockers
CKD	Chronic kidney disease
COPD	Chronic obstructive pulmonary disease
CRF	Chronic renal failure
CTS	Cathepsins
CUA	Calcific uremic arteriolopathy

CVDs	Cardiovascular diseases
DBA/2	Dilute brown agouti 2
DHA	2,8 dihydroxyadenine
DMPS	Dimercaptopropane sulfonate
DMSA	Dimercaptosuccinic acid
DTPA	Diethylene triamine pentaacetic acid
EBP	Elastin binding protein
ECM	Extracellular matrix
EDTA	Ethylene diamine tetraacetic acid
EGTA	Ethylene glycol-bis (β-aminoethyl ether)-N, N, N′, N′-tetraacetic acid
ELN	Elastin gene
Enpp1	Ectonucleotide pyrophosphorylase
ESRD	End-stage renal disease
FDA	Food and Drug Administration
FGF-23	Fibroblast growth factor 23
GAPDH	Glyceraldehyde 3-phosphate dehydrogenase
GFR	Glomerular filtration rate
HA	Hydroxyapatite
HDL	High-density lipoprotein
HSA	Human serum albumin
IS	Indoxyl sulfate
LDL	Low-density lipoprotein
LDLR	LDL receptor
LOX	Lysyl oxidase
LTBP	Latent TGF-β binding protein
LVH	Left ventricular hypertrophy
MAC	Medial arterial calcification

MAGPs	Microfibril-associated glycoproteins
MCRAs	Mineralocorticoid receptor antagonists
MGP	Matrix Gla-protein
MMPs	Matrix metalloproteinases
MSX-2	Muscle segment homeobox 2
Myh11	Smooth muscle myosin heavy chain 11
NIH	National Institutes of Health
NKF	National kidney foundation
OCN	Osteocalcin
OPG	Osteoprotegerin
OPN	Osteopontin
PEG	Polyethylene glycol
Pi	Inorganic phosphate
PPi	Pyrophosphate
PRPP	5-phosphoribosyl-1-pyrophosphate
PTH	Parathyroid hormone
PWV	Pulse wave velocity
RAAS	Renin-Angiotensin-Aldosterone system
RUNX-2	Runt-related transcription factor 2
sHPT	Secondary hyperparathyroidism
SMMHC	Smooth muscle myosin heavy chain
Spp1	Secreted phosphoprotein
STS	Sodium thiosulfate
TACT	Trial to assess chelation therapy
Tagln	Transgelin
VC	Vascular calcification
VDN	Vitamin D and nicotine

VDRAs	Vitamin D receptor activators
VLDL	Very low-density lipoprotein
VSMCs	Vascular smooth muscle cells
VVG	Verhoeff von Gieson
α-SMC Actin	Alpha smooth muscle actin

1 INTRODUCTION

Cardiovascular diseases (CVDs) refer to several types of conditions that affect the cardiovascular system – heart and blood vessels. CVDs remain the leading cause of death, being responsible for ~17.9 (31%) million deaths globally, and 840,000 (1 in 3) deaths in the United States alone [1, 2]. CVD is an umbrella term for many diseases, including blood vessel disease, heart valve diseases, heart rhythm problems, heart muscle diseases, and congenital heart diseases, among others. CVDs are often caused by key risk factors such as high blood pressure, high cholesterol, and habitual smoking and at least one of these risk factors are present in about half (49%) of the American population [3]. Certain medical conditions and poor lifestyle choices which are also considered as risk factors include age, sex, physical inactivity, excessive alcohol use, unhealthy diet, obesity, genetic predisposition and family history of CVDs, diabetes mellitus and chronic kidney disease (CKD) [4-6].

CKD, also known as chronic renal failure (CRF) is a condition characterized by gradual damage to and loss of kidney function over time. As the primary function of the kidneys is to filter extra water and wastes out of our blood, damage to kidneys causes wastes to build up in the body resulting in complications such as high blood pressure, anemia, weakening of bones, poor nutritional health, etc. The two major causes of CKD are diabetes and high blood pressure, being responsible for up to 2/3rd of cases. Other diseases and conditions that cause CKD include glomerulo nephritis, polycystic kidney disease, lupus, prolonged obstruction of the urinary tract, vesicoureteral reflux, and more.

Since CKD and CVDs share two major risk factors – diabetes and high blood pressure – patients with CKD are a group at high risk for developing CVD and cardiovascular events [5]. Concomitantly, heart diseases represent the most common cause of death amongst people with CKD and undergoing dialysis. The prevalence and burden of CVD only rises with declining kidney function.

Ectopic calcification has been observed in many CVDs and is recognized as a contributing risk factor for cardiovascular events including heart failure, pulmonary hypertension, and even death in CKD patients. Based on location, calcifications in CKD can be classified into calcifications of vessels viz. atherosclerotic intimal calcification (AIC) and medial arterial calcification in large and elastic arteries (MAC), calcification of heart valves and calcific uremic arteriolopathy (CUA). CKD patients may develop both types of vascular calcifications, elastin-associated MAC is more specific to CKD; In fact, in pediatric patients, it is the only form of vessel calcification seen.

Current treatment methods have been limited to preventing and retarding the progression of calcification. Notably, as yet, there is no consensus about screening for and intervening to retard the progress of VC and even the most dramatic interventions such as intense dialyses and renal replacement, make it clear that manifested vessel calcification cannot be removed. A few options to treat vascular calcifications are surgical methods like directional atherectomy to physically remove the mineral deposits and placement of stent grafts to keep the artery open [7, 8]. They are quite invasive and detrimental. A large number of patients as such remain underdiagnosed and those diagnosed have already calcified arteries. Therefore, they remain undertreated since preventative strategies can no

longer work at this stage. There is a dire need of an alternative pharmacological approach that promotes reversal of VC by resorption of calcified lesions without detrimental demineralization in normal tissues (i.e., bones and teeth).

Chelation therapy has been long investigated for reversal of atherosclerotic calcification. This process typically involves an injection of disodium ethylene diamine tetraacetic acid (EDTA), a synthetic chemical that binds, or chelates ionic calcium, trace elements, and other divalent cations [9]. Systemic chelation therapy requires high dosages of EDTA to be injected, which may result in unwanted side effects such as hypocalcemia, renal toxicity, and loss of mineral from bone [10, 11]. In our laboratory, we have developed a unique method to deliver chelating agents, and other therapeutics, in a site-specific manner to vascular calcification sites through targeted nanoparticles (NPs). Further, we have shown that such targeted delivery of EDTA through use of albumin NPs to a calcified site, reverses experimentally created vessel calcification while avoiding untoward side effects of systemic therapy.

In this dissertation, we take this approach forward in a clinically relevant animal model of CKD. We have studied the efficacy of targeted EDTA chelation therapy in a dietary adenine model of renal failure in rats. We also explored the feasibility of using targeted EDTA chelation therapy in a mouse model of dietary adenine which would serve as an aid in the near future to investigate if reversal of arterial calcification improves vascular homeostasis through the use of cell-lineage tracing. Additionally, we examined if removal of calcification by EDTA chelation therapy can reverse the associated phenotypic changes of vascular smooth muscle cells (VSMCs) in an organ culture model of porcine

carotid arteries. Overall, our goal was to present targeted EDTA chelation as an excellent alternative therapeutic approach to reverse MAC clinically.

The dissertation is organized as follows:

- In Chapter 2, we present a comprehensive review of:
  - → ***Cardiovascular System:*** Cardiovascular diseases, cardiovascular system, and structure of the aortic wall.
  - → ***Elastin:*** Structure, function, ultrastructure, mechanism of elastin synthesis and elastic fiber assembly, and elastin degradation in disease.
  - → ***CKD:*** Definition, classifications, consequences, and cardiovascular complications in CKD.
  - → ***VC:*** Types, mechanisms, and current treatment strategies.
  - → ***Animal models of VC:*** *In vivo* studies with animal models of VC, CKD and MAC, and adenine-induced CKD model of VC.
  - → ***Chelation Therapy:*** Definition, history of chelation therapy, types of chelating agents used, EDTA chelation therapy, clinical trials with EDTA chelation therapy.
  - → ***Targeted EDTA chelation therapy***: Nanoparticles as drug delivery agents, albumin nanoparticles, targeting of albumin nanoparticles to degraded elastin in calcification.
- Chapter 3 provides rationale for this research and specific aims designed for this project.

- In Chapter 4, we compare three different chelating agents – EDTA, EGTA, and BAPTA to deduce the best chelator for use in targeted chelation therapy
- In Chapter 5, we discuss whether EDTA, a chelating agent, loaded and elastin-antibody conjugated nanoparticles can be targeted to sites of elastin-specific medial arterial calcification for its reversal in a rat chronic kidney disease model.
- In Chapter 6, we demonstrate targeting of elastin-antibody conjugated albumin nanoparticles to sites of medial arterial calcification in a mouse adenine model of CKD-induced calcification. Monitoring of disease progression *in vivo* and VSMC cell status were explored for the potential use of this model to investigate whether reversal of MAC through targeted EDTA chelation therapy can restore vascular homeostasis.
- In Chapter 7 we explore the feasibility of an *ex vivo* organ culture model of porcine carotid arteries to better understand the mechanism of VC and direction of VSMC before and after treatment with EDTA-loaded NPs. The *ex vivo* model may serve as a bridge between cell culture and extensive animal models currently in use to provide complementary information about intrinsic mechanisms and treatment of VC.
- Chapter 8 summarizes and lists conclusions from the present research and provide future recommendations to take this research forward and take major steps towards clinical translation of targeted EDTA chelation therapy for permanent reversal of VC.

2 REVIEW OF LITERATURE

2.1 Cardiovascular diseases

Cardiovascular diseases (CVDs) are the number one cause of death globally; more people die annually from CVDs than of any other cause. An estimated 17.9 million people died globally from CVDs in 2016, representing approximately 30% of all registered deaths [1]. Out of the 17 million premature deaths due to non-communicable diseases in 2015, 82% are in low- and middle-income countries, and 37% of them are caused by CVDs [2]. In the United States alone, CVDs have remained the leading cause of death, responsible for as many as 840, 000 deaths in 2016. The annual total cost of CVDs in the US has been estimated at $351.2 billion in 2014-15 [12].

The term CVDs describe a range of conditions that affect the cardiovascular system – heart and blood vessels. They are grouped into disorders *of the blood vessels*, such as coronary artery disease, cerebrovascular disease, peripheral arterial disease, arterial calcification, abdominal aortic aneurysms (AAAs), deep vein thrombosis and pulmonary embolism; disorders *of the heart structure and muscle*, including congenital heart disease, rheumatic heart disease, carditis and cardiomyopathy; problems with *heart rhythms* known as arrhythmia; and disease *of the heart valves*, like calcification of the heart valves, valve prolapse and stenosis.

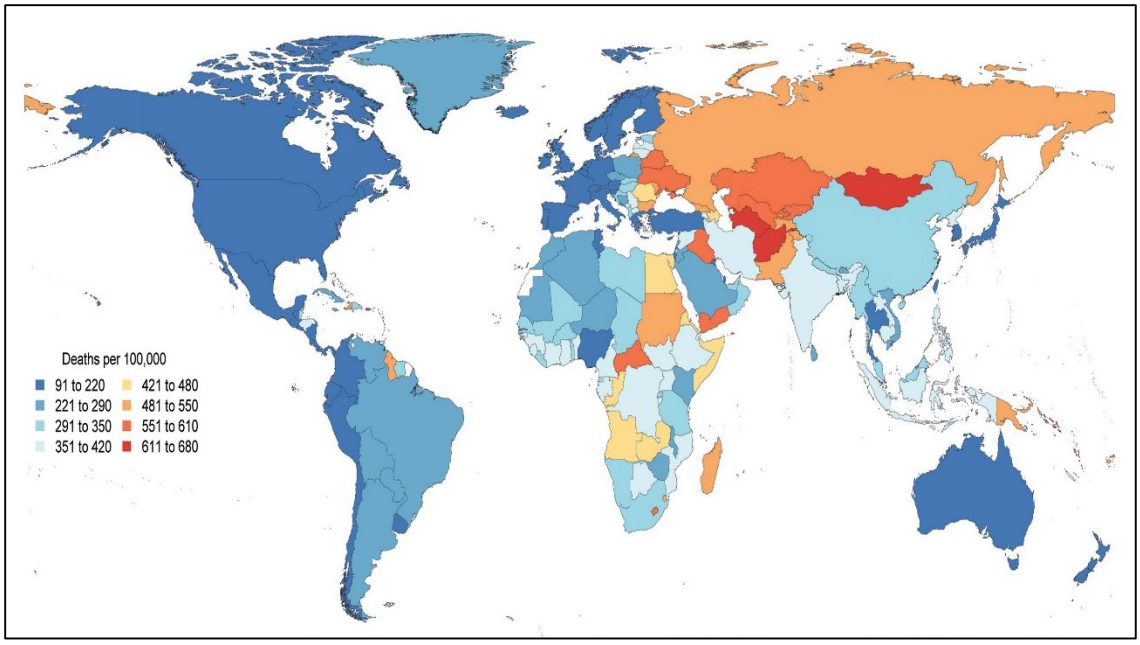

Figure 2-1: Global map, age-standardized death rate of CVD in 2015 [13].

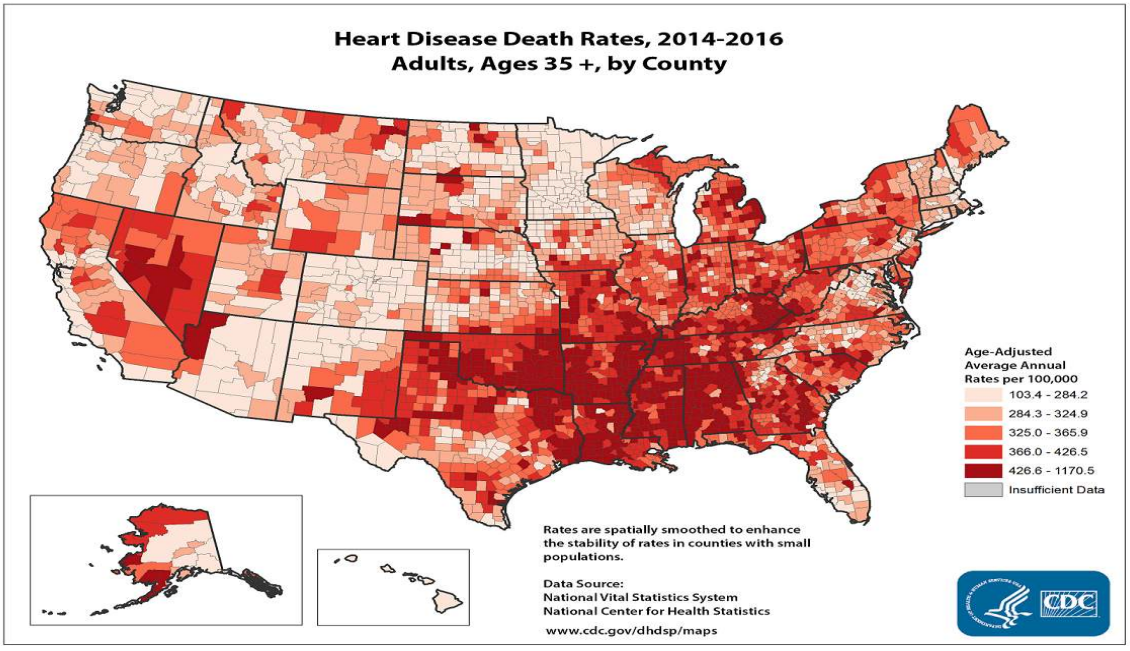

Figure 2-2: Heart disease death rates across the US [14].

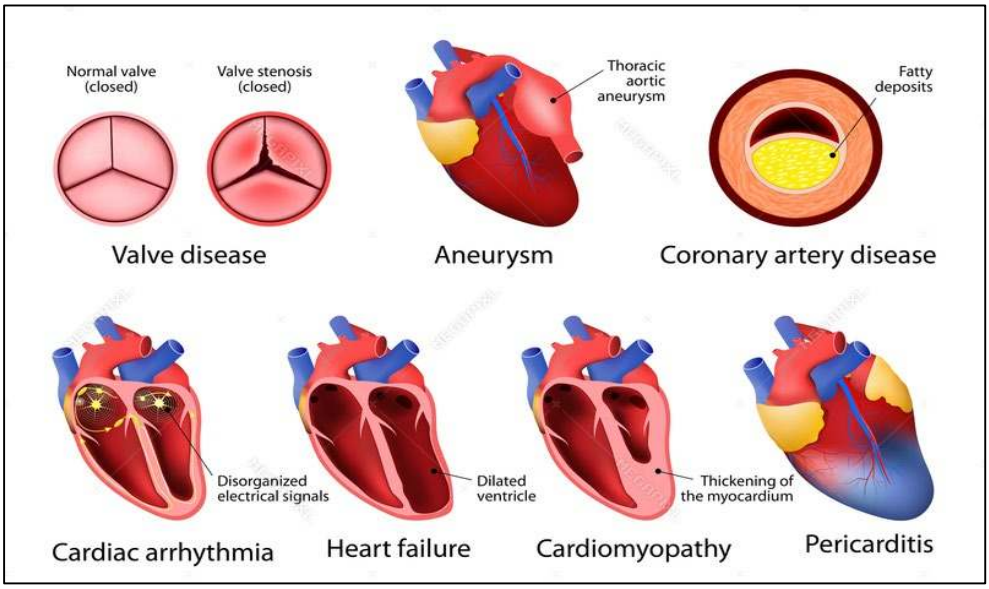

Figure 2-3: Types of Cardiovascular Diseases [15].

Risk factors for CVDs are classified as non-modifiable and modifiable. Non-modifiable risk factors are age, gender, ethnic background, socioeconomic status, and familial history of the disease. Physical inactivity, excessive tobacco use and alcohol consumption, unhealthy diet resulting in high cholesterol levels and obesity, uncontrolled blood pressure come under modifiable risk factors [3, 4, 16]. With better lifestyle choices, modifiable risk factors can be kept under check and reduce chances of having CVDs. Heart failure is the most common, costly, and potentially fatal outcome of many of the CVDs [17].

2.2 The Cardiovascular System

The Cardiovascular System (Figure 1-4), also known as the circulatory system, functions to carry blood through vessels to and from all parts of the body. It is a closed tubular system in which the blood is propelled by a principal muscular organ called the heart. There are two major circuits in the circulatory system, the systemic and the pulmonary, both made up of vessels viz., arteries, veins and capillaries [18].

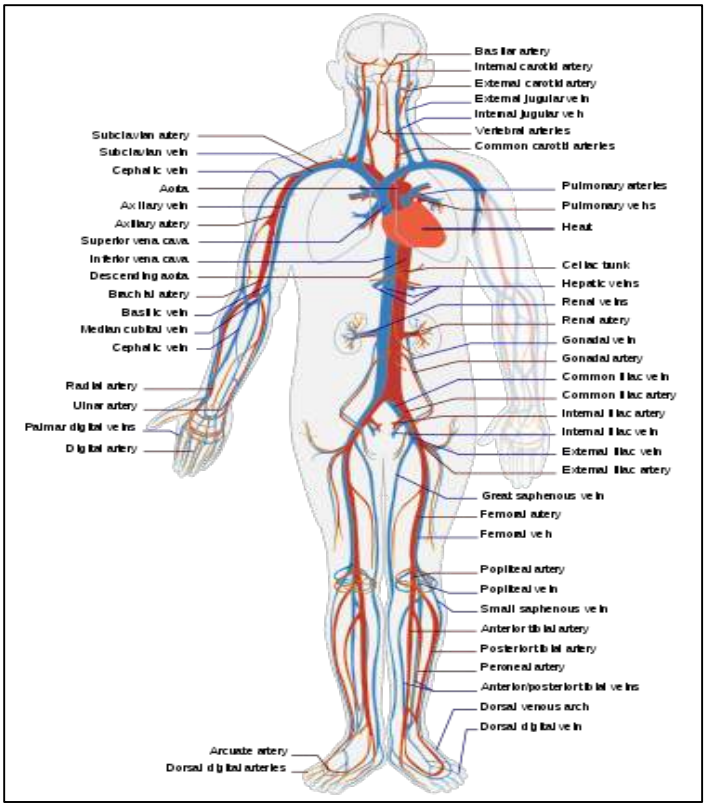

Figure 2-4: The human cardiovascular system (simplified). Red indicates oxygenated blood in the arteries, blue indicates deoxygenated blood in veins [18].

A third circuit known as the lymphatic system, whose primary function is to transport lymph, is also considered part of the circulation and helps the body to get rid of toxins, waste and other unwanted materials. Blood vessels vary with size and function, but all of them possess the same basic structure. Each type of vessel has a lumen - a hollow passageway through which the blood flows and is surrounded by the vessel wall. The vessel wall has three layers, or tunics, meaning "*coats"* in Latin.

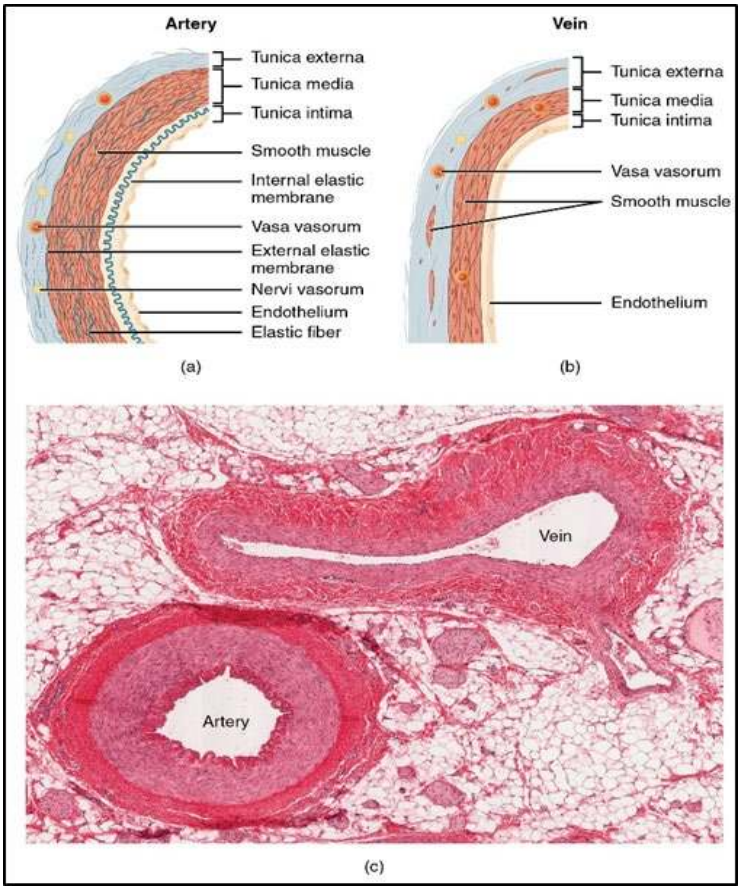

Figure 2-5: Structure of Blood Vessels. (a) Arteries, (b) veins, and (c) Micrograph showing relative differences in thickness [19].

The deepest layer, *tunica intima*, is lined by a specialized simple squamous epithelium known as endothelium. The middle layer, *tunica media*, is the thickest of the layers in arteries. It is rich in smooth muscle supported by connective tissue mainly made up of elastic fibers arranged in circular sheets. The outer layer is the *tunica adventitia* (this is the thickest layer in the veins) and is entirely made of connective tissue primarily composed of collagenous fibers and nerves that supply the vessel as well as the nutrient capillaries (called *vasa vasorum)* in the larger blood vessels.

Arteries carry blood from the heart to various organs and can be further subcategorized by their size. All arteries, as mentioned above have relatively thick walls that can withstand the high pressure of blood ejected from the heart. Those closest to the heart have the thickest walls, containing a high percentage of elastic fibers throughout the wall. These type of arteries are elastic arteries and are typically >10mm in diameter. Further from the heart, where the blood surge is stifled, the percentage of elastic fibers decreases, and there is increased smooth muscle in the medial layer. These are the muscular arteries with a diameter range between 0.1mm and 10mm. Muscular arteries branch to distribute blood to a vast network of arterioles. The transition from artery to arteriole is very gradual, with progressive thinning of the wall and decreased lumen size (the diameter of an arteriole is <0.5mm). Overall, the heart forces blood into the arteries, who through their elastic recoil, send blood on in pulsating waves. Therefore, it is crucial that the arteries possess strong, elastic walls to ensure fast, efficient blood flow in absence of which there would be a plethora of vascular complications.

2.3 Elastin Structure and Degradation

Elastin makes up roughly 50% of the arterial extracellular matrix (ECM) as discussed above and is the most prevalent structural protein. Aside from the arteries, elastin is present in the ECM of tissues like skin, lungs and renders them elastic properties. With a half-life period of 74 years, majority of elastin deposition in the body occurs during embryonic stage and early childhood [20, 21]. It rarely undergoes any remodeling and has a very low turn-over rate. Synthesis of elastin been well documented in fibroblast cells, smooth muscle cells, chondrocytes, and endothelial cells [22-25]

Elastin is made up of elastic fibers that have two key components, one amorphous and one fibrillary. The amorphous component is extensively cross-linked and comprises 90% of the mature fiber. The fibrillar component is a collection of microfibrils that are roughly 8-16 nm long and rich in acidic glycoproteins [26, 27]. These microfibrils are located around the periphery of the amorphous content and contain a number of glycoproteins like microfibril-associated glycoproteins (MAGP-1, -2, -3, -4, fibrillins, latent TGF-β binding protein (LTBP) and fibulins contribute to anchorage of elastin and provide its structural coating [28, 29].

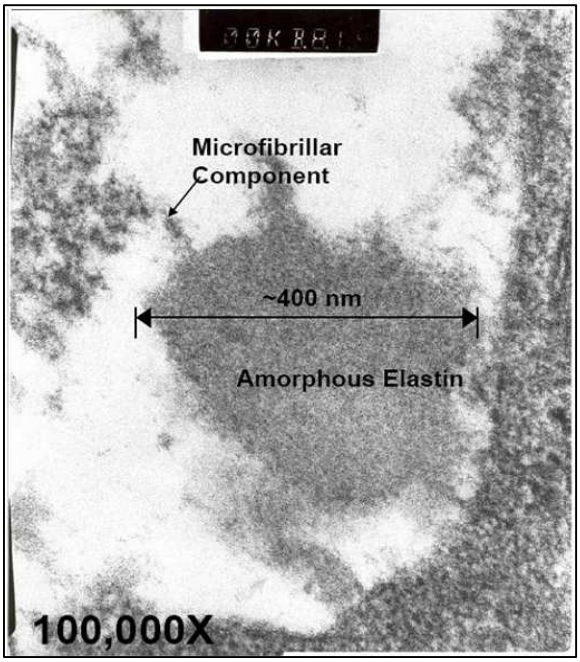

Figure 2-6: TEM of cross section of elastin and fibrillin deposited by rat vascular cells in culture [30].

The primary structure of elastin is mainly composed of hydrophobic amino acids, such as glycine and proline [31]. There are a couple of highly conserved peptide sequences in the elastin fiber – 'VPGVG' and 'PGVGV'. Due to these recurring amino acid residues (XPGX' where X and X' are hydrophobic), elastin is a highly hydrophobic protein [32].

The cellular production, orientation, assembly, crosslinking, and deposition of elastin is a tightly regulated hierarchical process and is not very well understood. Tropoelastin, a 72 kDa soluble precursor of mature elastin, is its monomeric form. Human tropoelastin is encoded by a single gene (ELN) with multiple isoforms and is present as a single copy on the chromosome-7 [33]. Post translational modification of tropoelastin results in the mature 60 kDa protein. Tropoelastin gene is expressed during prenatal development by smooth muscle cells, endothelial cells, and fibroblasts. As we age,

however, ELN expression decreases dramatically along with decreased elastin production. In middle-aged people, elastin production is mostly non-existent, and humans rely on elastin deposition that occurs in the womb and very early in life [34].

The process of elastogenesis is broadly classified into the following stages: (i) tropoelastin synthesis, (ii) coacervation, (iii) microfibrillar deposition, (iv) crosslinking, and (v) maturation. In order for a mature elastin fiber to form, tropoelastin molecules must interact and crosslink with each other. Fibrillin-1 largely makes up the microfibrils in the ECM that anchor the forming elastic fibers. Lysyl oxidases are a group of five enzymes including LOX, and LOXL 1-4, which cross-link tropoelastin and aid the process.

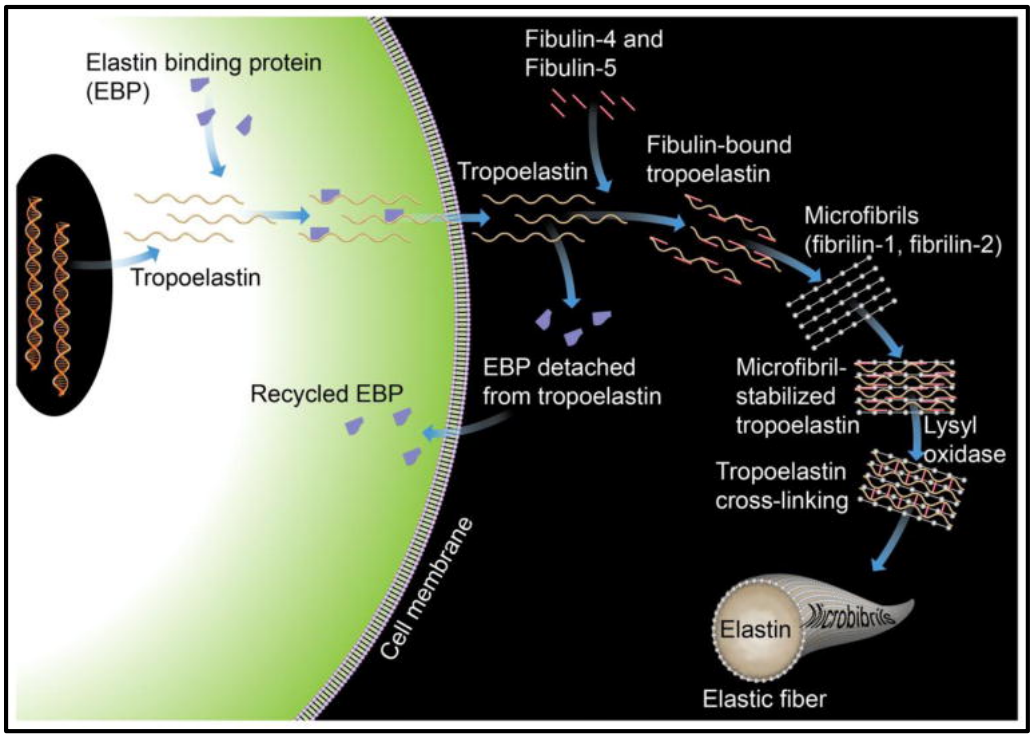

Figure 2-7: Illustration of elastin fiber synthesis and assembly [35].

Initially, the ELN gene is expressed by cells and tropoelastin molecules are secreted into the ECM. These tropoelastin molecules begin to self-aggregate or coacervate due to the inherent tendency of tropoelastin to coacervate owing to its excessive hydrophobicity [36]. The coacervating tropoelastin molecules form ~1μm spherules and remain attached to the cell surface until their deposition on microfibrils. Elastin binding protein (EBP), made of a 67 kDa peripheral subunit attached to two membrane-bound proteins of 61 kDa and 55 kDa MW, carries tropoelastin molecules to fiber formation sites on the surface of the cell. Tropoelastin initially binds to EBP and forms a stable complex. The 67 kDa subunit then loses its affinity for tropoelastin and the membrane-bound protein, when a sugar moiety binds to the EBP. This loss of affinity results in tropoelastin being released onto growing elastin fibers [26]. The microfibrils in ECM provide a scaffold for directing and propagating elastin growth and further coacervation and also recruit LOX enzymes for crosslinking [37-39].

Eventually, tropoelastin is oxidized by LOX enzymes and is followed by aldol condensation and Schiff base reactions among lysyl residues resulting in crosslinking of elastin fibers with desmosine and isodesmosine links [40]. The matured elastin produced as the final product is very stable and gives the tissues their ability to stretch and recoil [41]. This entire process of elastic fiber assembly is illustrated in Figure 1-7.

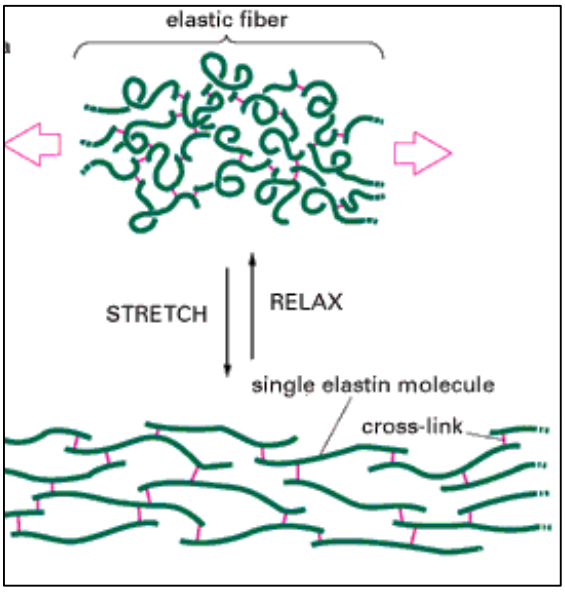

Figure 2-8: Depiction of elastic recoil [42].

One of the consistent features of many vascular diseases is the fragmentation and degradation of elastic lamina. Elastic lamina degradation is witnessed in vascular calcification [43, 44], diabetes [45], end-stage renal disease [46, 47], and aortic aneurysm [48]. Additionally, vascular proliferative diseases affecting smaller arteries like coronary arterial occlusion and atherosclerotic-mediated stenosis share elastin degradation as a common pathological feature [49, 50]. In such disease conditions, elastic lamina is degraded and the amorphous elastin core protein is exposed.

2.4 Chronic Kidney Disease

Chronic Kidney Disease (CKD) is a broad moniker for heterogeneous disorders affecting kidney structure and function. It is a worldwide public health problem with an ever-increasing incidence and prevalence, resulting in poor outcomes, and therefore a high treatment cost [51]. The National Kidney Foundation (NKF), in 2002, published 15 clinical practice guidelines on evaluation, classification, and risk stratification in CKD. The definition of CKD has evolved since then, but current international guidelines define this condition as decreased kidney function as indicated by glomerular filtration rate (GFR) of less than 60 mL/min per 1.73m^2, or kidney damage markers, or both, for a minimum of 3 months [52]. When GFR is found to be less than 15 mL/min per 1.73m^2, the patient is adjudged to have reached end-stage renal disease (ESRD) at which point the kidney is no longer believed to sustain life over the long term. The burden of CKD is substantial; According to WHO global health figures, 1.5% of the deaths worldwide were attributed to CKD in 2012 and it is further projected that the death rate from CKD will continue to increase to reach 14 per 100,000 people by 2030 [53]. CKD is common among adults in the US; more than 30 million American adults may have CKD, with its associated diseases being the 9th leading cause of death [54]. The two primary causes of CKD are diabetes and hypertension, being responsible for 2/3rd of the cases in high- and middle-income countries and also low-income countries. Diabetes accounts for 30-50% of all CKD and affects 285 million (6.4%) adults worldwide, and this number is only expected to increase by 69% in high-income countries and 20% in low-income and middle-income countries by 2030. Greater than a quarter of the adult worldwide population was estimated to have

hypertension in 2000, while this proportion is projected to rise by approximately 60% by 2025 [55]. Other conditions that affect the kidneys include glomerulonephritis, inherited diseases such as polycystic kidney disease, developing malformations, lupus and obstructions caused by kidney stones, tumors, or enlarged prostate in men. In developing countries, common causes of CKD may also include glomerular and tubulointerstitial diseases as a result of infections and exposure to drugs and toxins [56].

A conceptual model for development, progression, and complications of CKD includes antecedents associated with increased risk, disease stages, and complications including death. Risks are usually categorized either as susceptibility to kidney disease because of sociodemographic and genetic factors, or as exposure to factors which would lead to the disease. It is noted that early stages of diseases are often devoid of symptoms and detected during assessment for comorbid disorders, and tend to be reversible. Rapidly progressive diseases, however, can lead to kidney failure within months. Owing to its importance in the pathophysiology of complications, GFR is used to classify CKD into five stages: more than 90 mL/min per 1·73 m 2 (stage 1), 60–89 mL/min per 1·73 m 2 (stage 30–59 mL/min per 1·73 m 2 (stage 3), 15–29 mL/min per 1·73 m 2 (stage 4), and less than 15 mL/min per 1·73 m 2 (stage 5).

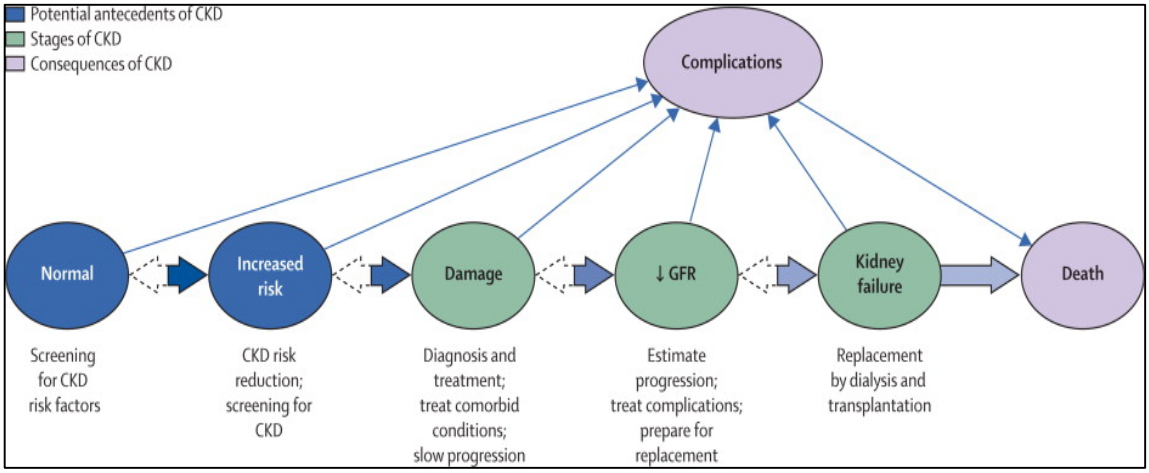

Figure 2-9: Conceptual model for chronic kidney disease and its complications [57]

Kidney failure is traditionally considered as the most serious outcome of CKD. When symptoms are severe, they can be treated only through dialysis or in more serious cases transplantation. As mentioned above, kidney failure at this stage is known as ESRD. However, there are several other consequences of CKD that include not only renal dysfunction and progressive renal failure but also complications of decreased kidney function and increased risk of cardiovascular disease. Additional complications include acute kidney injury, infection, cognitive impairment, and diminished physical function [58-63]. All these complications contribute to high morbidity and mortality and in general, poor quality of life. In patients with CKD, compared to general population, cardiovascular diseases (CVDs) are more frequent and severe. It often goes unrecognized and undertreated, and it is now increasingly apparent that individuals with various stages of CKD are more likely to die of cardiovascular complications than progress to ESRD. As

such, these individuals must be viewed as being in the highest risk group for cardiovascular disease and mortality [64, 65].

2.5 Cardiovascular Complications in CKD

CVD also represents the leading cause of mortality in CKD patients, and its prevalence and burden only increase with declining renal function [66, 67]. Cardiovascular complications are approximately three times more frequent in patients with CKD than in other known cardiovascular risk groups, and mortality is 10-fold more frequent in patients on dialysis than age- and sex-matched non-renal populations. As a matter of fact, patients with mild to moderate CKD (Stages 1-3 are much more likely to develop and die from CVD than progress to ESRD. Increased cardiovascular risk in CKD patients is partly because of traditional risk factors such as diabetes, hypertension, and hyperlipidemia. However, associations of reduced kidney function with cardiovascular risk are independent of these traditional risk factors, and they fail to adequately explain the observations made in these patients.

Non-traditional kidney-specific risk factors make noteworthy contributions to cardiovascular risk in these cases. Some of these non-traditional factors that play a role in the association of renal failure and CVD include anemia, hypervolemia, hyperphosphatemia, endothelial dysfunction, nitric oxide bioavailability, Asymmetric dimethylarginine (ADMA), dyslipidemia, inflammatory and oxidative stress, etc. [68-70]. Apart from left ventricular hypertrophy (LVH), which is present very early in the disease course even in normotensive CKD patients, structural alterations of the myocardium, as well as intra-and extra-cardiac blood vessels are hallmarks of this disease.

Cardiovascular calcifications also become highly prevalent as CKD progresses and are potent predictors of cardiovascular mortality in these patients [46, 71]. London *et al.* demonstrated that the extent and histoanatomic type of vascular calcification are predictors of subsequent mortality [72]. There are four different manifestations of calcifications in diseased patients: advanced calcification of the intimal plaques, medial calcification of large and elastic arteries, calcification of heart valves and myocardium, and a rare condition known as calcific uremic arteriolopathy (*also known as* calciphylaxis). All four of them are distinct yet have overlapping pathological mechanisms [71, 73, 74].

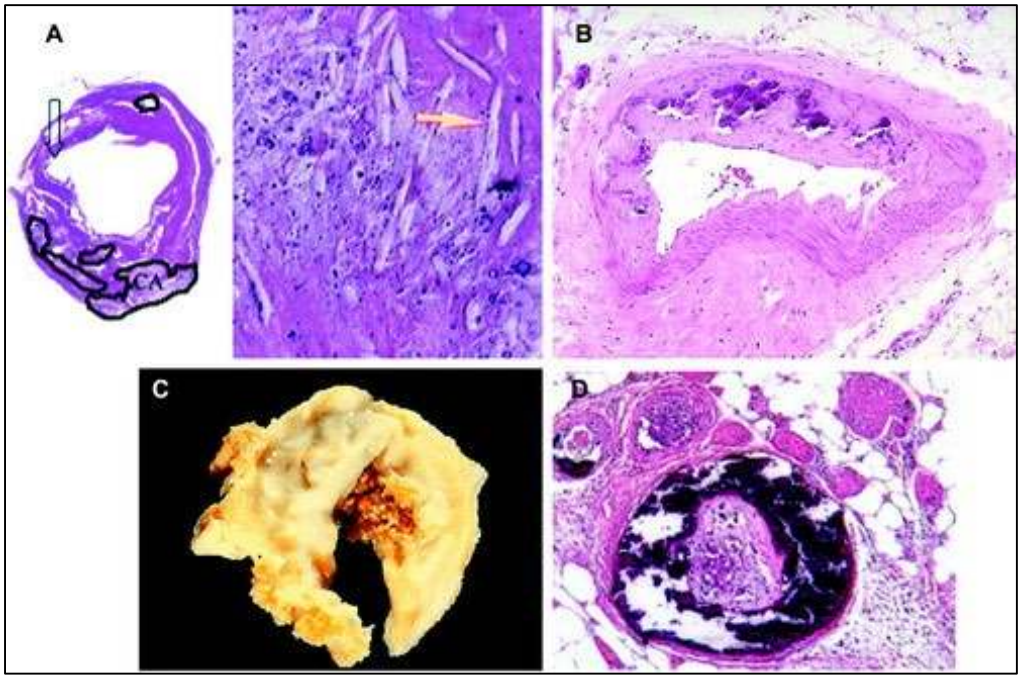

Figure 2-10: Types of cardiovascular calcifications. (A) Atherosclerotic calcification. (B) Medial calcification. (C) Valvular calcification. (D) Calciphylaxis [75]

2.6 Vascular Calcification

Accelerated vascular calcification is a hallmark of CKD patients and plays a pivotal role in the CVD burden and eventual mortality in these patients. In patients with late-stage renal disease, the risk of death linearly correlates with an increase in numbers of sites on the vasculature affected by calcification; in the aorta, carotid, and femoral arteries [76].

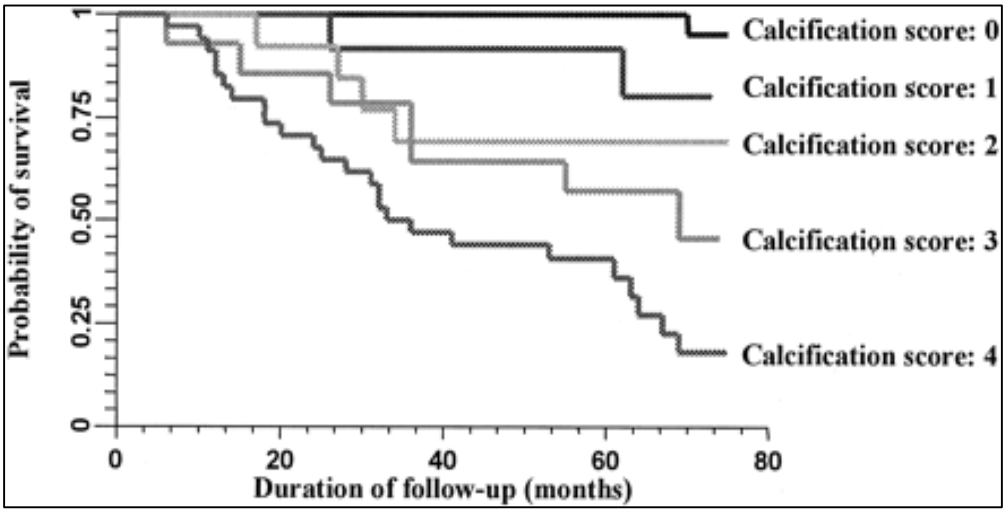

Figure 2-11: Probability of all-cause survival according to calcification score [76]

2.6.1 Types of Vascular Calcification

Two types of calcification are observed in the vasculature, both of which affect patients with long-standing kidney disease, particularly amongst those on dialysis – medial arterial calcification (MAC, *also known as* calcific arteriosclerosis or Monckeberg's sclerosis) and accelerated calcification of intimal plaque (*also known as* calcific atherosclerosis) [71, 77-79].

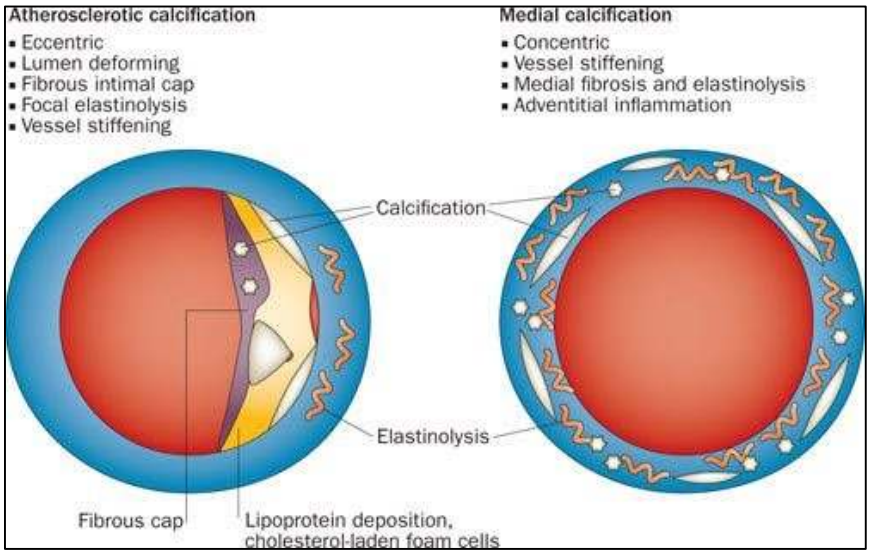

Figure 2-12: Atherosclerotic intimal calcification vs. Medial arterial calcification [80]

Intimal calcification is typically considered the last step in classical atherosclerosis and is a multifactorial process involving inflammation, macrophage infiltration, dyslipidemia, and advanced glycation end products (AGEs), etc. On the contrary, medial calcification is characterized by diffuse mineral deposition circumferentially along or within elastic lamellae of the medial layer of the arterial wall. It can occur independently or in conjunction with intimal calcification but is more common among the two in CKD or diabetic patients [73, 81]. Morphologically, atherosclerotic calcification occurs as dispersed, spotty, and patchy deposits of calcium in a matured plaque whereas MAC gives a “tram-line” or “railroad track” like appearance as more and more lengths of the arterial tree calcify.

Intimal calcification results in vessel narrowing and dysfunction, possibly causing a thrombotic event eventually. Atherosclerotic plaque burden is higher, and the lesions more distinctly calcified in CKD patients compared to normal populations.[82]. MAC, on the other hand, contributes to loss in vessel elasticity, increased arterial stiffness resulting in increased pulse pressures, increased systolic blood pressure, and LVH ultimately causing arrhythmias and heart failure [72]. While patients with CKD can develop both types of VC, MAC is more specific to CKD; it is the exclusive form of VC observed in pediatric CKD patients. MAC contributes significantly to cardiovascular mortality in CKD patients [83].

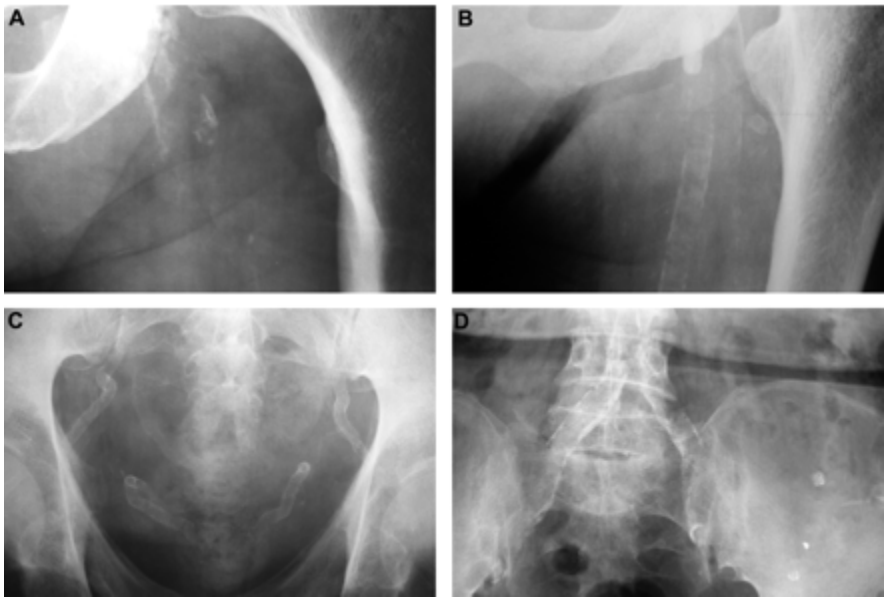

Figure 2-13: Radiographs of intima and media calcification as seen in the pelvis and the thigh of CKD patients. (A) Intima calcification is seen as discrete plaques with irregular and patchy distribution. (B &C) Media calcification present as a uniform linear railroad track. (D) Presence of both, intima and media calcification is reflected as discordances [72].

2.6.2 Mechanisms of Vascular Calcification

Calcification of arteries in CKD is a catenation of well-orchestrated and tightly regulated processes which involve cellular and molecular reprogramming, structural and functional changes in arterial cells and ECM. Several studies have described key events required for the initiation and promotion of calcification. An imbalance of calcification inhibitors and promoters in CKD drives calcification. Loss of inhibitors which tightly control spontaneous pathological precipitation of calcium – phosphate crystals, such as Matrix Gla-protein (mGP) [84], Fetuin-A [85], Klotho [86], Pyrophosphate (PPi) [87], Osteopontin [88], Osteoprotegerin [89] instigates calcification. Transcription factors such as Runt-related transcription factor (RUNX2, *also known as* Cbfa1) [90], Muscle segment homeobox 2 (MSX-2) [91], Bone-morphogenic proteins (BMP-2, 4 and 6), Osteocalcin (OCN), Alkaline phosphatase (ALP) [92] etc. which are critical for normal bone development, have been identified at sites of human arterial calcification in both general and CKD patients [93], in animals and also *in vitro.* In addition, development of a calcifiable ECM, induction of apoptosis and vesicle release accompanied by osteogenic/chondrogenic differentiation of vascular smooth muscle cells (VSMCs) are all important players which spur active calcification processes [90, 94, 95].

Table 1-1: List of inhibitors and promoters of vascular calcification in CKD.

Calcification Inhibitors	Calcification Promoters
	BMP-2,4 and 6
Matrix Gla-protein	Osteocalcin
Fetuin-A	Alkaline Phosphatase
Klotho	RUNX2
Pyrophosphate	Oxidative Stress
Osteopontin	MMP2, 3 and 7
Osteoprotegerin	SOX9
BMP-7	Ca^{2+} and PO_4^{2-}
	Apoptosis/Apoptotic bodies

Although a multitude of mechanisms are involved, ectopic, especially vascular, calcification in CKD is largely actuated by a dysregulation of mineral metabolism, in particular Ca and P. Hyperphosphatemia, a result of reduced renal phosphate clearance in combination with increased Ca X P product level are recognized as chief culprits of accelerated arterial calcification in CKD patients. Deposition of calcium phosphate salts in the media of the arteries occurs on the amorphous elastin that makes up the elastic lamellae. It is augmented in the context of elastin degradation by elastases and other such proteases. In particular, Matrix metalloproteinases (MMPs) and cathepsins (CTS) have been shown to be overexpressed and involved in calcified arteries. MMP-2, MMP-9, CTS-K, and CTS-L can degrade elastin laminae in the media [96-100].

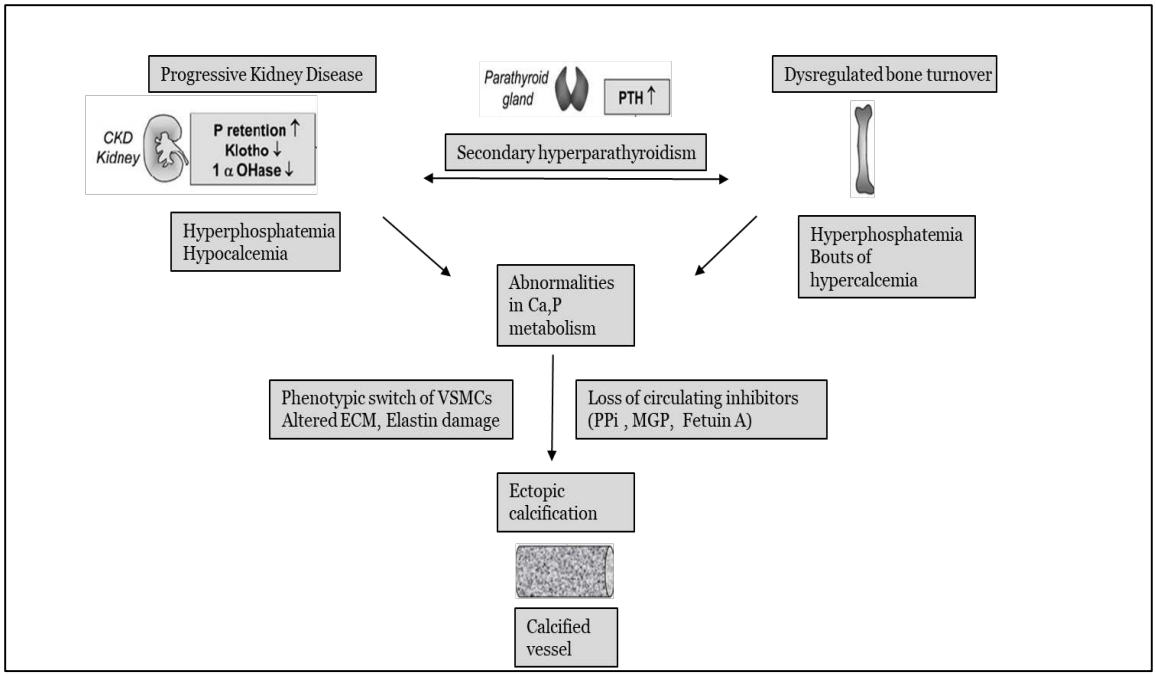

Figure 2-14: Mechanism of vascular calcification in chronic kidney disease [94].

2.7 Current Treatment Strategies

Therapeutic strategies and inventions that may stabilize and potentially reverse vascular calcification may be of immense value to patients with CKD. Most of the treatment methods in use have been limited to optimizing and managing the dysregulated mineral metabolism and bone turnover diseases, both of which are characteristic to CKD. It should be noted here that the strong relationship between progressing renal dysfunction and increased presence and severity of VC means that primary prevention may potentially have a positive impact on VC. A good number of clinical trials in patients with hypertension and normal renal function have shown that anti-hypertensive treatments reduce aortic stiffness [101, 102]. Different classes of antihypertensive drugs may have

different effects on arterial stiffness. Calcium channel blockers (CCBs), Angiotensin-converting enzyme inhibitors (ACEi), and Mineralocorticoid receptor antagonists (MCRAs) have a beneficial effect in reducing arterial stiffness and central blood pressure. The first study in humans to demonstrate an effect of CCBs on VC was a sidearm of the Nifedipine Study: Intervention as Goal for Hypertension Therapy (INSIGHT). In this particular study, nifedipine was found to inhibit the progression of coronary calcium in a sub-group of 201 high-risk hypertensive patients compared to co-amizolide (a diuretic). However, the exact clinical message of this study is unclear in the light of INSIGHT results which showed comparable effectiveness of nifedipine and co-amizolide in preventing overall cardiovascular events [103]. Other studies prior and after have evaluated the effect of CCBs for their effect on central blood pressure and arterial stiffness [104, 105].

It is now common knowledge that ACEi, Angiotensin receptor blockers (ARBs) and Aldosterone antagonists interfere with the Renin-Angiotensin-Aldosterone System (RAAS), and confer benefits on vasculature beyond simply controlling the blood pressure. The effects of ACE inhibition on coronary plaque progression in humans in relation to its calcium content have been investigated in a study named PERSPECTIVE. A substudy of the EUROPA trial, PERSPECTIVE tested the effect of perindopril on coronary plaque. Only plaques with a calcium score of 0-25% regressed with perindopril in comparison to a placebo, but plaques with moderate (25-50%) and high (50-100%) calcification progressed equally as in placebo group [106]. In another study with 478 young type I diabetic patients having albuminuria, ACEi/ARB treatment significantly lowered CAC progression over ~2.5 years compared to those without any treatment [107]. In a prospective randomized

trial with 31 patients having essential hypertension and LVH, the effects of combined therapy of an ARB (Valsartan) and ACEi (Perindopril) were studied and compared with those of respective monotherapies. The findings suggested that, compared to respective monotherapies, perindopril, and valsartan together exerted greater favorable effects. Further, an open randomized trial conducted by Frimodt-Møller M et al. investigated whether a more complete inhibition of RAAS by combining ACEi (Enalapril) and ARB (candesartan) compared to monotherapy has an additive benefit in CKD patients. They found that dual blockade of RAS resulted in additive BP independent reduction in Pulse wave velocity (PWV) and arterial stiffness compared to monotherapy [108].

Table 2-2: Primary prevention of vascular calcification

Treatment	Mechanism of Action/Outcome	References
Primary Prevention – Antihypertensive Drugs		
Calcium Channel Blockers (CCBs) *Nifedipine*	Slower progression of coronary calcification in patients on nifedipine vs. co-amilozide	Motro et al. 2001 [103]
Angiotensin-converting Enzyme Inhibitors (ACEi)/Angiotensin Receptor Blockers (ARBs) *Perindopril*	Coronary plaques with no or little calcium (0-25%) regressed on perindopril and not in placebo	Bruining et al. 2009 [106]
Perindopril/Valsartan	ACEi/ARB treatment was associated with substantially reduced odds of CAC progression	Maahs et al. 2006 [107]
Enalapril/Candesartan	Dual blockade of the RAAS resulted in additive BP independent reduction in PWV and arterial stiffness in CKD patients.	Frimodt-Møller M et al. 2012 [108]

Beyond primary prevention using antihypertensives, secondary prevention of VC by correcting hyperphosphatemia and secondary hyperparathyroidism (sHPT), which are universal consequences of renal failure embodies a central clinical approach. This is accomplished by oral phosphate binders, active vitamin D compounds, calcimimetics, adjusting calcium concentration in the dialysate, and surgical correction of sHPT. It is pertinent to note that phosphate control by dietary restriction to 800-1000 mg/day lowered urinary phosphate excretion along with a decrease in phosphorus absorption, but the regimens are notoriously hard, and there is a tendency to relapse. [109].

Oral phosphate binders are the mainstay in the management of serum phosphate levels in patients undergoing dialysis. These medications bind to phosphate in the gut, either by forming an insoluble complex or by binding it into a resin and are usually classified as calcium-containing (Calcium acetate, Calcium carbonate, Calcium ketoglutarate, etc.) and calcium-free (Magnesium carbonate, Lanthanum carbonate, Sevelamer hydrochloride, and Sevelamer carbonate, etc.). Although both kinds of phosphate binders are effective at regulating phosphate levels, the calcium-containing phosphate binders are hazarded for their concomitant calcium load and its effect on vascular calcification [110]. In a randomized study with 200 hemodialysis patients treated with either sevelamer or calcium salts for the treatment of hyperphosphatemia, serum phosphate was controlled equally with both agents whereas subjects treated with calcium experienced significant hypercalcemia and intact Parathyroid hormone (PTH) levels. Moreover, both coronary artery and aortic calcification progressed significantly with calcium but not with sevelamer (~6 months – 1 year) [111]. A total of 119 patients with no

evidence of coronary calcification showed little evidence of disease development over the next 18 months, either on calcium-containing phosphate binders or sevelamer. However, subjects with a history of at least mild coronary calcification had significant progression at 6, 12, and 18 months following treatment with those on calcium-containing phosphate binders showing rapid progression [112]. Several prospective studies show an evidently reduced rate of Coronary artery calcium (CAC) in ESRD patients on sevelamer compared with those on calcium carbonate or calcium acetate [113].

Ameliorating the effects of sHPT is a vital approach to treat disordered bone and mineral metabolism. Although high parathyroid hormone itself does not correlate positively with and may not cause vascular calcification, its management may help in minimizing hypocalcemia. Management of sHPT is achieved by active vitamin D compounds, calcimimetics, etc. Vitamin D plays an important role in multiple metabolic pathways, including regulation of mineral metabolism. Active vitamin D formulations, or vitamin D receptor activators (VDRAs) including calcitriol, alfacalcidiol, doxercalciferol, and paracalcitriol have been prescribed in the treatment of sHPT in CKD. Hemodialysis and peritoneal dialysis patients who received VDRAs experience better survival outcomes than those who do not, regardless of their PTH levels [114]. Calcitriol, alfacalcidiol, and doxercalciferol can effectively lower PTH but have the side effect of heightening gastrointestinal absorption of Ca and P causing an undesirable load [115]. In a 2-year follow up study in dialysis patients, progress of aortic arch calcification was associated with higher accumulative doses of alfacalcidiol [116]. Paracalcitriol may preferentially target the parathyroid gland while avoiding the gastrointestinal effect and thus is less

associated with VC [117]. Nevertheless, more suitably sized randomized controlled trials are needed to determine the optimal doses and type of VDRAs to be used in therapy.

Calcimimetics are compounds that mimic the effects of Ca *in vivo.* They can work as a treatment for hyperparathyroidism by binding to Calcium sensing receptors (CaSRs) in the parathyroid glands. By binding to CaSRs, calcimimetics allosterically modulate them to become more sensitive to existing levels of circulating Ca, and they, in turn, suppress excess secretion of PTH. The only significant randomized study to assess the effects of calcimimetics is the ADVANCE study with CINACALCET which showed that along with the use of VDRA therapy, cinacalcet slowed the progression of VC over VDRA therapy alone in hemodialysis patients [118]. However, a more recent EVOLVE study reported that cinacalcet failed to significantly reduce the risk of death or major cardiovascular events in patients with moderate-to-severe sHPT who were undergoing dialysis [119]. For progressive, biochemically-severe, and often symptomatic sHPT, surgical removal of a part of the parathyroid gland, known as parathyroidectomy, may be the treatment of choice. Subtotal parathyroidectomy has been shown to arrest the progression of CAC in dialysis patients [120]. In chronic hemodialysis patients who underwent total parathyroidectomy, retrospective evaluation of prognosis revealed that parathyroidectomy, atrial fibrillation (AF), and serum albumin were significant factors for total and especially cardiovascular mortality. Total parathyroidectomy was associated with better survival, probably due to decreased cardiovascular mortality [121].

Table 2-3: Secondary prevention strategies against VC.

Treatment	Mechanism of Action/Outcome	References
Secondary Prevention		
Hyperphosphatemia *Dietary Phosphate Control* *Phosphate Binders*	Reduction of circulatory phosphate imbalance and reduced hyperphosphatemia	Isakova, T., et al. 2011 [109] Hutchison, A.J., et al. 2011 [110] Chertow, G.M., et al. 2002 [111] Block, G.A., et al. 2005 [112] Russo, D., et al. 2007 [113]
Secondary hyperparathyroidism *Vitamin D Receptor Activators (VDRAs)* *Calcimimetics* *Parathyroidectomy*	Management of sHPT by minimizing hyperphosphatemia and hypocalcemia without causing hypercalcemia and overly suppressing PTH	Teng, M., et al. 2003 [114] Tentori, F., et al. 2006 [115] Ogawa, T. et al. 2010 [116] Sprague, S.M., et al. 2003 [117] Raggi, P., et al. 2011 [118] Investigators, E.T., et al. 2012 [119] Bleyer, A.J., et al. 2005 [120] Iwamoto, N., et al. 2012 [121]

In addition to these preventative treatment strategies, there have been several potential therapies that tried to directly target the calcification process. Pyrophosphate (PPi) is a powerful inhibitor of calcium crystallization that circulates at sufficient concentrations so as to prevent hydroxyapatite formation, thus serving as an endogenous inhibitor of calcification. PPi may be deficient in advanced renal failure and plasma levels of PPi may be reduced in dialysis patients. In general, an inverse association of PPi concentrations is seen with VC in CKD and ESRD patients [87]. Humans lacking ectonucleotide pyrophosphorylase (Enpp1), the enzyme that synthesizes extracellular PPi, are also known to develop several MAC at an early age. However, rapid hydrolysis of PPi *in vivo* limits this therapy and in turn prompted the development and use of nonhydrolyzable analogs, known as bisphosphonates.

Studies, although small, with etidronate show a beneficial effect in CKD and ESRD patients. In a study with a mean patient age of 63.2±8.2 and mean duration of dialysis of 7.4±5.5, 35 patients were administered etidronate for 14 days over three cycles. CAC progression in these patients was significantly less pronounced during treatment than compared to the period before treatment was initiated [122]. In another study with etidronate, patients with ESRD and undergoing dialysis three times per week were given etidronate orally for 23 months. Aortic calcification area (ACA) in these patients did not change over 23 months, but the control group had significantly elevated ACA scores [123]. Calcification scores of the coronary arteries, thoracic, and abdominal aorta collected by a multi-detector-row CT scanner showed that etidronic acid markedly reduced aortic calcification in patients with ESRD undergoing chronic hemodialysis [124]. There is still

a debate over efficiency of bisphosphonate therapy, and results differ by the agent in question; different studies suggest a beneficial role of etidronate, pamidronate to a little extent but not alendronate or ibadronate [125]. Owing to their potential effects on bone formation and accumulation in renal failure because of their clearance by kidneys, bisphosphonates are not recommended as a therapy for treatment of uremic vascular calcification.

Table 2-4: Treatments directed against calcification mechanisms

Treatment	Mechanism of Action/Outcome	References
Calcification Mechanisms		
Pyrophosphates Bisphosphonates	Reduce release of Ca^{2+} and prevents hydroxyapatite nucleation and growth	O'Neill, W.C., et al. 2010 [87] Nitta, K., et al. 2004 [122] Hashiba, H., et al. 2006 [123] Ariyoshi, T., et al. 2006 [124] Toussaint, N.D., et al. 2010 [125]
Thiosulfate	Binds with vascular calcium salts to form a highly soluble calcium thiosulfate salt	Araya, C.E., et al. 2006 [126] Mataic, D., et al [127] Adirekkiat, S., et al. 2010 [128] Mathews, S.J., et al. 2011 [129]

Sodium thiosulfate (STS) is a small molecule acting as a vasodilator, antioxidant, and a calcium chelator *in vivo.* The use of thiosulfate to treat VC was devised due to reports that it prevents nephrolithiasis in humans, reduced tumoral calcifications in renal failure

and significantly because it was successful in treatment of Calcific uremic arteriolopathy (CUA) [126, 127]. In hemodialysis and peritoneal dialysis patients with CUA, parenteral infusion of STS was able to reduce skin necrosis and calcium deposits within three months of administration. In two preliminary studies with hemodialysis patients, STS was able to delay the progression of CAC after 4-5 months of intravenous administration but with a flipside of decline in bone mineral density of the hip in one study [128, 129]. Additional clinical trials are underway, and at this time, STS is not recommended for use elsewhere.

Osteoclasts are the major mineral-resorbing cells in the body, and a landmark study from our laboratory found that when osteoclasts were co-implanted with elastin in rats subdermally, calcification was limited [130]. However, successful delivery and activation of osteoclasts to the site of calcification remains a challenge.

2.8 Animal models of Vascular Calcification

Numerous animal models have been developed to study the cellular and molecular mechanisms underlying VC, and to investigate various treatment strategies against it. A variety of protocols in different animal species that produced calcifications at different locations on the aorta have been documented in literature. Some well-known models include Calcium chloride ($CaCl_2$) injury of abdominal aorta, local intraluminal perfusion of pancreatic elastase, systemic delivery of warfarin and vitamin K, supraphysiologic dosages of vitamin D, nicotine used in combination with vitamin D, delivery indoxyl sulfate, etc.

The $CaCl_2$ injury model has been used in rats, mice, and rabbits [131, 132]. Local chemical damage to the abdominal aorta (or any other parts of the aortic tree such as carotid or thoracic) by direct periadventitial application of $CaCl_2$ causes localized medial calcification. There is minimal injury to the arterial wall, but the acute and excessive calcification is accompanied by elastin fiber breakdown and severe inflammation [133]. Warfarin inhibits γ-carboxylation of matrix Gla protein (MGP) and induces calcification of the arteries similar to what is seen in an MGP-deficient mouse. Vitamin K is also used in this model to restore normal coagulation as Warfarin is an anticoagulant, commonly prescribed to dialysis patients [134, 135].

Calcitriol and other such vitamin D analogs are used to treat diseases in which VC is common, such as osteoporosis and hyperparathyroidism. But toxic doses, either daily intraperitoneal injections (1μg/kg) or supraphysiologic doses in diet (7.5 mg/kg), of Vitamin D and its analogs, causes calcification [136-138]. This toxic effect of vitamin D is both indirect (by causing an increase of circulating levels of Ca and P) and direct through VSMCs. Calcitriol has been known to stimulate calcium flux into VSMCs and thus modulates increased expression of several proteins associated with calcification.

As discussed earlier, various other stimulants have also been administered in rodents to induce VC. Nicotine (5 ml/kg) amplifies the pro-calcific effects of vitamin D (25 mg/kg). Vitamin D and nicotine (VDN) induces a calcium overload in the arteries, resulting in medial and other widespread calcification [139]. The nicotine plus vitamin D model causes calcification similar to that in a senescent man and is naturally accompanied by systolic hypertension and LVH. Indoxyl sulfate (IS) is a uremic toxin that accelerates

the progression of CKD. In addition, IS promotes aortic wall thickening and aortic calcification along with colocalization of osteoblast-specific proteins. Thus, it is not only a nephrotoxic but also acts as a vascular toxin [140].

Intraluminal infusion of elastase degrades elastin in the arteries, which in turn localizes calcification in the abdominal aorta. This model was tested in swines and rabbits [141]. In the elastase-treated arterial segments of swines, elastic fiber damage, reduction of smooth muscle cells in certain areas and a significant number of necrotic lesions and calcium deposits were observed within three weeks. New Zealand rabbit elastase-induced aneurysm of the common carotid artery and subsequent calcification is one of the most commonly used models to test the safety and efficacy of endovascular devices [142].

Gene deletion in mice is an extremely useful technique to unearth the precise role of a particular protein in the development of VC. Several inhibitors, either local or systemic, such as MGP, fetuin-A, PPi are often dysregulated during the pathophysiological process of calcification [85, 87, 89]. Mice which are deficient in phosphaturic hormone fibroblast growth factor (FGF) 23 and its necessary cofactor Klotho exhibit extensive vascular and other soft tissue calcifications [85, 143]. Mice that lack MGP develop to term, but die within a couple of months as a result of arterial calcification leading to blood vessel rupture. MGP-deficient mice, besides, exhibit inappropriate calcification of various cartilages, including that of the growth plate, eventually leading to short stature, osteopenia, and fractures [84]. Osteoprotegerin (OPG) deficient mice also exhibit medial calcification of the aorta and renal arteries, suggesting that regulation of OPG, its signaling pathway, or its ligands play a role in the association between osteoporosis and VC [144].

Schafer et al. identified the serum protein α2-Heremans-Schmid glycoprotein (Ahsg, commonly known as fetuin-A) as an important inhibitor of ectopic calcification acting on a systemic level. Ahsg-deficient mice are normal phenotypically, but develop several calcifications of various organs on a mineral and vitamin D-rich diet, and on normal diet when the Ahsg deficiency is on a DBA/2 background [145].

Rodents have a generally high resistance to the development atherosclerotic calcification. The lipid profile of rodents differs significantly from humans in that rodents carry most of their plasma cholesterol in the form of high-density lipoprotein (HDL), known to be a protector against atherosclerosis. Humans, on the other hand, have 75% of their cholesterol on low-density lipoprotein (LDL). However, mice of C57/BL6 genetic background are an exception. Mice models based on interventions in lipoprotein metabolism through genetic and dietary manipulations are most commonly used to study atherosclerotic calcification. ApoE, a glycoprotein which is a constituent of all lipoproteins except LDL, serves as a ligand for receptors involved in the clearance of very low-density lipoproteins (VLDL) from circulation. Deletion of this particular ApoE gene results in a definite increase in plasma levels of VLDL, increase in LDL to a lesser extent and a 45% reduction in normal HDL levels leading to development of atherosclerotic lesions, mainly in the aortic root and ascending aortas. A high fat, high cholesterol diet leads to the development of more widely distributed and complex atherosclerotic plaques in these ApoE knockout mice [146-148]. The LDL receptor (LDLR) knockout mice represent another frequently used genetic model for atherosclerosis. LDLR knockout shows a modest increase in lipid levels, doubling of plasma cholesterol mainly due to elevated LDL levels

and little to no atherosclerosis when fed a regular chow diet. When fed with a 1.25% cholesterol-rich diet, LDLR knockout mice display an eight-fold increase in plasma cholesterol levels and show rapidly developing atherosclerotic lesions throughout the length of the aorta. Administration of high-cholesterol, high-fat diet to these mice causes a 2-fold increase in aortic calcification and decreased rate of bone formation [149, 150].

Table 2-5: Animal models for *in vivo* calcification studies.

Type of Animal Model	Method of induction of disease	Animal Species	References
Calcium Chloride model	Periadventitial application of $CaCl_2$	Rats, Mice, Rabbits	[131-133]
Warfarin/Vitamin K	Warfarin in drinking water/Vitamin K Subcutaneous injections	Rats	[134, 135]
Vitamin D	Daily intraperitoneal injections or supra-physiological vitamin D doses in diet	Rats	[136-138]
Genetically induced models	Knockout of regulators of calcification (FGF23, Klotho, MGP, OPG or Fetuin-A)	Mice	[84, 89, 143, 144, 151, 152]
Nicotine Model; usually used in combination with Vitamin D	Oral administration of Nicotine amplifies the calcifying effects of Vitamin D	Rat	[139]
Indoxyl Sulphate Model	Administration of Indoxyl Sulphate in water	Rats	[140]

Elastase Model	Intraluminal delivery of elastase causes breakdown of elastin fiber	Rats, Mice, Swine, Rabbits	[141, 142]
5/6th Nephrectomy Model of CKD	Reduction in renal mass is usually installed by a two-stage surgical procedure: partial nephrectomy of one kidney and total nephrectomy of the contralateral kidney	Rats, Mice	[153-155]
Dietary adenine induced CKD model	High adenine feeding leads to structural and functional damage to kidneys causing increased Serum Ca levels and calcification	Rats, Mice	[156-159]
Genetic models of atherosclerotic calcification	ApoE$^{-/-}$ knockout mice Ldlr$^{-/-}$ knockout mice	Mice	[146-150]

2.9 Animal Models of CKD with Vascular Calcification

Animal models of CKD generate a range of severity in calcification phenotype attributable to a lack of consistency in the genetic backgrounds used, degree of kidney damage induced, time course of study, and dietary regimen selected.

The 5/6th nephrectomy model or remnant kidney rat model reproduces experimental CRF by mimicking the progressive loss of nephrons that occurs in human CRF. It was first developed by Chauntin and Ferris in 1932 and has been used ever since [160]. In this model, reduction in renal mass is usually achieved by a two-stage surgical procedure:

partial nephrectomy of one kidney and then a total nephrectomy of the contralateral kidney. Different methods are employed to perform the nephrectomy; resection or ligation of the upper and lower poles of the kidney [161], cauterization or electrocoagulation of the renal cortex and arterial ligation [162]. Out of the three, arterial ligation of 2/3rd of extrarenal branches of the renal artery of the kidney, performed on one combined with resection of the other kidney is the most commonly used rat model of 5/6th nephrectomy model. However, the major limitations of 5/6th model for study of vascular calcification include requirement of the two-step surgical procedure combined with the need to use either an accelerating agent such as Vitamin D, excessive dietary phosphate levels or surgical removal and replacement of parathyroid glands [163].

Rats with autosomal dominant polycystic kidney disease result in spontaneous development of CKD over time. Heterozygous Han: SPRD rats (Cy/+) develop azotemia at 10 weeks and progress to uremia by about 40 weeks of age, accompanied by anemia, hypertension, hyperlipidemia, and sHPT [164, 165]. In this model, Moe et al. reported that all three components of CKD viz., abnormal serum biochemistries, abnormal bone remodeling and calcification of the tunica media are induced when fed a normal 0.7% P diet. 60% of the animals developed mild to severe calcifications of the aorta after 38 weeks of age [166]. The main disadvantage of this model, however, particularly for its usage in interventional studies, is the very slow progression of CRF and as such the late onset of the first calcified spots in the arteries, combined with limited reproducibility.

2.10 Adenine-Induced Chronic Kidney Disease Model

In normal conditions, adenine is salvaged by the enzyme adenine phosphoribosyltransferase (APRT) enzyme and is generally present in very low levels in circulation and urine. APRT is expressed ubiquitously in all mammalian cells and plays an important role in the purine nucleotide salvage pathway helping in recovery of bases and nucleosides following degradation of RNA and DNA. It represents the rate-limiting step in the conversion of adenine and 5-phosphoribosyl-1-pyrophosphate (PRPP) to adenosine monophosphate (AMP). ARTP catalyzes a phosphoribosyl transfer from PRPP to adenine, forming AMP and releasing pyrophosphate.

When adenine administration exceeds a certain level, APRT activity is insufficient and saturated. Adenine is then oxidized by xanthine dehydrogenase to 2,8 dihydroxyadenine (DHA) via an 8-hydroxyadenine intermediate product. Although DHA is protein-bound in plasma, it has a general poor solubility in urine and gradually precipitates in the kidney tubules, leading to the formation of kidney stones, i.e., nephrolithiasis [167]. If left untreated, it results in renal failure with permanent kidney damage. The autosomal recessive metabolic disorder, APRT deficiency represents the human counterpart of this phenomenon [168].

The adenine model has recently gained a lot of attention due to the relative ease in design and several encouraging outcomes. Long term high adenine feeding in rats results in certain metabolic abnormalities resembling CRF in humans. Among the disturbances observed are azotemia, accumulation of uremic toxins, imbalance of amino acids and electrolytes, and other hormonal imbalances [169]. Adenine forms crystals in the renal

tubules causing subsequent tubular injury, seen as lesions in mainly proximal tubules, some distal tubules and glomeruli, inflammation, and noticeable fibrosis. These marked kidney damages go along with characteristic biochemical changes like significantly elevated serum creatinine, blood urea nitrogen, and phosphorus. Renal pathology of the adenine model resembles the clinical situation quite well with the presentation of hyperphosphatemia, hypocalcemia, severe secondary hyperparathyroidism with high parathyroid hormone levels, hypovitaminosis of D, and renal osteodystrophy. Okada et al. optimized the adenine-induced CKD model in rats that closely resembles the clinical condition in humans [170]. It has since become a useful model to study complications of CKD in patients.

Several research groups made use of the adenine model to evaluate therapeutic agents for prevention of medial calcification [156, 159, 171-175]. The key advantage of the adenine model is that it does not mandate surgery to generate required levels of CKD. However, its major drawback is that up to 50% of the animals do not show medial aortic calcification despite the manifestation of a stable, comparable moderate-severe CKD. Another significant disadvantage is the severe weight loss that occurs with feeding of high adenine and ensuing mortality [176]. Price et al. introduced a variant on this model by lowering the protein content of the adenine-rich diet to 2.5% along with high amounts of Ca (1.06 %) and P (0.92%). This combination resulted in the development of uniformly severe medial calcification in the aortas of all rats 4 weeks after the induction of CKD. Lowering the protein content of the diet dramatically increases the frequency and extent of medial artery calcification [157].

Table 2-6: Studies with adenine-model of CKD in rodents

Reference	Animals	Diet	Duration of adenine feeding
Price et al. [157]	13 wk old SD rats	0.75% Ad 0.92% P 1.06% Ca 2.5%/25% Protein	4 wk
Katsumata et al. [156]	12 wk old Wistar Rats	0.75% Ade 0.92% P 1.06% Ca	4 wk
Lomashvilli et al. [177]	300g SD rats	0.75%/0.5% Ad 0.92% p 10.6% Ca	4 wk
Yamada et al. [178]	10 wk old SD rats	0.75% Ad 1.2% P 1.0% Ca	4 wk/6 wk
Neven et al. [159]	10 wk old Wistar rats	0.75% Ad 0.92% P 1.1% Ca	4 wk
Henley et al. [171]	350-390g SD rats	0.75% Ad 0.9% P 1.1% Ca	4 wk
Pasch et al. [179]	6 wk old Wistar rats	0.75% Ad 0.8% P 1.05% Ca	4 wk

2.11 Chelation Therapy

Chelation has its origin in the Greek word '*chela'* meaning claw of a lobster, thus describing the concept of clinging or holding with a strong grip. The term *chelate* was first applied by Sir Gilbert T. Morgan and H. D. K. Drew in 1920. They suggested the term for the caliper-like groups which function as two associating units and fasten to a central atom so as to produce heterocyclic rings [180].

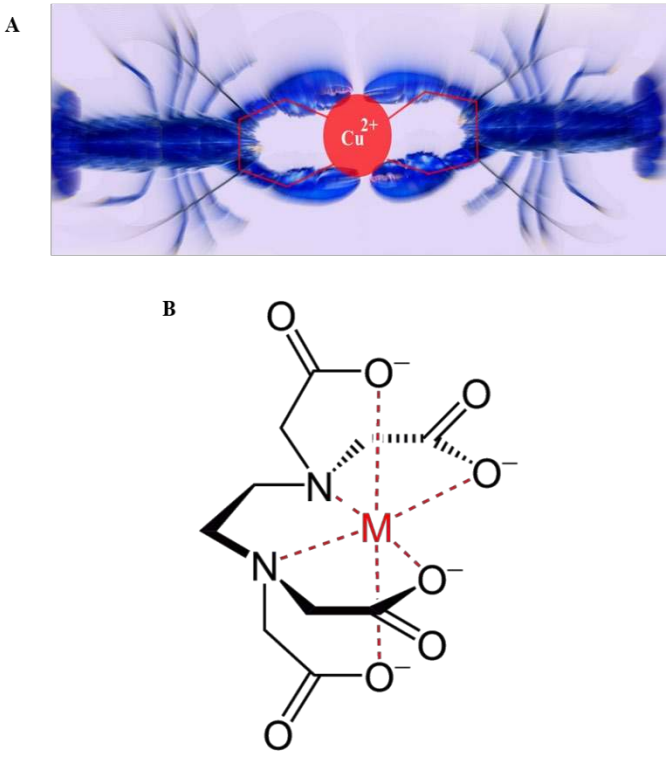

Figure 2-15: Chelating agent-metal ion complex. (A) Depiction of chelating agent binding to metal ion in a crab-like grip. (B) EDTA-Metal ligand complex [181].

Chelation therapy mainly involves the usage of Ethylene diamine tetraacetic acid (EDTA), a chemical that binds to, or chelates ionic calcium, trace elements, and other divalent cations. Chelation therapy can be traced back to the early 1930s when Ferdinand

Munz, a German chemist first synthesized EDTA while he was looking for a replacement for citric acid as a water softener [182]. Usage of chelation for therapy began during World War II when some chemists at the University of Oxford were researching for an antidote to lewisite, an arsenic-based chemical weapon [183]. It was learned that EDTA was particularly effective in treating lead poisoning. Following this, chelation therapy was used to treat workers who had painted US naval vessels with lead-based paints and were suffering from lead poisoning. It remains in use for some very specific medical purposes, although it needs to be administered under extremely careful supervision, owing to its many inherent risks. In fact, it is one of the preferred medical treatments against many forms of metal poisoning (e.g., lead, arsenic, mercury, iron, copper, and nickel) [184]. Heavy metal poisoning can be caused by drinking polluted water, breathing heavily polluted air, and due to several conditions that lead to a buildup of toxic metals in the body, such as Wilson's disease, hemochromatosis, thalassemia, sickle-cell disease, etc.

2.12 Types of chelating agents

There are multitudes of chelating agents with different affinities for different metals, physical characteristics, and their mechanism of action in the body. These agents may be administered intravenously, intramuscularly, or orally depending on the agent and need. Some chelating agents that have been used as chelation therapeutics for various medical purposes against metal intoxication are listed in Table 2-7.

Apart from its usage in alternative medicine to treat metal toxicity as discussed, chelation therapy has also been advocated for conditions like atherosclerosis, diabetes, autism, Alzheimer's, and Parkinson's disease. However, all these claims are largely

unproven, and chelation therapy is only approved by the U.S. Food and Drug Administration (FDA) to treat metal poisoning [185, 186].

Table 2-7: Chelation therapy for metal intoxication

Type of chelating agent	Target metal and medical application	Route of Administration	References
EDTA	Lead, Calcium	Intravenous	[187-190]
Calcium disodium EDTA	Mercury, Lead	Intravenous	[191-193]
STS (Sodium thiosulfate)	Antioxidant Cyanide Poisoning Skin Diseases like Acne	Intravenous	[194] [195]
DTPA (Diethylene triamine pentaacetic acid)	MRI contrast agent, Radioactive poisoning with Plutonium, Americum, etc.	Intravenous	[196] [197]
Dimercaprol *also known as* BAL (British anti-Lewisite)	Arsenic, Mercury, Lead poisoning Copper poisoning (Wilson's disease) Lewisite poisoning	Intramuscular injection	[198] [199] [200, 201]
DMSA (Dimercaptosuccinic acid)	Mercury, Arsenic and Lead poisoning	Oral	[202-204]
DMPS (Dimercapto-propane sulfonate)	Acute Arsenic poisoning Polonium poisoning Mercury poisoning	Oral Intravenous	[205] [206]

D-Penicillamine	Lead, Arsenic, Mercury poisoning Copper poisoning in Wilson's disease	Oral or Intravenous injections	[207] [208]
Deferoxamine and Deferasirox	Iron poisoning (Thalassaemia) Aluminum poisoning (Chronic renal dialysis)	Intravenous injection or infusion	[209, 210]

2.13 EDTA Chelation Therapy

EDTA binds to and forms strong complexes with iron, mercury, lead, calcium, trace elements, and other divalent cations. Table 2-8 shows EDTA and its binding affinity to various metal ions.

Table 2-8: EDTA and its Log K binding constants to various metal ions.

Metal	Fe^{3+}	Hg^{2+}	Cu^{2+}	Pb^{2+}	Ni^{2+}	Zn^{2+}	Cd^{2+}	Co^{2+}	Al^{2+}	Fe^{2+}	Mn^{2+}	Ca^{2+}	Mg^{2+}
Log K	25.1	21.8	18.8	18.5	18.0	16.5	16.5	16.3	16.1	14.3	13.7	10.7	8.7

Higher binding constants indicate the binding potential of the chelating agent to the respective metal ion. Owing to its large binding affinity to Pb^{2+}, EDTA has been used for decades to treat lead poisoning, as we discussed before. EDTA also has an appreciable binding affinity to Ca^{2+}, therefore has been used to treat hypercalcemia, removal of calcium

from fixed tissues and has long been advocated as an alternative treatment approach for CVDs [9, 187, 211].

There have been many case studies and clinical trials to claim that EDTA chelation therapy is effective against atherosclerosis, coronary heart disease, and peripheral vascular disease. It began with Norman Clarke, Sr. and his coworkers in the 1950s who observed that some of the workers at a battery factory had improved angina pectoris following chelation therapy. He subsequently administered chelation therapy to patients with angina and other occlusive vascular problems, hypothesizing that "EDTA could dissolve disease-causing plaques in the coronary systems of humans" [188]. In a subsequent longer study, Clarke et al. showed that 87% of patients out of 283 showed improvement in their symptoms [212]. Quite a few investigators made similar observations about the role of EDTA in the treatment of cardiovascular disease [213-217]. In a retrospective study of 2,870 patients treated with NaMgEDTA, Olszewer and Carter noted that EDTA chelation therapy benefited patients with cardiac disease, peripheral vascular disease, and cerebrovascular disease. The conclusions were unjust due to a lack of comparison with people who did not receive the treatment. The same researchers carried out a double-blind study in which patient progress was evaluated by measuring blood pressure changes, performance in stress tests before, during, and after EDTA treatment. It was claimed that the treatment showed substantial improvements in walking and master exercise tests [218]. McDonagh et al. reported a case study with 30 patients diagnosed with atherosclerotic vascular disease and showed that EDTA chelation therapy decreased intra-arterial obstruction and reduced stenosis [219]. In a retrospective case study in 470 patients acting

as their own control, Claus Hancke and his group observed that 80-91% of them showed improvement. Amongst 92 patients referred for surgical intervention, only 10 ultimately required surgery during, or after chelation therapy [220].

Results from other randomized, placebo-controlled studies, however, do not indicate any benefit from EDTA on CVD. The first of these studies was conducted by Diehm et al. with 45 patients who had a high-grade arterial obstruction and intermittent claudication, by measuring their ability to perform pain-free walking exercises along with many other parameters. Measurements made during the 4-week treatment period, and for 3 months after treatment, showed that both EDTA and control Bencyclan groups showed comparable improvements [221]. Guldager and coworkers published a double-blind, placebo-controlled trial with 153 patients who received either EDTA (3g of Na_2EDTA) placebo. At the end of the 5-9 week treatment phase, there were no significant inter-group differences in any of the outcome parameters, and the situation remained unchanged even after 6 months of follow-up [222]. Another placebo-controlled, double-blind study was published by van Rij et al. randomizing 32 patients with intermittent claudication into treatment and control groups. No clinically significant differences in main outcome measures (subjective and measured walking distances, ankle/brachial pulse indices) between chelation therapy and placebo groups were detected up to 3 months following treatment [223]. In 2002, Knudtson et al. enrolled 84 patients over 21 years of age with coronary artery disease proven by angiography, or documented myocardial infarction and stable angina. Based on exercise time to ischemia, exercise capacity, and quality of life

measurements, they found no evidence to support a beneficial effect of chelation therapy [224].

The use of chelation therapy to treat heart diseases and other conditions grew in the United States by approximately 68% to about 111,000 people. The Trial to Assess Chelation Therapy (TACT) was the first large-scale, NIH funded, multi-centered study commissioned from 2008 to 2013 to determine the safety and efficacy of EDTA Chelation Therapy (disodium EDTA) for individuals with a history of heart attacks. It was a study with a large enough design to detect if there are any moderate benefits towards risks associated with the therapy. Overall, patients who received chelation therapy had a modest 18% reduced risk of subsequent cardiac events such as heart attack, stroke, and hospitalization for angina. These results, by themselves, are not sufficient to recommend routine use of chelation therapy for post-heart attack situations. Interestingly, among patients with diabetes (these patients made up 37% of the entire study population), researchers found that those receiving chelation had a markedly lower risk of cardiovascular events (25% in diabetic patients vs. 38% in placebo) and death due to any cause was 43% lower [190, 225]. A new follow-up study, Trial To Assess Chelation Therapy 2 (TACT2) commenced in December 2016 and is underway until 2021. NIH is sponsoring TACT2 to repeat the TACT1, but only in patients with diabetes and a prior heart attack to confirm the apparent benefit of EDTA chelation therapy in this group of patients [226]. Despite countless claims and opinions against the use of EDTA chelation therapy in the treatment of CVDs, there is enormous potential, as long as the possible side-effects can be circumvented.

2.14 Nanoparticles as drug delivery systems

In the treatment of vascular diseases, direct administration of drugs has shown limited success largely because of rapid drug clearance, short half-life, and severe systemic side effects. In addition, disturbed flow condition in the arteries is an important factor to consider while developing an effective therapy for vascular disease [227]. Nanoparticles (NPs) have certain unique features that enable them to be used in drug delivery to specific tissues or organs to maximize the beneficial effects of the drug by improving local availability and lower off-target complications. The tunability of their shape, size, and surface chemistry makes NPs suitable to be programmed for site-specific delivery. NPs achieve their central goal of site-specificity by exploring considerations of normal versus diseased tissues to optimize their residence time [228-230].

Several types of nanocarriers have been developed for use in medicine, each with their own advantages and disadvantages. These include micelles, reverse micelles, dendrimers, liposomal nanocarriers, polymeric nanoparticles, nanogels, and nanocoatings. Among these, only polymeric and liposomal nanoparticles have been extensively studied for drug delivery in vasculature because of their high biocompatibility and biodegradability. Further, they present a variety of possibilities for surface-modification and high drug payload [231, 232]. Polymeric nanocarriers have proven to be more effective in delivering drugs to vascular wall than their liposomal counterparts, owing to liposome's inherent issues such as thinner membranes affecting their durability, and destabilization due to addition of polyethylene glycol (PEG). As NPs being targeted to vascular disease have to be administered intravenously into circulation, an immune response, known as

opsonization, to the blood proteins that are absorbed onto the particle surface will occur [233]. This will result in the particles being quickly eliminated from circulation by the Mononuclear phagocyte system (MPS) [234], and the desired therapeutic effect is not achieved. Surface addition of PEG chains to polymeric NPs, a process termed PEGylation, increases their hydrophilicity, reduces immunogenicity, and increases their retention time by making them “stealthy”. [235].

Targeting of NPs can be achieved either by passive or active targeting mechanisms. Passive targeting is commonly used in oncology because the tumor results in enhanced permeability and retention (EPR) effect [236, 237]. NPs preferentially accumulate near tumor sites due to blood vessel leakage, or limited lymphatic drainage. Active targeting is a result of surface modifiers such as ligand/receptor, antigen/antibody, or any other form of molecular recognition, to ensure that the NPs are guided to the tissue of interest [238, 239].

2.14.1 Albumin use for formulation of nanoparticles

Albumin is a versatile macromolecule for drug delivery because it is known to be non-toxic, non-immunogenic, biocompatible, and biodegradable. In recent times, albumin-based nanoparticles have emerged as attractive drug carriers, since a significant amount of drug can be loaded into the particle matrix because of high binding sites present in the albumin molecule [240]. Albumin can be obtained from a variety of sources, including egg white (ovalbumin), bovine serum albumin (BSA), and human serum albumin (HSA). Albumin NPs are expected to be well tolerated, as evidenced by clinical studies with registered HSA-based particles such as Albunex™[241] and Abraxane™ [242].

Albumin nanoparticles can be prepared using a variety of techniques [240]; desolvation, emulsification, thermal gelation, nanospray drying, and nab™. In the process of desolvation, albumin is phase-separated out from a solution by the addition of a desolvating agent due to its diminished solubility. Glutaraldehyde is then used as a crosslinker to harden the coacervates. Other crosslinkers, such as polyethyleneimine (PEI), formaldehyde, and 1-ethyl-3-(3-dimethylaminopropyl) cardodiimide (EDC) have been suggested as alternatives to glutaraldehyde for reduced toxicity [243].

2.15 Targeted or Site-specific EDTA Chelation Therapy

The usage of systemic chelation therapy with EDTA, as discussed above, requires high dosages resulting in possible unwanted side effects such as hypocalcemia, renal toxicity, and bone loss [10, 244]. The major drawback to any systemic treatment is that very small amounts of the drug (in this case, chelating agent) actually reach the site of mineralization. Another notable hurdle for systemic attempts to reverse VC is that calcium is typically present in blood, bones, and teeth, and is required for normal functions in these tissues. Therefore, removal of calcium from arteries through systemic approaches can have major and potentially disastrous complications. Targeted and site-specific delivery of EDTA could lower the dosage required and present attractive advantages such as improved bioavailability and control over release of the chelating agent.

In our laboratory, we have developed a nanoparticle approach with albumin-based NPs that only targets degraded elastin fiber, which is a salient feature of calcified arteries. As noted previously, elastic fibers are made up of a core of crosslinked amorphous elastin, and several microfibrillar glycoproteins (such as fibrillins and fibulins) on the periphery of

the amorphous core. Consequent to elastic fiber degradation and calcification, the surrounding microfibrillar proteins are lost, and the amorphous core is exposed. This exposed core serves as a potential target for nanoparticles conjugated on their surface with an elastin-specific antibody [245].

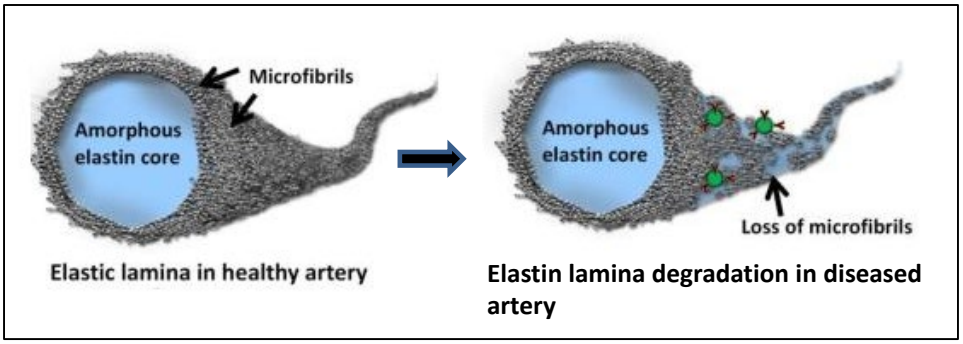

Figure 2-16: Elastic fiber degradation leads to exposed amorphous core

Several key studies performed and published from our laboratory have shown the success of such site-specific targeted therapies with albumin NPs aimed to target damaged elastic fiber in the treatment of elastin-specific diseases including abdominal aortic aneurysm [246-248], emphysema and chronic obstructive pulmonary disease (COPD) [249].

3 PROJECT RATIONALE AND SPECIFIC AIMS

Therapeutic strategies and interventions that may stabilize and potentially reverse vascular calcification (VC) are of immense value to patients with chronic kidney disease (CKD). As discussed at length in the previous chapter, most of the treatment methods in use have been generally limited to optimizing and managing the dysregulated mineral metabolism and bone turnover diseases, both of which are characteristic to CKD itself. It is pertinent to note here that there is no consensus yet about screening for, and interventions to retard the progression of VC. Even with the most dramatic interventions in use, namely intense dialysis and renal replacement therapy, VC that has already manifested in patients cannot be regressed.

Current clinical practice entirely focuses on prevention and retardation of progression. Unfortunately, most patients remain underdiagnosed, and those diagnosed already have heavily calcified vessels thereby remaining undertreated since preventative strategies no longer work at this stage of diagnosis. Therefore, it becomes essential that the process of treatment of VC involves direct interference with mineralization in the arteries and resorption of calcified lesions. Promoting this process of reversal, while simultaneously avoiding demineralization from tissues that normally contain calcium (i.e., bones and teeth) remains the most critical challenge with respect to developing a successful treatment regimen for VC in CKD. Unfortunately, there is no FDA-approved treatment available at this time to reverse calcification in millions of patients with CKD. Finding a treatment approach that attacks and dissolves mineralization in the calcified arteries of

these patients, while eluding systemic loss of calcium, thus improving arterial elasticity remains a pressing health care necessity.

Chelating agents are chemical compounds known to react with metal ions to form stable and water-soluble complexes. They have long been of great importance in treating intoxications and metal overload in the body. Some critical qualities of a chelating agent to exert its clinical effect are high affinity towards the toxic metal, forming the metal-chelator complex with rapid elimination, and low toxicity. EDTA is a well-known chelator and has a high affinity towards a variety of metal ions, including Ca^{2+}. Ethylene glycol tetraacetic acid (EGTA) is a polycaroboxylic acid similar to EDTA and can also act as a chelating agent. It is reported to have a better affinity towards Ca^{2+} than EDTA. A polycarboxylic acid derivate of EGTA, known as (1,2-bis(o-aminophenoxy) ethane- N, N, N', N' tetraacetic acid (BAPTA), is also known for its calcium-specificity and ability to bind two Ca^{2+} ions in solution, Both EGTA and BAPTA have been used to chelate Ca^{2+} in buffers, especially in the presence of other metal ions like Mg^{2+}. Because of their affinity for Ca^{2+}, we theorize that these chelating agents can chelate and remove Ca from mineralized deposits.

Our innovative tactic is to target the amorphous elastin core that is exposed when elastin fibers degrade and calcify. NPs conjugated with an anti-elastin antibody will accumulate at the calcified sites, sparing healthy arteries and other tissues. This will allow us to deliver any agent to these degraded and calcified elastin fibers. The chelating agent released at these sites will dissolve and remove calcium from the mineralized deposits. Site-specific delivery of chelating agent helps us to avoid systemic side effects commonly

seen with intravenous chelation therapies currently in use. If successful, this approach will create a new paradigm in the quest to invent a novel therapy for permanent reversal of vascular calcification.

Specific Aim 1: **To compare and contrast the chelating agents EGTA and BAPTA with EDTA and deduce the chelating agent most effective in demineralizing calcium for use in targeted chelation therapy of VC.**

Rationale: EDTA is a popular chelating agent in the treatment of metal intoxication due to lead, and calcium owing to its well-published affinity towards many metal cations. EGTA is useful for making buffers to chelate Ca ions when they are less concentrated than others, as found in living cells and chelating certain heavy metal poisons. BAPTA-AM has been known to maintain intracellular Ca^{2+} homeostasis. In this aim, we would like to compare the chelating ability of these three chelating agents *in vitro* to select the best among the three for our targeted EDTA chelation therapy experiments.

Specific Aim 2**: To investigate whether EDTA, a chelating agent, loaded nanoparticles (NPs) can be targeted to the sites of elastin-specific medial arterial calcification (MAC) and whether the calcification can be reversed in a renal failure model in rats.**

Rationale: We have already shown elastin antibody-conjugated nanoparticle delivery system delivers EDTA to the sites of vascular calcification in a calcium chloride abdominal aorta injury, and calcification is eliminated from these sites. One significant limitation of this study was that the calcification that manifests in the $CaCl_2$ model is restricted to the injury site in the abdominal aorta. Moreover, the calcification caused is because of an

inflammatory response to the periadventitial application of CaCl2 and may not be relevant clinically. Diabetic or renal failure patients would have calcification due to different pathomechanisms, and not due to chemically created injury. To address this limitation, we have chosen a renal failure model in rats caused by dietary administration of adenine.

Specific Aim 3: **To establish and validate adenine-induced CKD model of medial arterial calcification in mice by monitoring disease progression *in* vivo and exploring VSMC status for potential use in investigating targeted EDTA chelation therapy and effect of reversal of calcification on vascular homeostasis and function.**

Rationale: As cited earlier, we and several research groups have shown VSMCs undergoing differentiation and osteoblast-like transformation in VC. Recently, we have shown that osteogenic transdifferentiation of VSMCs occurs when cultured on surfaces of HA and calcified elastin. Interestingly, when cells were removed from the calcific environment and cultured normally, they revert to their VSMC phenotype. However, whether this is possible *in vivo* remains a challenge. Lineage tracing studies will be useful to investigate the fate of VSMCs *in vivo* after elimination of calcification by EDTA treatment. Since mice need to be used for lineage tracing studies, there is a need to establish a mouse model where CKD-related MAC is manifested and can be targeted. We would also like to develop imaging modules to track the progression of disease before and after treatment to assess improvement in vascular health following clearance of mineralized deposits and reverting of VSMCs to their contractile phenotype.

Specific Aim 4: **To develop an *ex vivo* porcine carotid artery organ culture model of vascular calcification for evaluating whether treatment with EDTA loaded nanoparticles conjugated with an anti-elastin antibody eliminates calcification and reverts VSMCs to their normal phenotype**

Rationale: A large number of studies have been conducted using cell cultures from mice, bovine, and human to better understand the core mechanism of VC. High morphological and genetic variation at higher passage numbers limit the suitability of monolayer cell cultures to examine the influence of interaction between different cells and thus do not provide a full picture of VC and ensuing phenomena. Organ cultures are simple, relatively easy, and a better fit to inspect VC and nearly resemble an *in vivo* condition. An *ex vivo* organ culture model from a larger animal than rodents would be a logical step forward. We intend to use a porcine carotid artery organ culture model of Pi-induced calcification to scrutinize VC and VSMC cell fate after chelation therapy.

4 SPECIFIC AIM 1

TO COMPARE EGTA AND BAPTA WITH EDTA AND DEDUCE THE CHELATING AGENT MOST EFFECTIVE IN DEMINERALIZING CALCIUM FOR USE IN TARGETED CHELATION THERAPY

4.1 Introduction

EDTA is a popular chelating agent for divalent ions, which is widely used in biochemistry, molecular biology, and cell biology. In addition to Ca, EDTA forms especially strong complexes with Mn, Cu, Fe, Pb, and Co. Ethylene glycol-bis (β-aminoethyl ether)-N, N, N′, N′-tetraacetic acid or Ethylene glycol tetraacetic acid, or simply known as Egtazic acid is an aminopolycarboxylic acid and can act as a chelating agent, just like EDTA. In comparison to EDTA, it has a lower affinity for Mg^{2+}, in turn making it more selective for Ca^{2+}. EGTA is known for its high specificity for Ca^{2+}, more so in the presence of Mg^{2+} [250]. It has been used to buffer solutions that resemble living cell environment, where Ca2+ ions are 1000-fold or so lesser concentrated than Mg2+ ions. Although EDTA is in more widespread use currently, EGTA is also used in some applications like treating animals with cerium poisoning, separation of thorium from monazite and as a component in elution buffers for protein purification. A synthetic derivative of EGTA, 1,2-bis(o-aminophenoxy)ethane-*N,N,N′,N′*-tetraacetic acid (BAPTA), is also known for its preference for Ca^{2+} ions in solution [251]. It is known to reduce elevation of cleaved Caspase-3, block cell death by inhibiting Reacting oxygen species (ROS) and eliminate intracellular changes of Ca^{2+} [252, 253].

Here, we try to assess the Ca chelating ability of the three chelating agents with a simple *in vitro* experiment using hydroxyapatite (HA) to select the better chelator for use in targeted EDTA chelation therapy.

4.2 Materials and Methods

4.2.1 Demineralization of HA *in vitro* by chelating agents

5 mg of hydroxyapatite powder was suspended in 30 mL solutions of three different chelating agents – EDTA, EGTA, and BAPTA. Two different concentrations (0.5 mg/mL, 5mg/mL) of each chelating agent were used. DD water was used as control group. At regular intervals, 1mL of supernatant was withdrawn to quantify Ca that was released into the supernatant. Samples were analyzed using the Spectro Acros ICP Spectrometer (SPECTRO Analytical Instruments, Kleve, Germany) at Clemson University Agricultural Service Laboratory and Ca amounts were normalized to the initial amount of HA in the solution.

4.2.2 Measurement of MMP activity in tissue homogenates

MMP activity in homogenates of lung tissue samples from emphysematous mice was measured using internally quenched peptide substrates for MMPs 2&9 (Ex/Em = 280/360 mm, MMP Substrate III, Anaspec, CA). One milligram of the substrate was dissolved in 50µl of DMSO, and the solution was diluted in 10 ml of development buffer (50 mM Tris Base, 5 mM $CaCl_2.2H_20$, 200 mM NaCl, 0.02% brij-35). 2 µl of the substrate stock solution and 2 µl of the homogenized tissues were mixed with 96 µl of the development buffer supplemented with any of the three chelating agents (EDTA, EGTA,

BAPTA) and incubated for one hour at 37°C. A fluorescent plate reader was used to read endpoint fluorescent intensity.

4.3 Results

4.3.1 Ca demineralized from HA by chelating agents

Three chelating agents (EDTA, EGTA, and BAPTA) at two different concentrations (0.5 mg/mL and 5 mg/mL) were tested to classify the best performing chelating agent with the highest propensity to release Ca. HA powder (5 mg in 30mL of chelating agent solutions was extracted at different time intervals and Ca measured through ICP analysis. EDTA was the stronger chelating agent amongst the three over a time period of 48 hours, removing Ca from HA at higher efficiency (~63 µg of Ca/mg of HA) than both EGTA and BAPTA, with 5 mg/mL EGTA (61.73 µg of Ca/mg of HA) reaching the level of demineralization of EDTA. Even at a higher concentration of 50 mg/mL, BAPTA was not as competent as EDTA in demineralizing Ca from HA powder in suspension with Ca released into the supernatants peaking at 51.4 µg of Ca/mg of HA for 5 mg/mL concentration. Negligible amounts of Ca were recorded with the control DD H_20. The release kinetics of all the three chelating agents are shown in Figure 4-1.

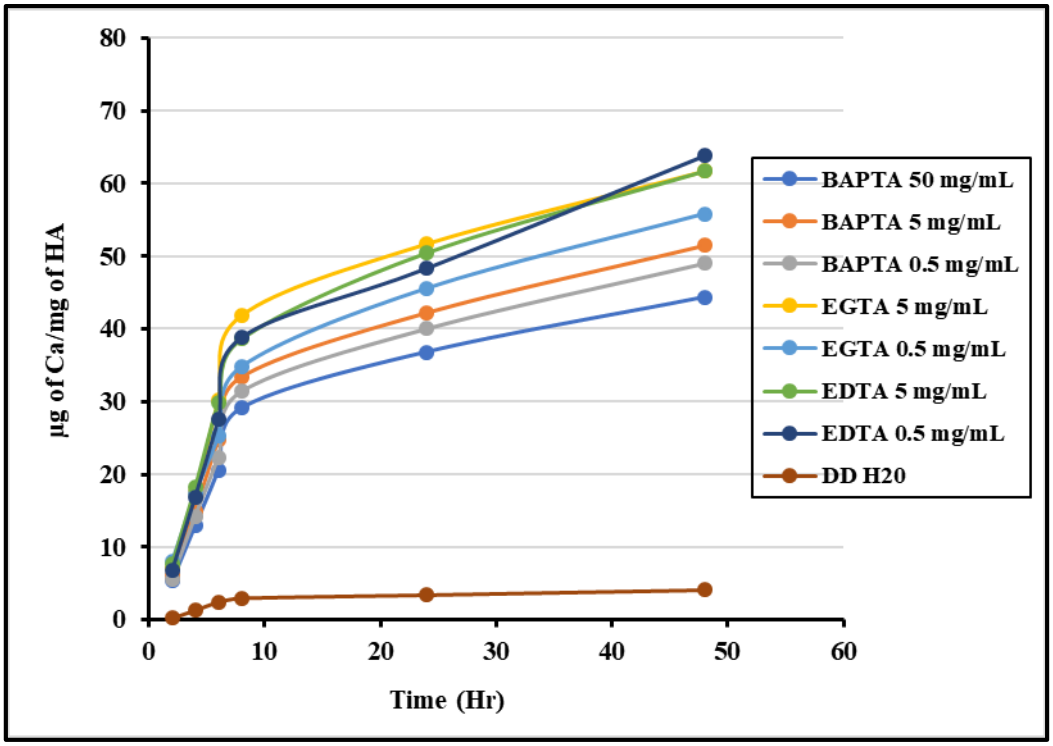

Figure 4-1: Demineralization and Ca release kinetics from HA by chelating agents. EDTA releases Ca most efficiently compared to EGTA and BAPTA at both the concentrations used.

4.3.2 Measurement of MMP activity in tissue homogenates

To compare the MMP inhibitory effect of the three chelating agents on the tissue homogenates of lungs from emphysematous mice, MMP activity was measured using a specific FRET substrate for MMP 2&9. No significant reduction of MMP activity was seen when the development buffer was supplemented with any of the three chelating agents, indicating that Zn^{2+} required for MMP activity was not chelated from solution (Figure 4-2).

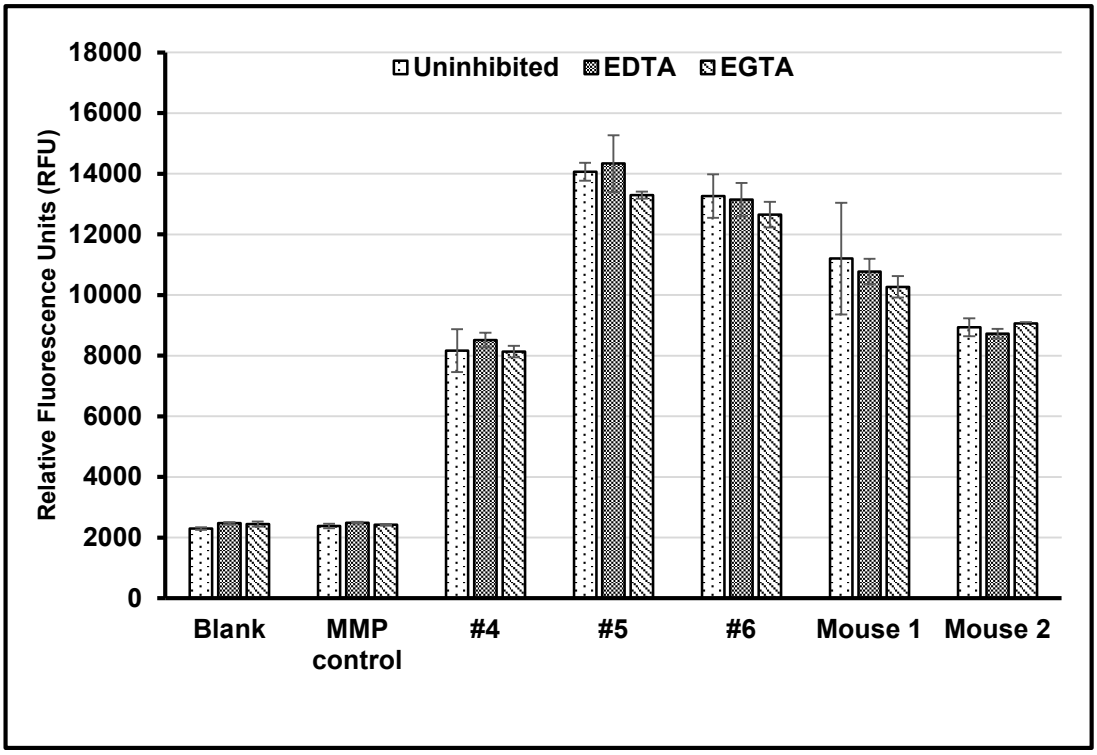

Figure 4-2: MMP activity by chelation of Zn^{2+}measured using specific FRET substrates for MMP 2&9.

4.4 Discussion

In this pilot study, we tested the efficacy for three different chelating agents known for their affinity of Ca^{2+} to compare their calcium demineralization potential. Demineralization of Ca^{2+} from HA shows that EGTA and BAPTA are not as effective in dissolving Ca^{2+} ions as EDTA. Reduction of MMP activity by chelation of Zn^{2+} was not observed with any of the three chelating agents. Although more studies are needed to confirm better demineralization of calcium deposits with different chelating agents,

including testing with Magnesium-based deposits (e.g., Whitlockite), calcified elastin fibers, and lesions. For now, EDTA was the chelator of choice.

5 SPECIFIC AIM 2

TO INVESTIGATE WHETHER EDTA, A CHELATING AGENT, LOADED NANOPARTICLES CAN BE TARGETED TO SITES OF ELASTIN-SPECIFIC MEDIAL ARTERIAL CALCIFICATION AND WHETHER THE CALCIFICATION CAN BE REVERSED IN A RENAL FAILURE MODEL IN RATS

5.1 Introduction

Patients with chronic kidney disease (CKD) have an elevated burden of cardiovascular disease (CVD) and compared to age-matched individuals with normal renal function[76, 254], are more likely to die due to CVD than to progress to renal failure. Although a cause of such excessive cardiovascular mortality has not been singled out, a major contributing factor is thought to be vascular calcification [76, 255].

Current therapies to treat VC, particularly in CKD, predominantly consist of controlling the mineral disturbance and are mainly preventive in action [256, 257]. EDTA is a promising chelating agent that can dissolve and remove calcium deposits if delivered near the calcification[258]. We demonstrated earlier that elastin antibody-conjugated NPs can be targeted to calcification sites and that EDTA delivered by these NPs reverses elastin-specific MAC in a rat model of $CaCl_2$ injury[259]. However, in that study, the aortic injury was created locally through a chemical insult, and systemic abnormalities usually associated with diseases like renal failure were not present.

Several research groups have employed the adenine-induced model of uremia and renal failure to characterize and investigate treatment methods for vascular calcification [159, 177, 179]. All these studies showed a common limitation that up to 50% of the rats fed with adenine diets do not show medial calcification in spite of a stable and comparable

CKD. Price et al. introduced a variant to this model by lowering the amount of protein in the diet to 2.5% and higher amounts of P than in a standard rodent diet[157]. Renal pathology of this model mimics the clinical situation with the development of hyperphosphatemia, hypocalcemia, severe secondary hyperparathyroidism, and other biochemical changes such as elevated serum creatinine and elevated blood urea nitrogen that lead to vascular calcification. Hence, this model is considered a useful tool to study complications of arterial calcification in CKD patients and to evaluate therapeutic agents in the prevention of uremia-related MAC[176, 260].

In the present study, we used the adenine diet with high P and high Ca-induced CKD rat model to test if albumin NPs loaded with EDTA delivered systemically would target calcific sites and remove vascular mineral deposition without the side effects associated with systemic EDTA chelation.

5.2 Materials and Methods

5.2.1 Preparation of BSA DiR Nanoparticles for in vivo targeting studies

DiR (1, 1-dioctadecyl-3, 3, 3, 3-tetramethylindotricarbocyanine iodide) (PromoCell GmbH, Heidelberg, Germany) loaded bovine serum albumin (BSA) (Seracare, Milford, MA) nanoparticles were prepared using desolvation method and conjugated to an anti-elastin antibody (US Biological, MA, USA) for targeting purposes as described [247]. Briefly, 250 mg of BSA was dissolved in 4 mL of DI water. 25 mg of DiR dye dissolved in acetone was added to BSA solution and stirred for one hour at room temperature following the addition of glutaraldehyde (EM grade 70%, EMS, PA, USA) at a concentration of 42 µg/mg BSA. The mixture was added dropwise to 24 mL of ethanol

while sonicating (Omni Ruptor 400 Ultrasonic Homogenizer, Omni International Inc, Kennesaw, GA) on ice for 30 minutes. Nanoparticles thus obtained were separated by centrifugation and washed. These particles were PEGylated (DSPE-PEG (2000) Maleimide) (Avanti Polar Lipids, Inc., Alabaster, AL) and conjugated to anti-elastin antibody following a previously described protocol [245, 246].

5.2.2 Preparation of EDTA-loaded nanoparticles for treatment

EDTA-loaded NPs were obtained by dissolving 200 mg of BSA (Seracare, MA) and 100 mg of EDTA (Fisher Scientific, NJ) in 4 mL of deionized water and pH was adjusted to 8.5 with 6N NaOH. The aqueous solution was added drop-wise to 16 mL of ethanol under probe sonication for 1 hour. For crosslinking, glutaraldehyde at ten µg per mg of BSA was added during sonication. The elastin antibody was conjugated in a method similar to the DiR NPs [245].

5.2.3 Experimental renal failure in rats – Adenine rat model

Renal failure was induced in rats by feeding adenine diets having high P and Ca levels. High adenine feeding resulted in crystallization of 2,8-dihydroxyadenine in renal tubules and interstitial spaces, thereby causing nephritis, fibrosis and all metabolic anomalies associated with chronic renal failure [176, 260]. Male Sprague-Dawley rats (Charles River Laboratories) were fed standard diets containing 18% protein until their body weights were close to or exceeding 300g. Animals were then fed a customized adenine (0.75%) diet (Harlan Teklad, Madison, WI, USA) made of 2.5% protein along with higher levels of calcium and phosphorus (1.06% and 0.92% respectively) [157]. Rats were maintained on this diet for 28 days while their body weights and behavior were carefully

monitored. If the weight loss was found to be more than 20% of baseline body weight, adenine diet was replaced with rat chow for all the adenine diet-fed animals to maintain consistency and allow them to recover their weights. Adenine diets were reintroduced once the animals recovered their weight, and the total adenine diet feeding time was 28 days. Control rats were fed normal chow diets without adenine for the length of the experiment. Disease progression in live animals was monitored via high-frequency ultrasound imaging (Vevo2100, VisualSonics, Toronto, Canada). Clemson University Animal Research Committee approved all animal use protocols (AUP) for the experimental models. All animals receive humane care in compliance with NIH Public Law 99-158, November 20, 1985, "Animals in Research," revised in 2015.

5.2.4 Targeting and Biodistribution of NPs

After 28 days of adenine diet feeding, six rats were injected with elastin antibody conjugated and DiR-loaded NPs via the tail vein. 24 hours later, the rats were euthanized and organs harvested for further analysis. Serum was collected for biochemical analysis using a standard autoanalyzer. The entire body and individual organs were imaged using a Caliper IVIS Lumina XR (Hopkinton, MA) with Ex/Em of 745/795 nm to calculate percentage fluorescence and targeting NPs to the site of injury in the aorta. Percentage Fluorescence was then calculated using the equation:

$$\%Fluorescence = \left(\frac{\frac{fluorescence\ in\ tissue}{total\ fluorescence\ in\ all\ organs}}{The\ dry\ weight\ of\ tissue} \right) * 100\%$$

5.2.5 Treatment with EDTA nanoparticles and intravenous EDTA solution

For the treatment study, rats were fed adenine diets for 28 days and divided into five groups randomly (n=6 per group). The first group of rats received tail vein injections of PBS to act as a no-treatment control (Saline-IV). The second group of rats received tail vein injections of blank BSA NPs without EDTA but conjugated with anti-elastin antibody suspended in PBS as controls (Blank-NPs). The third group of rats was given intravenous injections of EDTA solution (EDTA-IV) in PBS twice a week for two weeks at a dosage of 3mg/kg body weight. The fourth group received tail vein injections of NPs loaded with EDTA and conjugated with anti-elastin antibody suspended in PBS twice a week for two weeks (EDTA-NPs). The last group received EDTA-NPs and was allowed to survive for four weeks after treatment (EDTA-NPs-LT). Animals were euthanized by exsanguination while under isoflurane, aortas (from the arch to the iliac bifurcation) were collected as a unit and fixed in 10% neutral buffered formalin. Other organs including kidneys, hearts, liver, spleen, and lungs were also harvested. Serum was collected from animals of all the groups for biochemical analysis. The complete schematic of the present study is elucidated in Figure 4-1.

5.2.6 Whole-mount aorta alizarin red S staining

The whole aortic tree from ascending aorta to iliac bifurcation was carefully cleaned of adherent tissues and soaked in freshly made 2% alizarin red solution (pH 4.1-4.3) for 10 minutes and washed with DI water for ten more minutes. The aortas were then imaged by the stereomicroscope (Leica M125 stereo microscope, Leica Microsystems Inc. Buffalo Grove, IL).

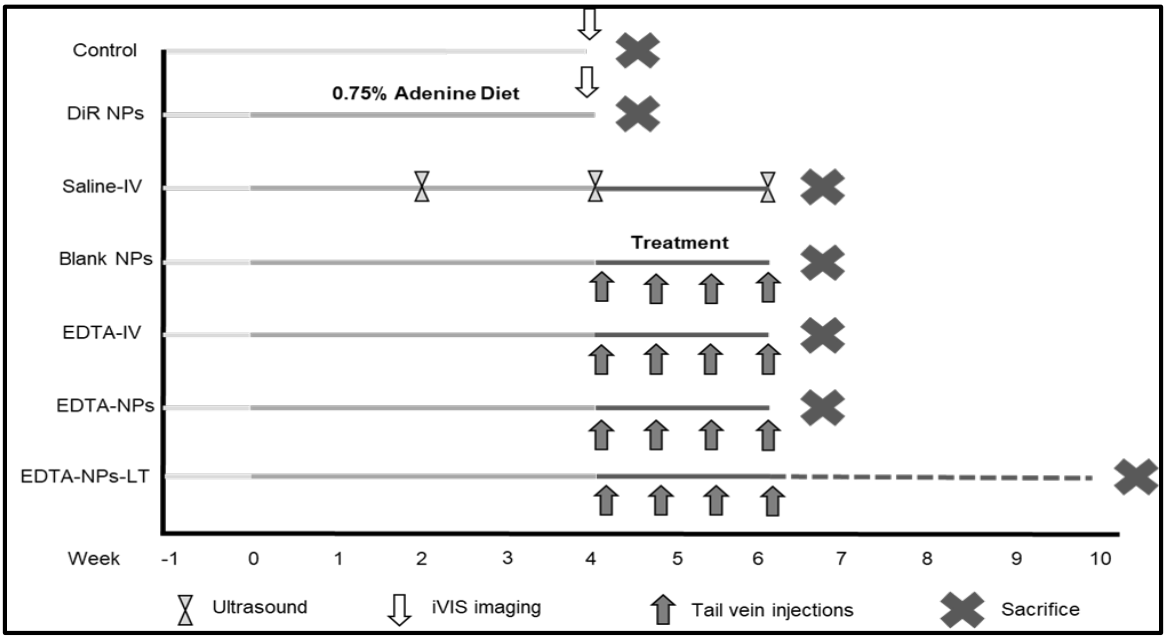

Figure 5-1: Schematic representation of Specific Aim 1 study design.

5.2.7 Histology of aorta and kidneys

Aortas and kidneys were fixed in buffered formalin, embedded in paraffin and sectioned per standard procedures. Five-micrometer sections were mounted on positively charged glass slides. Slides were baked overnight at 56°C in an oven to adhere tissues to the slides and melt the paraffin. Subsequently, the slides were deparaffinized with xylenes followed by dehydration with graded ethanol. Aorta slides were stained with hematoxylin and eosin for overall tissue morphology, Verhoeff-van Gieson (VVG) for elastin fibers and Von Kossa stain with neutral fast red counterstain for calcium deposits. Kidney slides were stained with hematoxylin and eosin for morphology, Periodic acid-Schiff stain (PAS) for polysaccharides and mucosubstances, and with trichrome for muscle and collagen.

5.2.8 Immunohistochemical analysis of the aorta

Aortas fixed in formalin were embedded in paraffin and sectioned as described earlier. Subsequently, xylenes and graded ethanol were used to deparaffinize the sections, and heat-induced antigen epitope retrieval was performed using citrate buffer (Thermo Scientific, MA). The slides were then incubated overnight at 4°C with primary antibodies — Mouse anti-Rat Alpha Smooth Muscle Actin (Biolegend, San Diego, CA), Rabbit anti-Rat Caspase-3 (Cell Signaling Technology, Danvers, MA), Rabbit anti-Rat MMP-2 and Rabbit anti-Rat MMP-9 (Enzo Life Sciences, NY). Staining with relevant secondary antibodies was completed using IHC kit (Enzo Life Sciences, NY). Slides were visualized by either 3,3′-Diaminobenzidine (DAB) or 3-Amino-9-ethylcarbazole (AEC) chromogens followed by an appropriate counterstain.

5.2.9 Quantification of aortic calcium

Calcium content in the aortas was measured after lyophilizing the part of the tissue at renal bifurcation that showed some alizarin red S stain in the whole mount. The lyophilized tissue was hydrolyzed in 6N HCl at 95°C and dried under a continuous stream of nitrogen for about 45 minutes. The residue was subsequently reconstituted in 0.01N HCl, and samples were analyzed using the Spectro Acros ICP Spectrometer (SPECTRO Analytical Instruments, Kleve, Germany) at Clemson University Agricultural Service Laboratory.

5.2.10 Ultrasound analysis of the aorta

A high-frequency ultrasound machine (Vevo2100, VisualSonics, Toronto, Canada) was used to image and monitor the aortas of the rats at different time intervals by utilizing

a linear array probe (MS 400D, frequency 18-38MHz). While being imaged, the animals were given light anesthesia by inhalation of 2% isoflurane and were placed in the supine position on the imaging table. Aortic stiffness parameters circumferential strain and pulse wave velocity (PWV) were calculated from the M-Mode and EKV images obtained with the scans, respectively.

Circumferential Green-LaGrange strain was calculated with the assumption that the strain is uniform around the vessel using the equation given below

$$Circumferential\ Strain = \frac{1}{2}\left(\left(\frac{Dsystolic}{Ddiastolic}\right)^2 - 1\right) * 100$$

5.2.11 Bone integrity as evaluated by micro CT scanning

Femoral bones harvested from the rats were wrapped with parafilm to prevent drying and scanned using a high performance *in vivo* micro CT scanner (Skyscan 1176, Bruker BioSpin, Billerica, MA). Reconstruction was carried out employing a Feldkamp algorithm using the built-in Skyscan Nrecon software. Functional mechanical testing of bone was performed on the rat femurs using a Bose test instrument (Electroforce 3200, Bose, MN, USA) and exposing them to escalating forces until fracture. At fracture, maximum load (N) was determined.

5.2.12 Statistics

All the results, including graphs in the figures, are given as mean±S.D. Statistical analysis was performed using a one-way analysis of variance (ANOVA). Results were considered to be significant when p-values ≤0.05. Tukey's HSD was then used post-hoc to identify the treatment groups with a significant difference.

5.3 Results

5.3.1 Nanoparticle preparation and characterization

EDTA-loaded NPs were prepared based on the procedure described previously our laboratory. They were then characterized by TEM and particle size analyzer for size and surface zeta potential. NPs had a final average size of 254.42±31.8nm; Zeta potential of the NPs was measured as -24.42±4.49mv. The average yield of NPs after centrifugation was 53.18±1.50%. EDTA loading into the NPs was 25.88±0.172% (Figure 5-2 A). EDTA was released from these particles over a period of 72 hours (Figure 5-2 B).

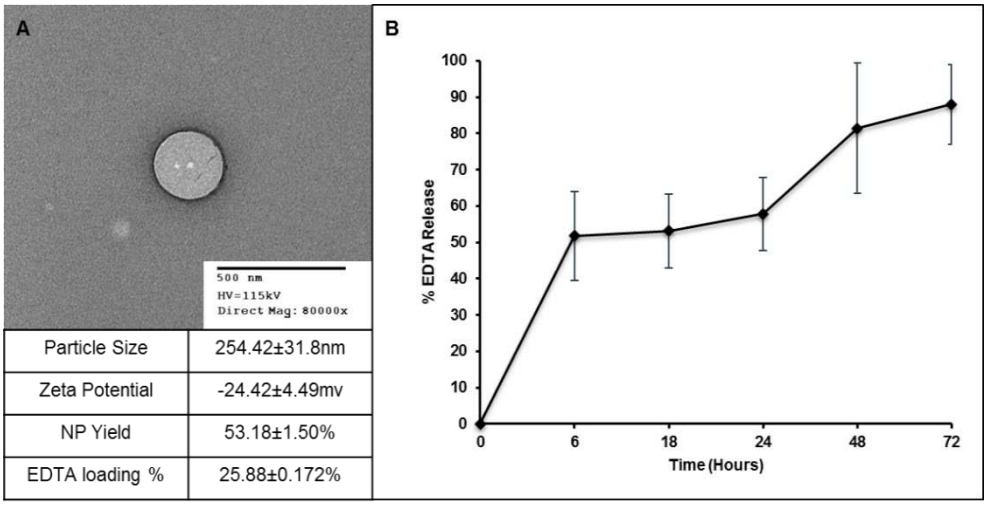

Particle Size	254.42±31.8nm
Zeta Potential	-24.42±4.49mv
NP Yield	53.18±1.50%
EDTA loading %	25.88±0.172%

Figure 5-2: EDTA NPs characterization and release kinetics. (A) TEM Imaging for NP particle size. Table below the TEM shows average particle size, surface zeta potential, average final yield of NPs and drug loading percentage. (B) *In vitro* EDTA release from NPs.

5.3.2 Adenine-induced renal failure model

Rats were fed adenine diets containing higher phosphate and calcium for 28 days to induce renal failure and vascular calcification. Body weights measured during the experiment indicated that the adenine diet-fed rats lost weight, possibly due to malnutrition and starvation (Figure 5-3). Modulating the adenine diet feeding, as explained in the methods section, enabled us to eliminate possible mortality in this model. All the animals survived until the end of the study, at which time they were electively euthanized.

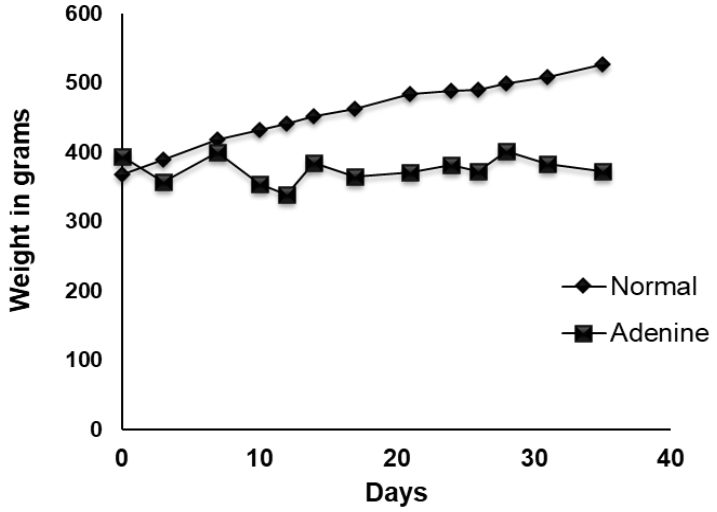

Figure 5-3: Body weights of rats monitored during adenine-diet feeding.

5.3.3 Morphology of kidneys and serum biochemistry

Harvested kidneys from the adenine-fed rats showed extensive morphological damage with crystal deposition in comparison to a standard diet-fed kidney (Figure 5-4 A). Histology of kidneys from adenine-fed rats revealed increased infiltration of inflammatory cells and fibrosis. Structural changes were severe and predominant in these rats validated by increased vacuolation of tubules, tubular atrophy, and an increased number of tubules with cell debris (Figure 5-4 B). Induction of CKD was further evidenced by higher serum creatinine and blood urea nitrogen (BUN) concentrations in the adenine-fed rats compared to normal animals. Furthermore, these animals also exhibited high serum phosphate and uric acid concentrations (Table 5-1).

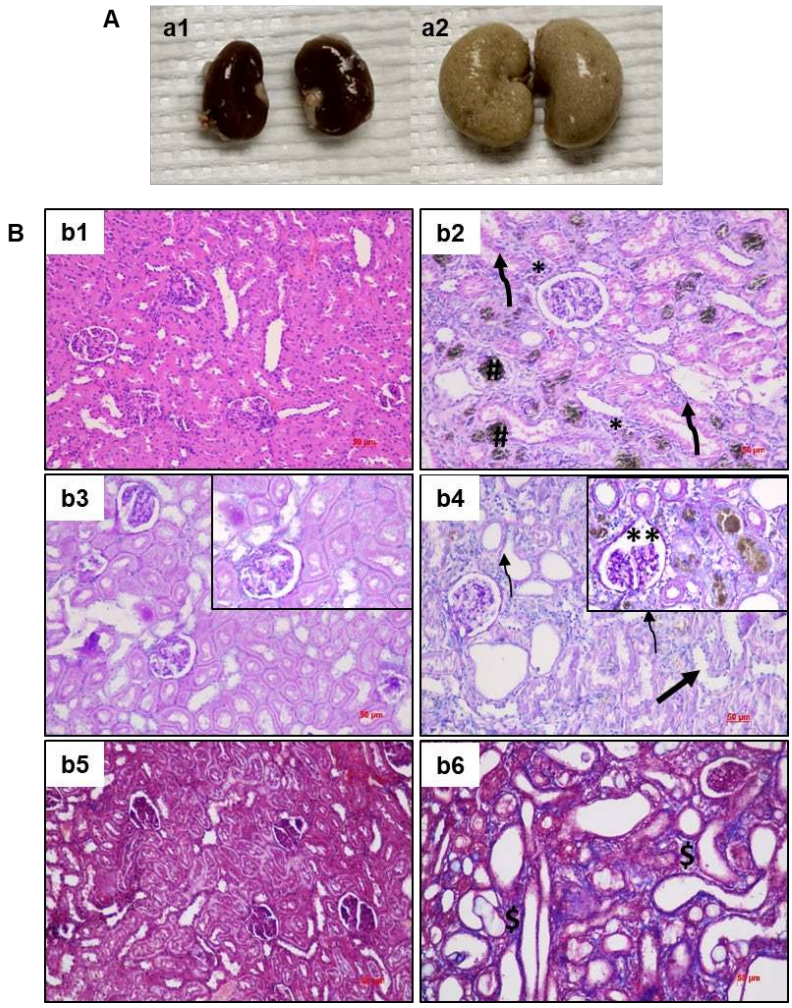

Figure 5-4: Morphology and histology of rat kidneys. (A) Gross morphological images of normal diet- and adenine diet-fed kidneys. (B) Histological staining of kidneys in normal- and adenine diet-fed kidneys – H&E (b1-b2), Periodic acid-Schiff (b3-b4), and Masson's trichrome (b5-b6).

Table 5-1: Serum biochemistry of adenine-fed rats (n=6 per group)

	Normal diet	Adenine diet
Serum Creatinine (mg/dL)	0.25±0.11	2.79±1.30*
Serum Phosphate (mg/dL)	7.58±0.25	11.42±4.34*
Serum Calcium (mg/dL)	10.00±0.29	10.27±0.42
BUN (mg/dL)	15.50±1.50	53.34±10.09*
Uric Acid (mmol/L)	0.73±0.12	1.44±0.15*
GFR	>60	15.34±4.11

* represents statistical significance (Student's unpaired t-test, $p < 0.05$)

5.3.4 Organ distribution of NPs and targeting to damaged aorta

Elastin antibody conjugated and DiR dye loaded NPs were injected through the tail vein of the rats after 28 days of feeding adenine. The NPs targeted the calcified and degraded aortic elastic lamina sites within 24 hours while sparing the healthy regions of the aorta in 4 out of 6 rats injected with DiR-NPs, which correlated with elastin damage. Animals that were fed normal diets did not show any targeting of the NPs to the aorta (Figure 5-5 A). The percentage fluorescence intensity normalized to the tissue weight for various organs showed 69.16±14.27% targeting of NPs to the calcification sites (Figure 5-5 B). Representative histological sections of the aortas showed that there was indeed degraded elastic lamina in the medial layers of the aorta as shown by VVG staining (Figure 5-6 a1-b1) and calcification of the damaged/degraded elastic lamina as shown by von

Kossa staining (Figure 5-6 a2-b2). NPs loaded with DiR dye were infiltrating the calcification site through adventitia in the adenine fed rats and reached the medial calcification sites (Figure 5-6 a3-b3).

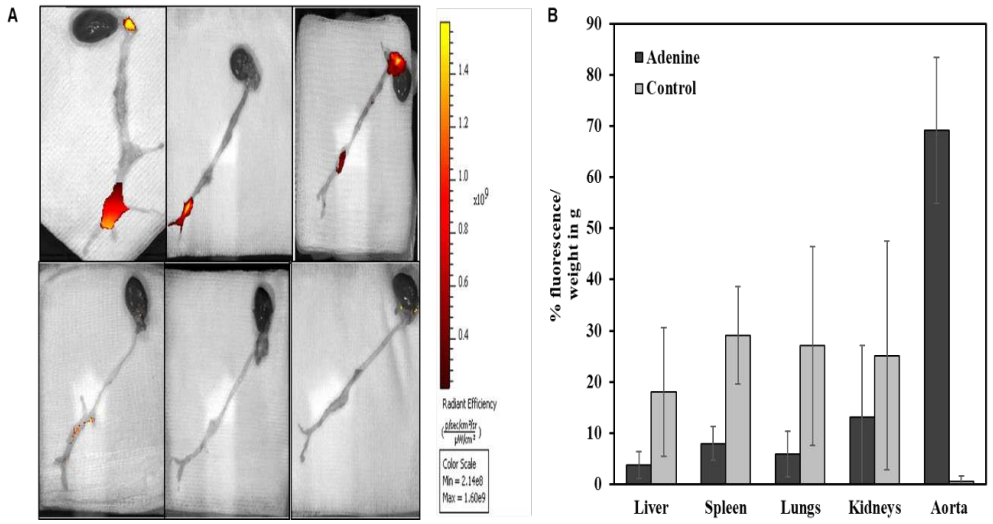

Figure 5-5: Nanoparticle targeting to diseased rat aortas (n=6). (A) NP accumulation in aorta following systemic IV injection of EL-DIR-NPs. (B) Organ distribution of NPs as measured by fluorescence intensity on iVIS imaging system.

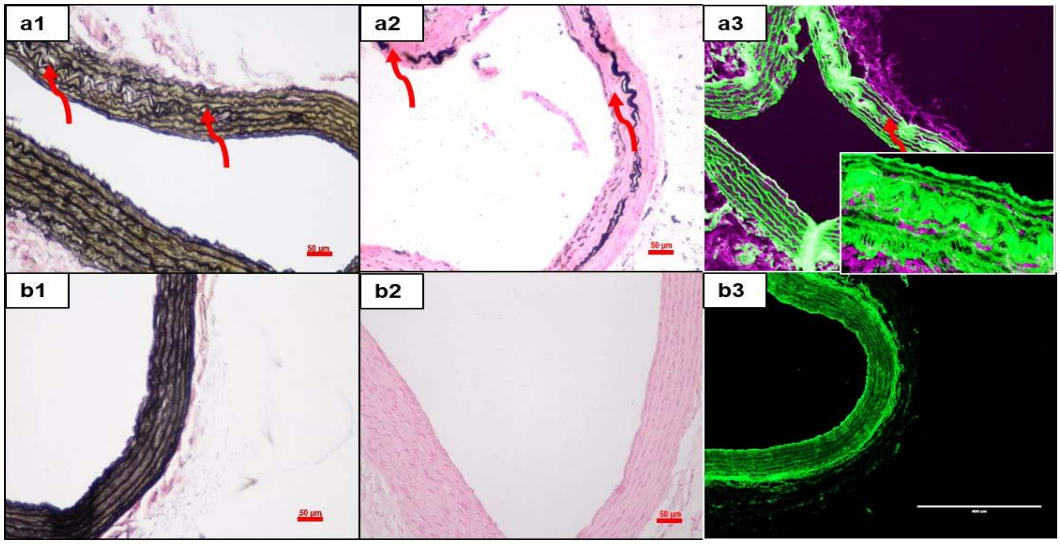

Figure 5-6: Histology of the aortas in adenine diet- and control diet- fed rats (n=6 per group).

5.3.5 Targeted EDTA Chelation Therapy leads to reversal of calcification

Quantitative calcium content of the aortic tissues showed the highest calcium content (13.47±3.5 μg/mg of the aorta) in intravenous saline (Saline-IV) group. There was a slight decrease in systemic intravenous EDTA (EDTA-IV) group (9.82±3.3% μg/mg), but the decrease was not statistically significant. EDTA-loaded targeted NPs (EDTA-NPs) group showed the least calcium content (6.4±3.2% μg/mg). This was significantly different from the Saline-IV group, which was further reduced in EDTA-NPs-LT group suggesting that removal of calcification continued even after NP therapy was halted (Figure 5-7). Aortic calcification evaluated by stereomicroscopic images of alizarin red-stained whole aortas corroborated the quantitative calcium results. Rats treated with EDTA-NPs and EDTA-NPs-LT showed significant elimination of the calcific spots, suggesting a reversal of mineral deposition (Figure 5-8 A: a4, a5). Representative histology of the aortas stained with von Kossa stain showed pronounced calcification of the medial layer in the Saline-IV and Blank-NP groups (Figure 5-8 B: b1, b2). This was to some extent reduced in aortas treated with EDTA-IV (Figure 5-8 B: b3), but it was completely absent in EDTA NPs and EDTA-NPs-LT groups, clearly suggesting that EDTA-removed calcium deposits and calcification did not return even after EDTA treatment was stopped for four weeks (Figure 5-8 B: b4, b5).

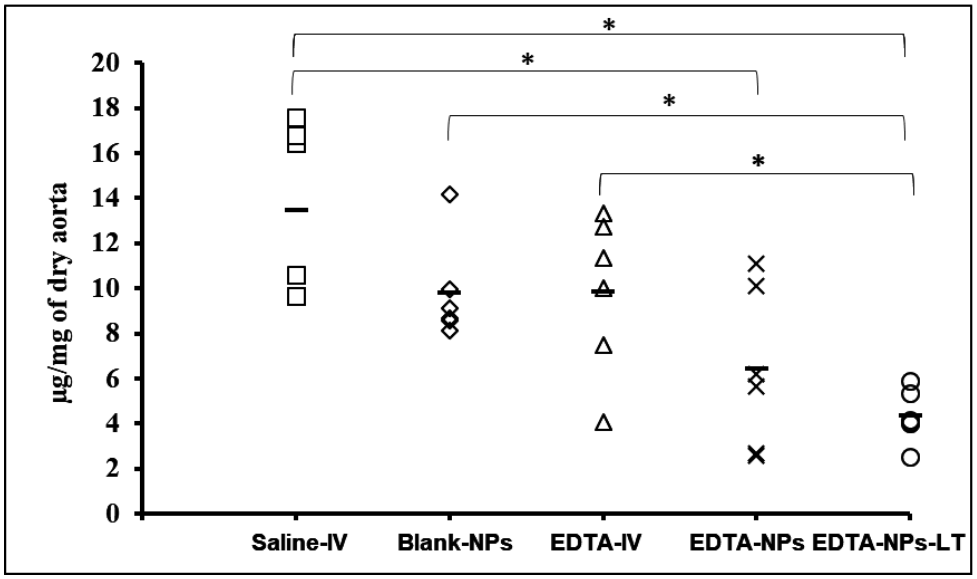

Figure 5-7: Quantification of calcium in the aorta of all the treatment groups. (n=6). (*, $p<0.05$, One –way ANOVA with Tukey's HSD). Solid line represents mean value.

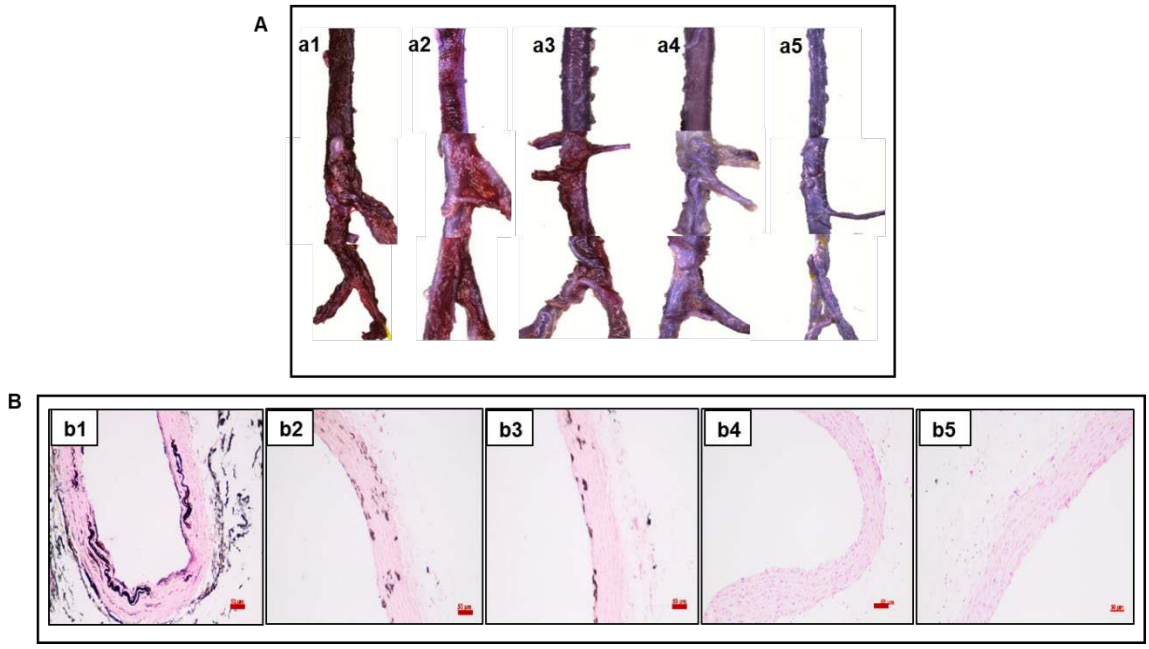

Figure 5-8: Histological staining of aorta for calcification in all the treatment groups. (A) Whole mount aortas stained with alizarin red S to visualize calcium. (B) Cross-sections of aortas stained with von Kossa stain for Ca deposits.

5.3.6 Serum biochemistry following EDTA nanoparticle treatment

Serum biochemistry measurements following chelation therapy show reduced creatinine and P levels in all the groups, including the Saline-IV and Blank-NP groups. This may be due to the adenine diet being discontinued during therapy. BUN, Uric Acid, however, remained high in all the groups. No morphological of histopathological differences were seen in kidneys from all the treatment groups compared to kidneys from adenine-fed rats before the treatment (Table 4-2).

Table 4-2: Serum biochemistry following chelation therapy. (n=6 per group).

	Saline-IV	**Blank-NPs**	**EDTA-IV**	**EDTA-NPs**	**EDTA-NPs-LT**
Serum Creatinine	0.53±0.10	0.70±0.23	0.63±1.1	0.73±0.26	0.46±0.00
Serum Phosphate	8.46±0.54	8.66±0.46	8.62±0.48	7.95±0.88	8.10±0.50
Serum Calcium	10.167±0.24	10.333±0.359	10.15±0.3	10.30±0.30	10.36±0.23
BUN	30.167±3.1	31.66±7.63	36.50±5.85	46.16±14.53	25.80±5.11
Uric Acid	1.62±0.18	1.58±0.34	1.42±0.21	1.317±0.2	1.26±0.1

5.3.7 Immunohistochemical analyses of the aorta for SMC phenotype and MMPs

Staining for alpha-smooth muscle actin indicated the loss of SMCs in the Saline-IV group due to calcification compared to a normal diet-fed control rat (Figure 5-9 A: a1, a2). SMC staining increased significantly in the EDTA-NPs and EDTA-NPs-LT groups, indicating that the removal calcification allowed restoration of SMC phenotype in the medial layer (Figure 5-9 A: a3, a4). To explore if the loss of VSMCs was because of apoptosis, Caspase-3 staining with 3,3′-Diaminobenzidine chromogen was performed. Caspase-3 marker was not detectable in a normal diet-fed rat, and it increased around the calcific sites in Saline-IV group (Figure 5-9 B: b1, b2). Apoptotic activity was considerably reduced in EDTA NPs and EDTA-NPs-LT groups, clearly suggesting that apoptotic cells were replaced by healthy cells (Figure 5-9 B: b3, b4).

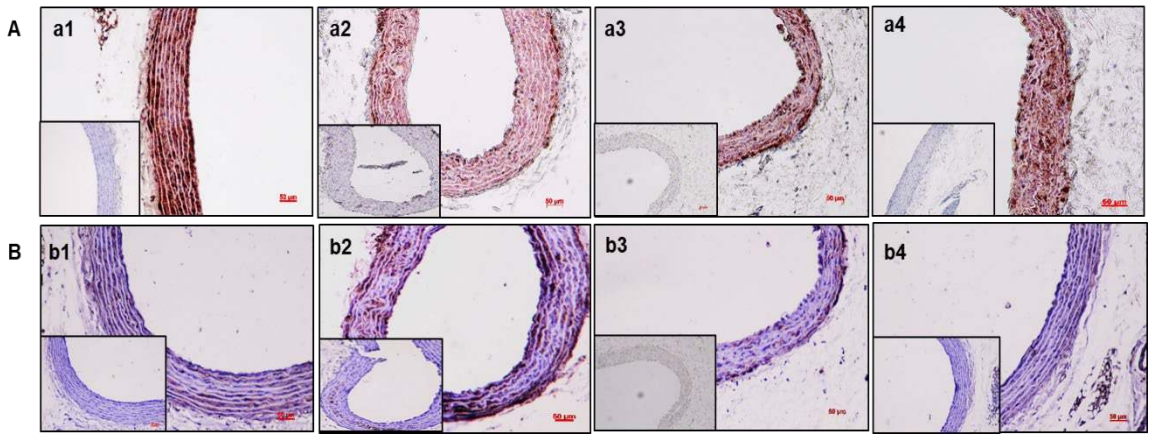

Figure 5-9: Immunohistochemical staining of the aortas for VSMC status in the treatment groups. (A) Representative images of IHC staining for anti-alpha smooth muscle actin. (B) IHC staining for caspase-3 showing apoptotic activity. (Insets in each image show respective secondary antibody controls).

Anti MMP-2 staining showed that MMP-2 activity was present in the calcified regions of the aorta in Saline-IV with no detectable MMP activity in a normal diet-fed rat (Figure 5-10 A: a1, a2). Treatment with EDTA-NPs slightly reduced MMP-2 activity, while EDTA-NPs-LT group showed the absence of MMP-2 staining in the medial layers (Figure 5-10 A: a3, a4). Staining for MMP-9 also was present in the calcified regions of the medial layers of the adenine diet-fed rat aortas in Saline-IV and absent in a normal rat aorta (Figure 5-10 B: b1, b2). MMP-9 activity was significantly reduced in both the EDTA NP treatment groups –EDTA-NPs and EDTA-NPs-LT (Figure 5-10 B: b1, b2).

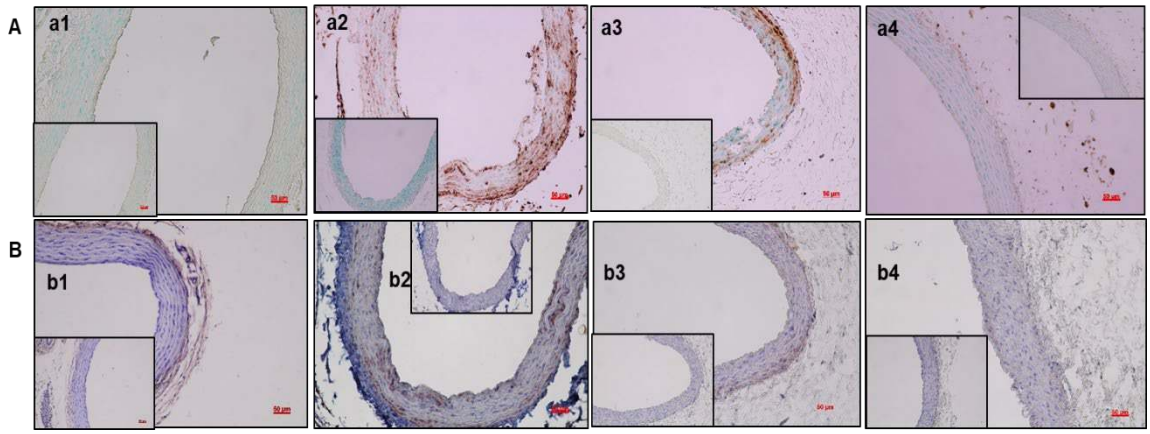

Figure 5-10: Immunohistochemical staining of the aortas for matrix metalloproteinases (MMPs) in the treatment groups. (A) Representative images of IHC staining for MMP-2. (B) IHC staining for MMP-9. (Insets in each image show respective secondary antibody controls).

5.3.8 *In vivo* ultrasound imaging

Ultrasound images of abdominal aortas were obtained during adenine diet feeding and after therapy. Healthy aortas from standard chow-fed rats showed thin and elastic aortas. In rats fed with the adenine diet, substantial calcification was seen in the medial layer of the abdominal aorta (Figure 5-11 A: a1, a2). Among the treatment groups, calcification was observed to be noticeably reduced only in the EDTA-NPs group; the Saline-IV, Blank-NPs and EDTA-IV groups all showed the persistence of calcification (Figure 5-11 A: a3 – a6). Circumferential strains of the healthy aortas, as calculated from the Green-LaGrange strain equation, were 11.99±1.043% (n=6). Strains in the rats fed with adenine diet for 28 days showed decreased circumferential strains, suggesting stiffening of the artery due to aortic mineralization. Saline-IV, Blank-NPs, and EDTA-IV groups did not reduce calcification; thus, aortic stiffness remained unimproved. Only EDTA-NPs group showed a statistically significant improvement in circumferential strain (9.22±1.05%) compared to the rest of the groups, suggesting that removal of the mineral content led to more elastic aortas (Figure 5-11 B).

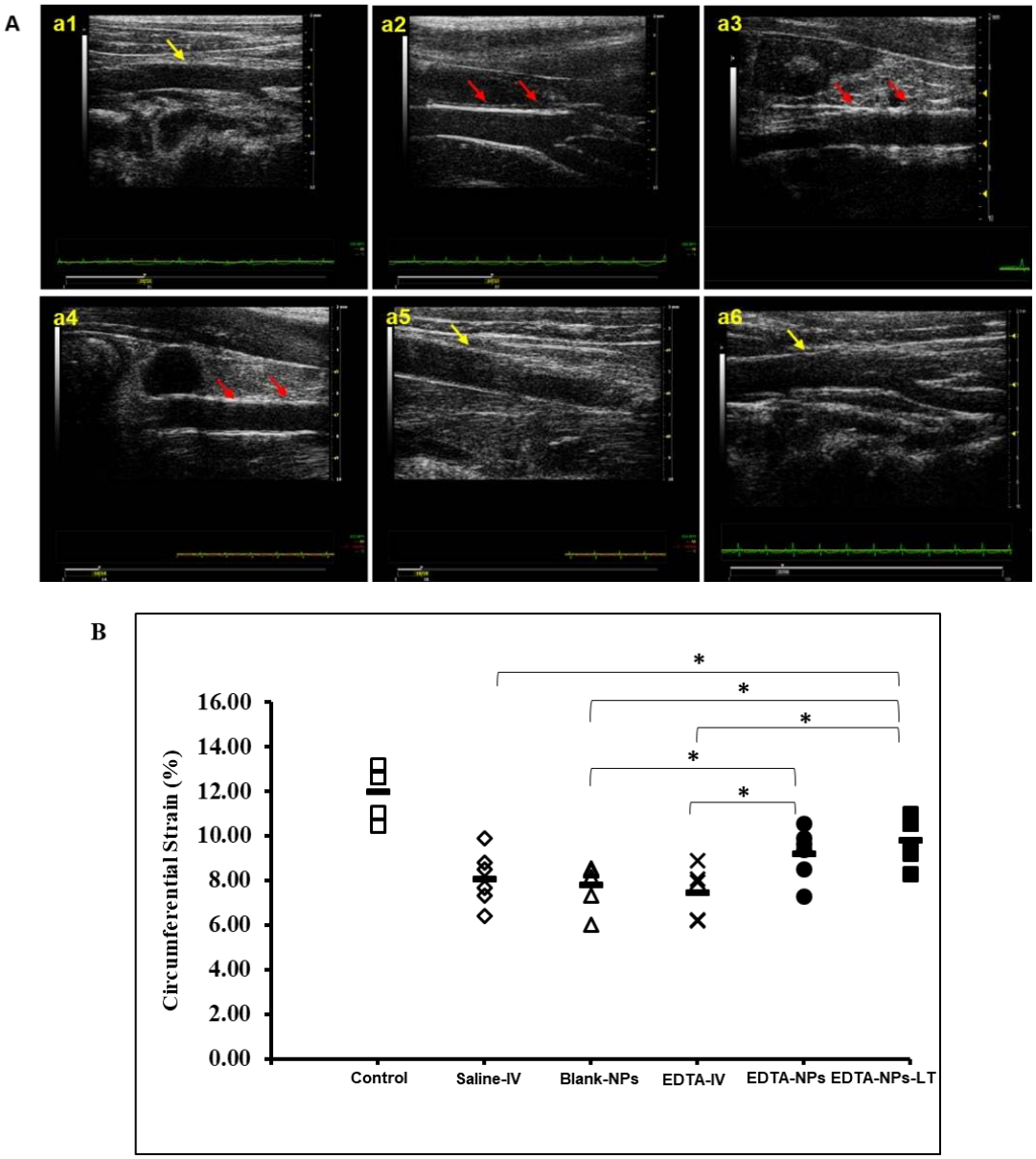

Figure 5-11: *In vivo* ultrasound imaging of the rat aortas. (A) Representative 2D B-mode images from control and all treatment groups. (B) Circumferential strain, as calculated from Green-LaGrange equation using M-Mode images. (n=6). (*, $p<0.05$, One –way ANOVA with Tukey's HSD). Solid line represents mean value

5.3.9 Bone morphology and functional testing

Representative 2D-image from micro CT scans of the femurs about 10 mm below the trochanter revealed reduced mineralization in all the groups. EDTA-NPs group did not show any additional reduction in mineralization compared to any other group fed with adenine diet, indicating that EDTA NPs did not cause structural damage to the bone (Figure 5-12 a). Functional studies on bone stability indicated that the maximum load needed to fracture the femurs did not differ significantly among the four treatment groups. This confirmed that bone stability was not affected by EDTA-NPs treatment (Figure 5-12 b).

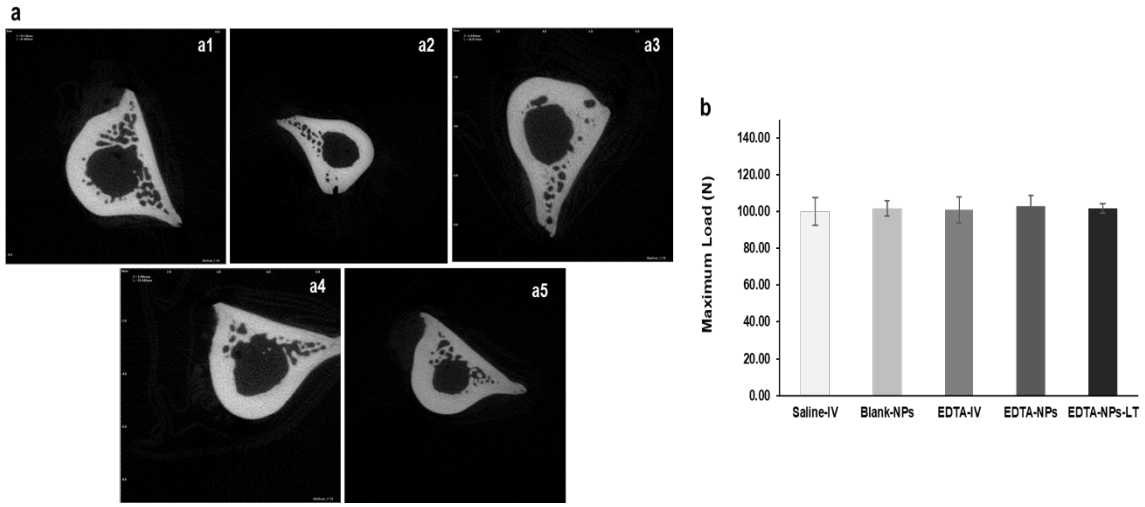

Figure 5-12: Morphology and functional testing of rat femurs from all the treatment groups. (a) Representative two-dimensional slices from microcomputed tomography of rat femurs from the different treatment groups. (b) Maximum load before breaking for femoral bone in the treatment groups.

5.4 Discussion

In this aim, our goal was to test whether elastin-specific MAC could be reversed by targeted EDTA chelation therapy in a clinically relevant model of CKD. To our knowledge, we, for the first time demonstrated that targeted nanoparticles injected systemically could target the calcified arteries and remove calcification in a CKD model in rats despite altered blood biochemistry.

Over the last few years, several research groups have made use of the adenine model for studying mechanisms of MAC in CKD [157, 175, 178, 260-262]. We were able to successfully induce CKD in rats fed with 0.75% adenine supplemented by high concentrations of Ca and P. Along with the expected structural damage to kidneys, biochemical abnormalities like elevated serum creatinine, serum phosphate, and higher levels of the BUN were seen. This closely resembled CRF in humans, making the model useful for the study of our targeted chelation therapy.

Several research groups have reported that one of the chief limitations of the adenine model is that a small dose of adenine (0.2%) causes inconsistent calcification, and a high dose (0.75%) causes excessive mortality [176, 260]. In our studies, carefully controlled 0.75% adenine-feeding led to medial vascular calcification without undue mortality. Albumin NPs conjugated with elastin-antibody, which recognizes only damaged elastin in the vasculature, were used to deliver EDTA to the calcification sites in animals fed adenine diets. Fluorescence intensity of DiR dye-loaded animals showed accumulation of NPs at calcification sites. The healthy regions of the aorta in these animals and the entire aorta in the rats fed rat chow diets were spared, demonstrating that NPs targeted only

degraded elastin. In previous studies, we showed that nanoparticles conjugated with generic IgG antibody do not target damaged elastin site [245, 246, 248, 259], suggesting that our elastin antibody conjugation led to site specificity. NPs also accumulated in liver and spleen, possibly because they are taken up by Kupffer cells in the liver and due to reticuloendothelial clearance [263]. This is very common for many nanoparticle therapies [264, 265]. Moreover, we observed that the NPs entered the media from the adventitial side through the vasa vasorum [245, 246]. Such adventitial delivery is advantageous: Often, intraluminal thrombus or atherosclerosis can hinder particles targeted from the lumen side.

Having established targeting efficiency of NPs to the calcified sites, we proceed to test reversal of calcification by delivering EDTA-loaded NPs. We prepared albumin nanoparticles loaded with EDTA following an established procedure [259]. Previously, we showed that such nanoparticles release EDTA slowly over a period of 72 hours. Our previous studies also showed, both *in vitro and in vivo,* that when EDTA was delivered in proximity to calcific deposits, EDTA removed the calcification [258, 259]. In this study, we chose to inject NPs twice a week for two weeks based on the release profile for EDTA. We included systemic EDTA injections as controls, at a dosage similar to the chelating agent released from our nanoparticles. After the two weeks of injections, we observed that the EDTA-loaded NPs reversed calcium deposits in the rat arteries, as confirmed by *in vivo* ultrasound, whole-mount aorta alizarin red stain, histology with von Kossa stain, and quantitative calcium levels. When EDTA alone was injected systemically, calcification was reversed only slightly; therefore, multiple injections or a higher concentration of EDTA will be required to achieve reversal. That can lead to systemic side effects as shown

previously with systemic EDTA therapy[179, 266, 267]. As expected, when the rats were injected with saline only and blank NPs as controls, the calcium deposits were not removed, and aortas remained calcified and stiff. We checked the status of kidneys in all animals at the end of the therapy by measuring blood biochemistry (Table 4-2). As the adenine diet was not continued during the two-week therapy, we did find reduced creatinine and P levels in all groups (including Saline-IV and Blank-NP groups) while BUN, uric acid remained high. This showed that EDTA therapy did not affect kidney function. Stopping the adenine diet might have improved kidney function in all groups, but once vascular calcification developed, it did not regress as can be seen in saline and Blank-NP groups. We saw a significant reduction in vascular calcification only after targeted therapy.

Elevated MMPs have been reported to have a strong correlation with elastic fiber degradation, stiffness, and calcification. Particularly, MMP-2 and MMP-9 up-regulation have been associated with arterial stiffening in diabetic patients with CKD [268]. Immunohistochemical staining for MMP-2 and MMP-9 showed that both were indeed present in the calcified regions of the aorta in adenine-fed rats. This suggests that MMP-2 and MMP-9 may be involved in elastin degradation and eventually causing elastin calcification in the adenine model. We showed that MMP-9 and MMP-9 knockout mice did not show vascular calcification in a $CaCl_2$ injury model [131]. Significant reduction in both MMP-2 and MMP-9 after removal of calcification suggests that the inflammatory cascade is reversed after removal of calcification. It may be that locally delivered EDTA chelated Zn^{2+} ions required for MMP activity and inhibited MMPs as shown earlier by others[269, 270], but this needs to be studied in detail.

We also evaluated cellular status in the aorta after adenine diet-induced calcification and after the therapy. Others showed that after adenine diet, SMCs lost phenotype and underwent apoptosis, and those apoptotic bodies aggravated calcification [94, 271]. In the *in vivo* studies described here, we saw the loss of SMC phenotype and increased apoptosis in cells close to medial calcification. Surprisingly, we found that after removal of calcification, there was an increase in SMC-type staining in the medial layers of the aorta. Further cell tracing studies are necessary to investigate if the higher SMCs seen after -treatment we due to dedifferentiation or repopulation by recruitment of HSCs, pericytes, or by EMT.

High-frequency ultrasound imaging helped us study changes to the aorta *in vivo.* It was shown that a reduced circumferential strain is an indicator of aortic stiffness[272]. Circumferential strains measured from M-mode images in healthy aortas were as reported in the literature. We observed that circumferential strain is reduced after adenine-diet feeding; this indicated increased aortic stiffness caused by calcification. EDTA NPs treatment removed calcium deposits and improved the circumferential strain levels, aortic elasticity, and health.

One important observation was that MMP activity and calcification did not return even after EDTA therapy was suspended for four weeks (EDTA-NP-LT group) although that CKD was present in the animals. EDTA targeted therapy did not cause any undue side effects in bone and mineral metabolism and biomechanics. Micro CT scanning to study bone morphology showed reduced mineralization in all groups. This was expected, as uremia is associated with reduced bone mineral density [179]. EDTA NPs group showed

no additional reduction in mineral density when compared to the Saline-IV and the Blank-NPs group. We showed earlier that polyphenols such as PGG, when delivered with nanoparticles, do regenerate degraded aortic elastin [247]. Thus, there is an exciting opportunity of dual nanoparticle therapy to first remove calcium deposits using EDTA and then restore medial elastin layers with PGG.

In conclusion, we demonstrated that targeted delivery of minimal doses of EDTA is an effective way to reverse calcification in an experimental rat model of CKD. This establishes the enormous potential for targeted EDTA chelation therapy as a viable clinical alternative to reverse vascular calcification in CKD patients.

6 SPECIFIC AIM 3

TO ESTABLISH AND VALIDATE ADENINE-INDUCED CKD MODEL OF MEDIAL ARTERIAL CALCIFICATION IN MICE BY MONITORING DISEASE PROGRESSION *IN VIVO* AND EXPLORING VSMC STATUS FOR POTENTIAL USE IN INVESTIGATING TARGETED EDTA CHELATION THERAPY AND EFFECT OF REVERSAL OF CALCIFICATION ON VASCULAR HOMEOSTASIS AND FUNCTION.

6.1 Introduction

In our studies with adenine model in rats, the animals were placed back on the standard diet during the course of chelation therapy after renal failure was established and calcified manifested. We do not know at this point if persistence of high circulating levels of Ca and P due to continuing adenine diet will result in return of calcification. There is a likelihood that the degraded elastin and calcium-binding sites will remain open after chelation and calcification may return in due course.

Moreover, our laboratory and several other research groups have shown that VSMCs begin to undergo osteogenic differentiation with transformation into osteoblast-like cells during the process of calcification [273, 274]. VSMC phenotypic alteration is accompanied by increased expression of proteins associated with bone such as Osteocalcin (OCN), Osteopontin (OPN), Runt-related transcription factor (RUNX-2), Bone morphogenic protein-2 (BMP-2) and increased Alkaline phosphatase (ALP) activity [79, 275, 276]. Increased levels of Ca and P levels, as seen in CKD patients, may accelerate mineral deposition and result in early calcification around elastin fibers [275]. More recently, we have shown that osteogenic transdifferentiation of VSMCs occurs when cultured on surfaces of HA and calcified elastin [273]. Remarkably, when cells were

removed from the calcific environment and returned to normal culture, they revert to their VSMC phenotype [274]. However, the feasibility of this phenotypic reversal of VSMCs, once the calcification is removed, *in vivo* remains unseen and open to investigation.

It would be intriguing to explore whether reversal of calcification through targeted EDTA chelation therapy can revert this expected phenotypic transformation of VSMCs *in vivo.* Our imminent goal is to investigate this phenomenon in an animal model of MAC caused by CKD. To test this hypothesis, extensive cell lineage tracing studies are needed to examine smooth muscle cell fate during calcification and after therapy. Mice present the possibility of genetic manipulation, thus offering avenues to inspect cellular and molecular mechanisms of disease progression and therapeutic effects in detail.

In the current aim, we sought to establish and validate the adenine-induced CKD model of MAC in mice in our laboratory for monitoring the progression of calcification *in vivo* and to explore VSMC status in calcified aortas. Our primary objective was to target our nanoparticle delivery system to diseased regions of calcified aortas in mice for potential delivery of chelating agent EDTA and therapeutics. We further studied global gene expression profiles of VSMCs to ascertain transdifferentiation into osteogenic phenotype. This model will provide a basis for investigating if targeted EDTA chelation therapy can restore VSMC cellular status and reinstate vascular homeostasis.

6.2 Materials and methods

6.2.1 Adenine-induced renal failure in mice

Six- to eight-week old mice with C57BL/6J genetic background (Jackson Laboratories) were housed in standard cages with wood chip bedding and paper roll for enrichment at ambient temperature (21-22°C) in a 12-hour light cycle. Mice were allowed to acclimatize to the conditions of the animal facility for a period of 7 days before the start of the experiment. For adenine-rich feeding, customized diets were purchased (Envigo Teklad, Madison, WI, USA). A 0.2% adenine diet was formulated to have similarities to the ones described in literature with 20% casein to make the diet more palatable for the mice, containing 0.9% P and 0.6% Ca. A high phosphate containing diet was also formulated with 20% casein, 0.6% Ca but with a 1.8% concentration of P. The mice were fed with the 0.2% adenine diet for a period of 4 weeks to induce CKD followed by 0.2% and high P diet for a further 4 weeks to produce arterial calcification (Ade+hP). The second group of mice was fed the 0.2% adenine and 0.9% P diet throughout the length of the study (Ade+nP). Animals were monitored regularly for expected loss of body weight and diets were intermittently switched to standard chow diet to allow weight recovery, resulting in zero unexpected mortality. Control group mice were fed standard chow diet throughout.

6.2.2 *In vivo* micro CT scan

A desktop *in vivo* X-ray micro-CT system (Skyscan 1172, Bruker Biospin) was used to obtain micro-CT images. With this system, both the X-ray source and the detector rotate around the animal. The mice were anesthetized with inhalation of isoflurane. A 0.2µ aluminum filter and a 90 kV tube voltage with an exposure time of 200ms were chosen as

the *in vivo* scanning parameters. Animals were placed on their back in the bed of scanner, and images were obtained at 18µm resolution with a rotational step of 0.7°. These settings allowed us to scan the axial length of the thorax in ~20 times of total exposure time. Transverse, Coronal, and Sagital virtual cross-sections were reconstructed by Feldkamp cone-beam algorithm using the in-built NRecon software. Finally, 3D models of reconstructed aortic scans were created by segmenting them out from other bodily tissues and fluids using a set of operations provided on the CTAn software.

6.2.3 Ultrasound imaging of aortas *in vivo*

Mice were scanned with a high-frequency ultrasound machine (Vevo2100, VisualSonics, Toronto, Canada) to image and monitor their aortas at regular time points during the study by utilizing a linear array probe (MS550D, frequency 22-55 MHz). Animals were placed in the supine position on the imaging table and anesthetized during scanning through inhalation of 2% isoflurane. Aortic stiffness parameters circumferential strain and pulse wave velocity (PWV) were calculated from the M-Mode and PW (Pulsed-wave) Doppler mode images obtained with the scans, respectively.

6.2.3.1 Measurement of aortic circumferential strain

Circumferential Green-LaGrange strain was calculated with the assumption that the strain is uniform around the vessel using the equation given below

$$Circumferential\ Strain = \frac{1}{2}\left(\left(\frac{Dsystolic}{Ddiastolic}\right)^2 - 1\right) * 100$$

6.2.3.2 Measurement of local pulse wave velocity (PWV)

Local PWV measurement made on a short segment of an artery can work as an early diagnostic tool to identify local stiffness of the arterial wall. PWV velocity at several short segments of the aorta was calculated indirectly using the parameters obtained from Color Doppler and PW Doppler mode images using the formula:

$$Pulse\ Wave\ Velocity\ (PWV) = \frac{D}{\Delta T}$$

where D is the distance between two points along the aorta traveled by the pulse wave and ΔT is the transit time or time delay between the two points. Time from the R wave on the ECG to the 'foot' of the Doppler waveform is calculated for the two points and the difference is recorded as transit time.

6.2.4 Targeting and Biodistribution of NPs

At the end of customized diet feeding in all the three groups, mice were injected with DiR-loaded and elastin antibody conjugated (ELN-DiR-NPs) via the tail vein. 24 hours later, the mice were euthanized, and organs harvested for further analysis. Serum was collected for biochemical analysis using a standard autoanalyzer. The entire body and individual organs were imaged using a Caliper IVIS Lumina XR (Hopkinton, MA) with Ex/Em of 745/795 nm to calculate percentage fluorescence and targeting NPs to the site of injury in the aorta. Percentage Fluorescence was then calculated using the equation:

$$\%Fluorescence = \left(\frac{\frac{fluorescence\ in\ tissue}{total\ fluorescence\ in\ all\ organs}}{The\ dry\ weight\ of\ tissue} \right) * 100\%$$

The overall design of the study is illustrated in Figure 6-1.

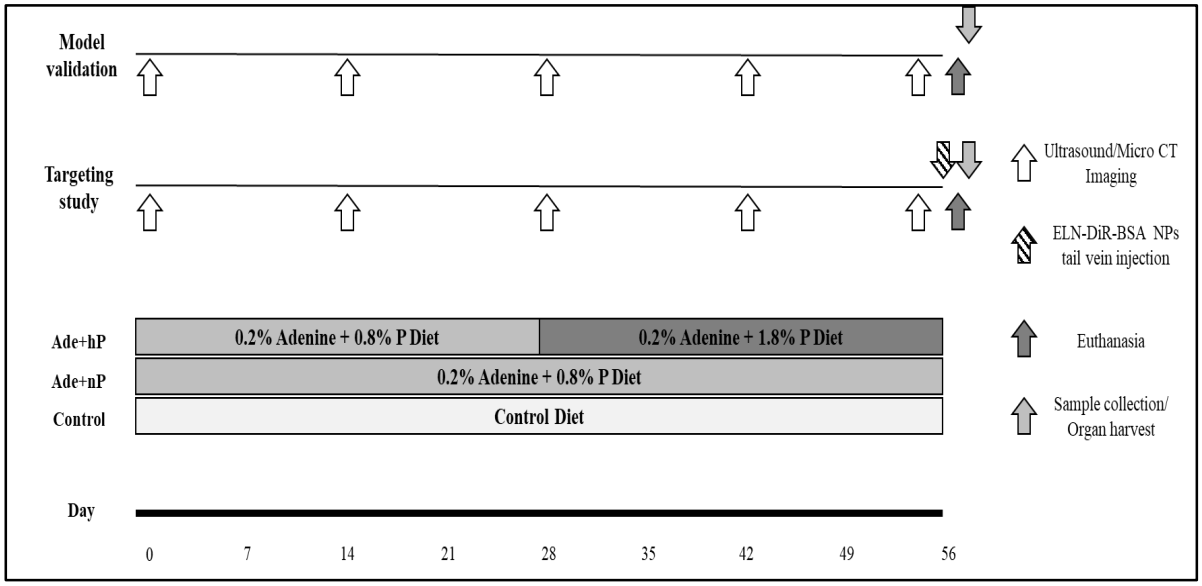

Figure 6-1: Schematic diagram of the adenine mice study. (n=6 per group per experiment).

6.2.5 Alizarin red staining of the whole mount aortas

Briefly, whole aortas were carefully cleaned of adherent tissues and soaked in freshly made 2% alizarin red solution (pH 4.1-4.3) for 10 minutes and washed with DI water for 10 more minutes. The aortas were then imaged by the stereomicroscope (Leica M125 stereo microscope, Leica Microsystems Inc. Buffalo Grove, IL). This will indicate regions of possible calcification on the aorta which are further analyzed as described next.

6.2.6 Histology of kidneys

Kidneys were fixed in buffered formalin, embedded in paraffin and sectioned according to standard procedures. They were then stained with Hematoxylin and Eosin for overall morphology, Periodic acid-Schiff stain (PAS) for polysaccharides and mucosubstances, Trichrome for muscle and collagen.

6.2.7 Histology of aorta cross-sections

Segments of aortas from regions where DiR fluorescence was seen on the iVIS system were embedded Tissue Tek OCT compound, and 5 μm sections were mounted on charged slides by cryosectioning. Slides were fixed in cold acetone, air-dried at room temperature and then used for staining. The following histological stains were used: Hematoxylin and eosin (H&E) for overall tissue morphology, Alizarin Red with Light Green SF yellowish counterstain to detect calcification, von Kossa stain with neutral fast red counterstain for calcium deposits and Verhoeff-van Gieson (VVG) stain for elastin fibers.

6.2.8 Quantification of aortic calcium

Calcium content in the aortas was measured after lyophilizing a section of the whole aorta. The lyophilized tissue was hydrolyzed in 6N HCl at 95°C and dried under a continuous stream of nitrogen for about 45 minutes. The residue was subsequently reconstituted in 0.01N HCl, and samples were analyzed using the Spectro Acros ICP Spectrometer (SPECTRO Analytical Instruments, Kleve, Germany) at Clemson University Agricultural Service Laboratory.

6.2.9 Immunohistochemistry for VSMC status

Briefly, OCT compound was washed off the tissue sections (5 μm), and they were placed in a water bath containing citrate buffer (10 mM Sodium Citrate, 0.05% Tween 20, pH 6.0) inside a pressure cooker to achieve heat-induced unmasking of antigens. Endogenous peroxidases were quenched with 3% hydrogen peroxide. Non-specific background was eliminated by treating the sections with Background Buster (Innovex) for 1hr at RT. Primary Antibodies against were applied overnight at 4°C against Alpha smooth muscle actin (ACTA2) (Novus Biologicals, Centennial, CO), Smooth Muscle Myosin Heavy Chain (SMMHC), Runt-related transcription factor (RUNX-2) (Santa Cruz Biotechnology, Inc., Dallas, TX), Bone morphogenic factor-2 (BMP-2), Osteopontin (OPN) (Rockland). Following primary antibody incubation, relevant secondary antibodies were applied and signal was enhanced by ABC method (Vector, Burlingame, CA). Slides were visualized by either 3,3′-Diaminobenzidine (DAB) or NovaRed peroxidase substrate chromogens (Vector, Burlingame, CA) followed by a light hematoxylin counterstaining prior to mounting.

6.2.10 Clariom S microarray analysis for differential gene expression

Total RNA (miRNAeasy Micro Kit, Qiagen) was prepared using aortas isolated from adenine+hP and control group mice. Purified RNA was labeled with the help of a GeneChip Wash and Stain Kit (Affymetrix, Santa Clara, CA), then hybridized to Clariom S Mouse Array (Affymetrix, Santa Clara, CA) according to manufacturer instructions. Data resulted in 22,206 detected probes that were used for subsequent analysis, and expression patterns are displayed as a heat map.

6.2.11 Statistics

All the results, including graphs in the figures, are given as mean±S.D. Statistical analysis was performed using a one-way analysis of variance (ANOVA). Results were considered to be significant when p-values ≤0.05. Tukey's HSD was then used post-hoc to identify the treatment groups with a significant difference.

6.3 Results

6.3.1 Body weights, serum biochemistry and histomorphology of kidneys

As a convention, mice fed the customized diets were monitored for loss of body weight caused due to starvation, daily quantities of water consumed and urine excreted. Mice fed the adenine containing diets lost weight at a steady rate (~20% over a period of 5 days) (Figure 6-2). To avoid death of animals due to starvation and weight loss [277, 278], we modulated the feeding to allow for intermittent weight recovery when they reach 20% weight loss before placing them back on the adenine diets. As with the rats, this allowed us to eliminate mortality caused in mice due to this mode. Mice fed adenine-diets also were observed to consume higher quantities of water and passed higher amounts of urine when compared to the control diet-fed mice [279, 280] (data reported by animal housing facility and not shown due to the requirement of metabolic cage usage). Biochemical analyses performed on sera extracted from these mice suggest that severe dysfunction of kidneys is induced in these mice with reported increases in Serum Creatinine (2-fold), Serum Phosphorus (1.5-fold) and Blood Urea Nitrogen (BUN) levels (2.5 fold). (Table 6-1).

In adenine-diet fed mice, discoloration and deformity of the kidneys were obvious after 28 days of adenine feeding compared to the control mice (Figure 6-3A). Renal histology in the adenine-diet fed mice shows deposition of crystalline structures in the tubular lumen and peritubular inflammatory cell infiltration alongside several dilated tubules (Figure 6-3 b1-b2). PAS staining showed dilated bowman's spaces in some glomeruli, tubular atrophy, and thickened basement membranes (Figure 6-3 b3-b4). Severe tubulointerstitial fibrosis can be seen with Masson's Trichrome stain (Figure 6-3 b5-b6).

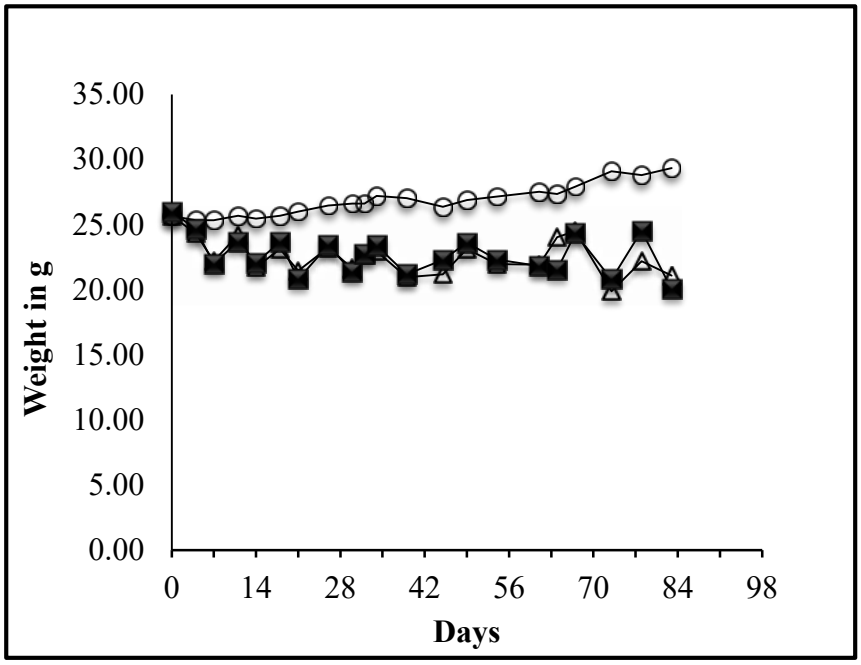

Figure 6-2: Body weights of the three groups of mice.

Table 6-1: Serum biochemistry for renal function parameters in adenine-fed mice.

	Control diet	Adenine diet
Serum Creatinine	<0.17	0.40±0.10*
Serum Phosphate	8.5±1.09	14.03±4.32*
Serum Calcium	9.02±0.19	8.42±1.68
BUN	19.6±3.2	49.43±12.74*
Glucose	198.2±27.01	141.83±56.19
GFR	>60	>60

* represents significant difference in adenine mice from control mice

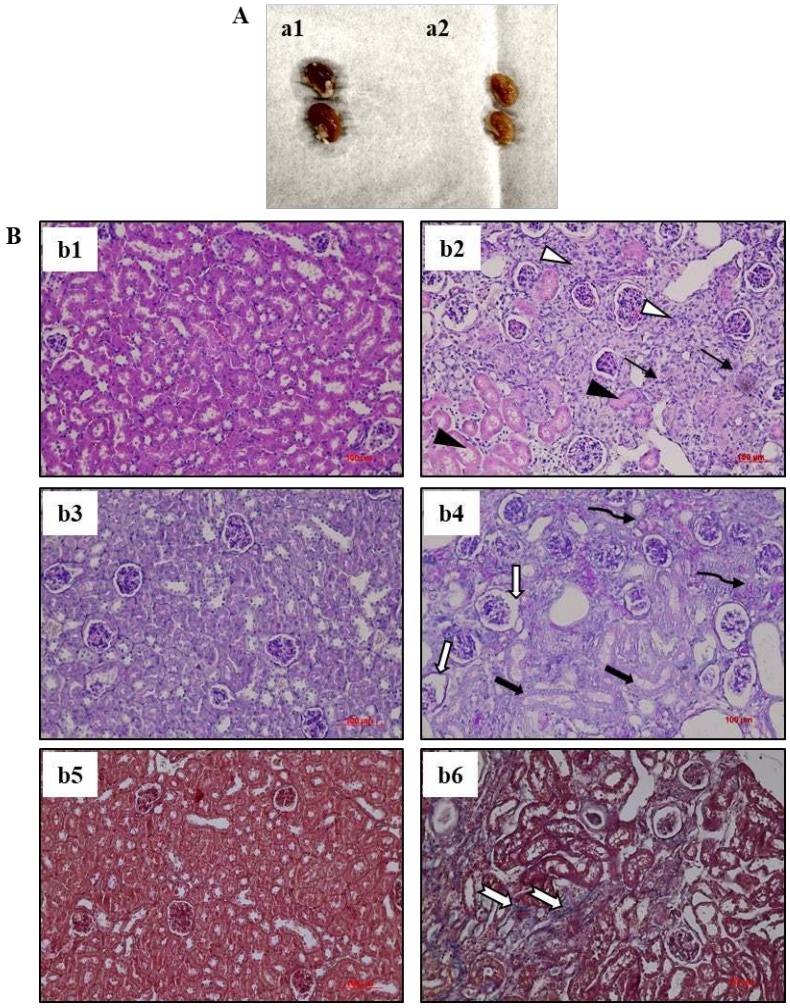

Figure 6-3: Morphology and histology of kidneys in mice. (A) Gross morphological images of normal diet- and adenine diet-fed kidneys. (B) Histological staining of kidneys in normal- and adenine diet-fed kidneys – H&E (b1-b2), Periodic acid-Schiff (b3-b4), and Masson's trichrome (b5-b6). (n=6 animals per group). *Scale bar = 100µm.*

6.3.2 *In vivo* Micro CT scanning for visualization of aortic calcification

Calcification of the aorta was evident on CT images of Ade+hP group mice. Three-dimensionally scanned and reconstructed images visually confirmed presence of calcification in the aorta, mainly in the infrarenal region (Figure 6-4 A1-A3). However, CT

imaging performed on the same group of mice at their 28-day time point did not show any tangible calcification (data not shown) while images from Ade+nP group mice were devoid of any aortic calcification throughout the duration of the feeding (Figure 6-4 B1-B3), thus confirming that 0.2% adenine feeding needs to be followed by 0.2% adenine + 1.8% P feeding as described in literature. Control group mice also did not present any calcification throughout the length of the study, as was expected (Figure 6-4 C1-C3). 3D models fabricated using the CTAn software allowed us to color and visualize aortic calcification in the Ade+hP group providing another *in vivo* assessment tool to track disease progression (Figure 6-5).

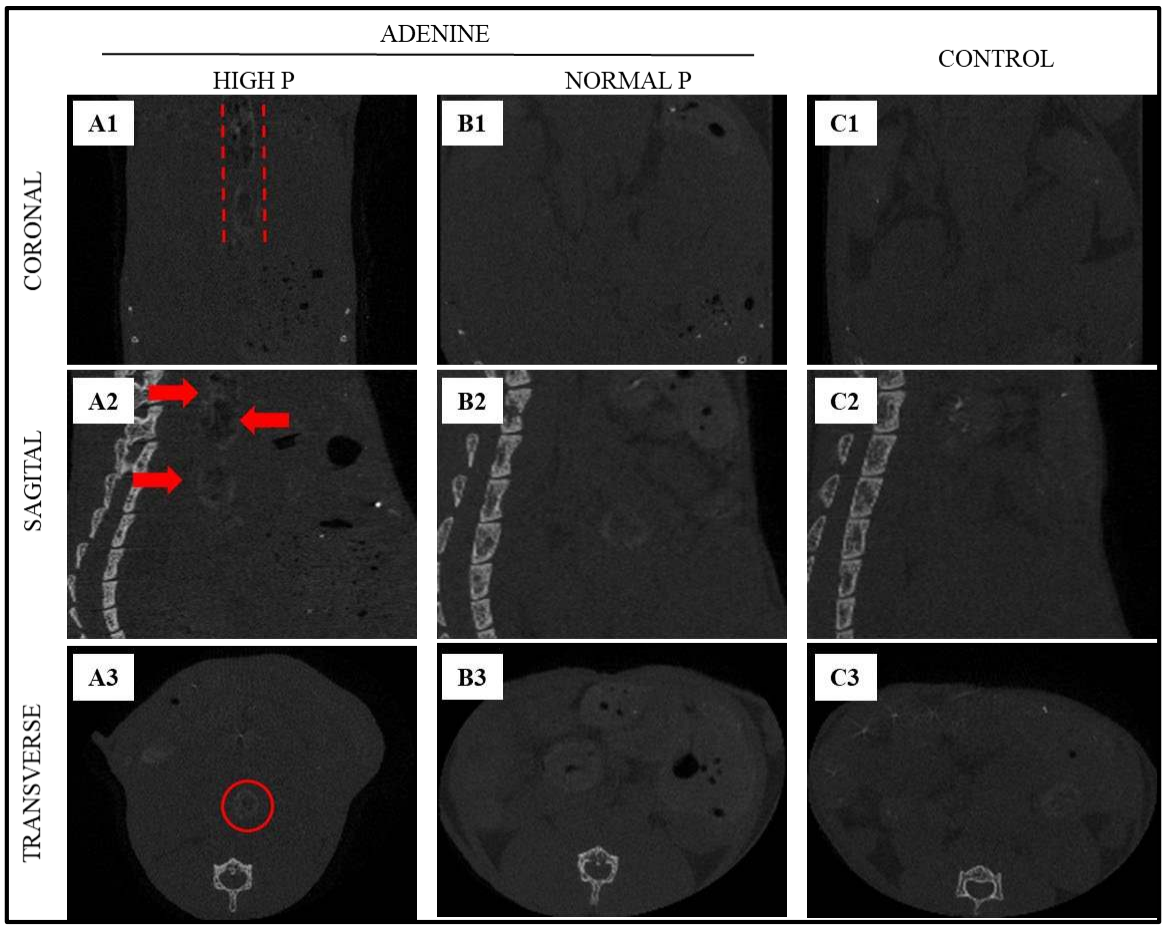

Figure 6-4: Representative images from *in vivo* 3D micro-computed tomography (Micro CT) scanning and reconstruction. Coronal, sagittal and traverse sections from all the three groups of mice are shown – Ade+hP (A1-A3), Ade+nP (B1-B3) and Control (C1-C3). Calcification visualized on the reconstructed scans of Ade+hP is illustrated by red dotted lines, arrows and circle in coronal, sagittal and transverse scan images respectively. (n=6 animals per group).

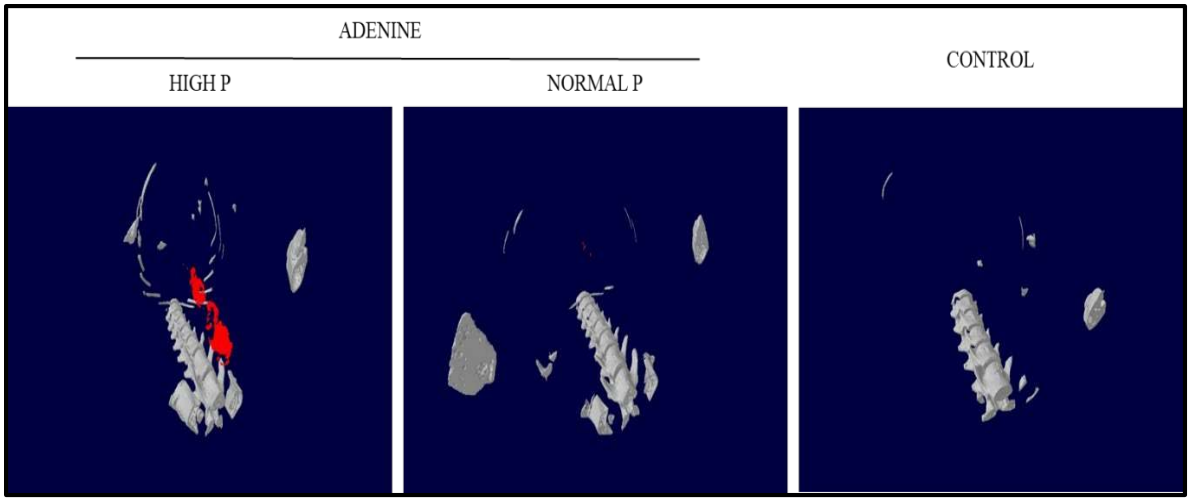

Figure 6-5: 3D modeling of reconstructed mouse abdominal micro CT scans. Bone tissue is pictured in white while possible aortic calcification in the Ade+hP group is colored in red. (n=6 animals per group). *Scale bar = 400µm.*

6.3.3 Ultrasound imaging to monitor aortic calcification

Local PWV values were calculated using the distance between the two points in a region of aorta divided by the transit time (Figure 6-6). Baseline PWVs in the three groups did not differ from each other as was expected. No significant differences were seen in the local PWVs at the 4 week feeding time point as well. However, following 4 weeks of high P diet feeding, PWVs in the Ade+hP group (2.41±0.53 ms^{-1}) were significantly higher than in the Ade+nP (1.77±0.21 ms^{-1}) and control groups (1.61±0.16 ms^{-1}) (Figure 6-7 A-B).

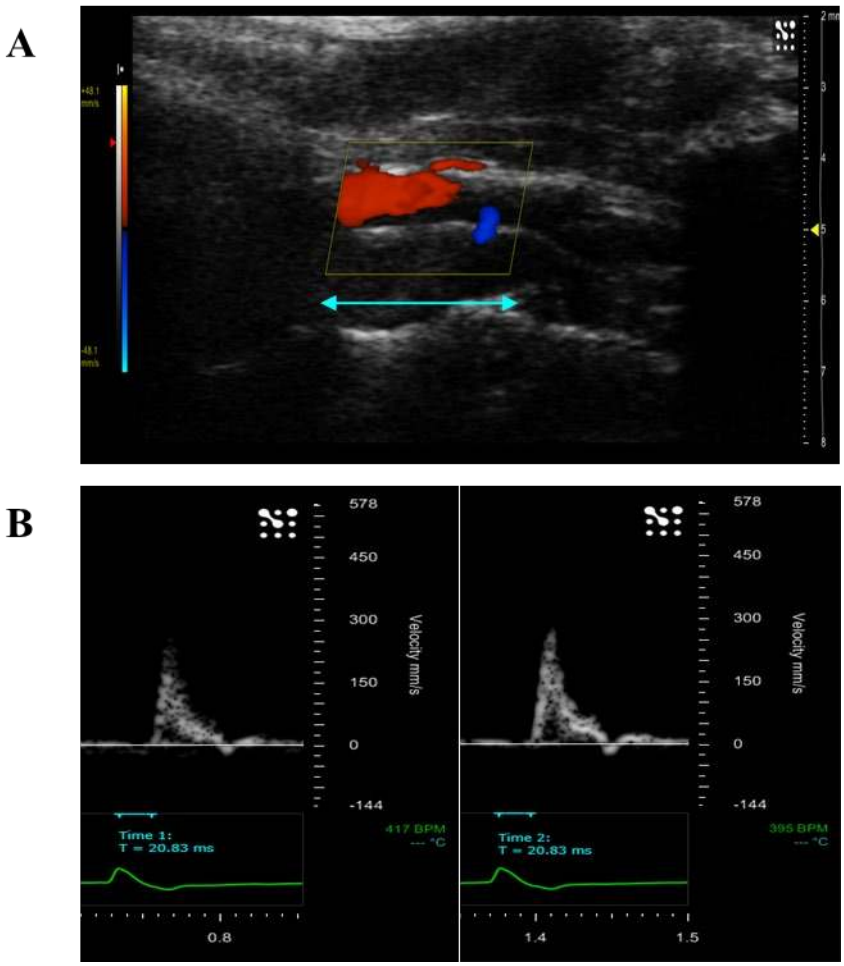

Figure 6–6: Local Pulse Wave Velocity (PWV) calculated as the distance traveled by the pulse wave over transit time. (A) Colored Doppler and (B) Pulse-wave Doppler images showing calculations of distance traveled and transit times respectively.

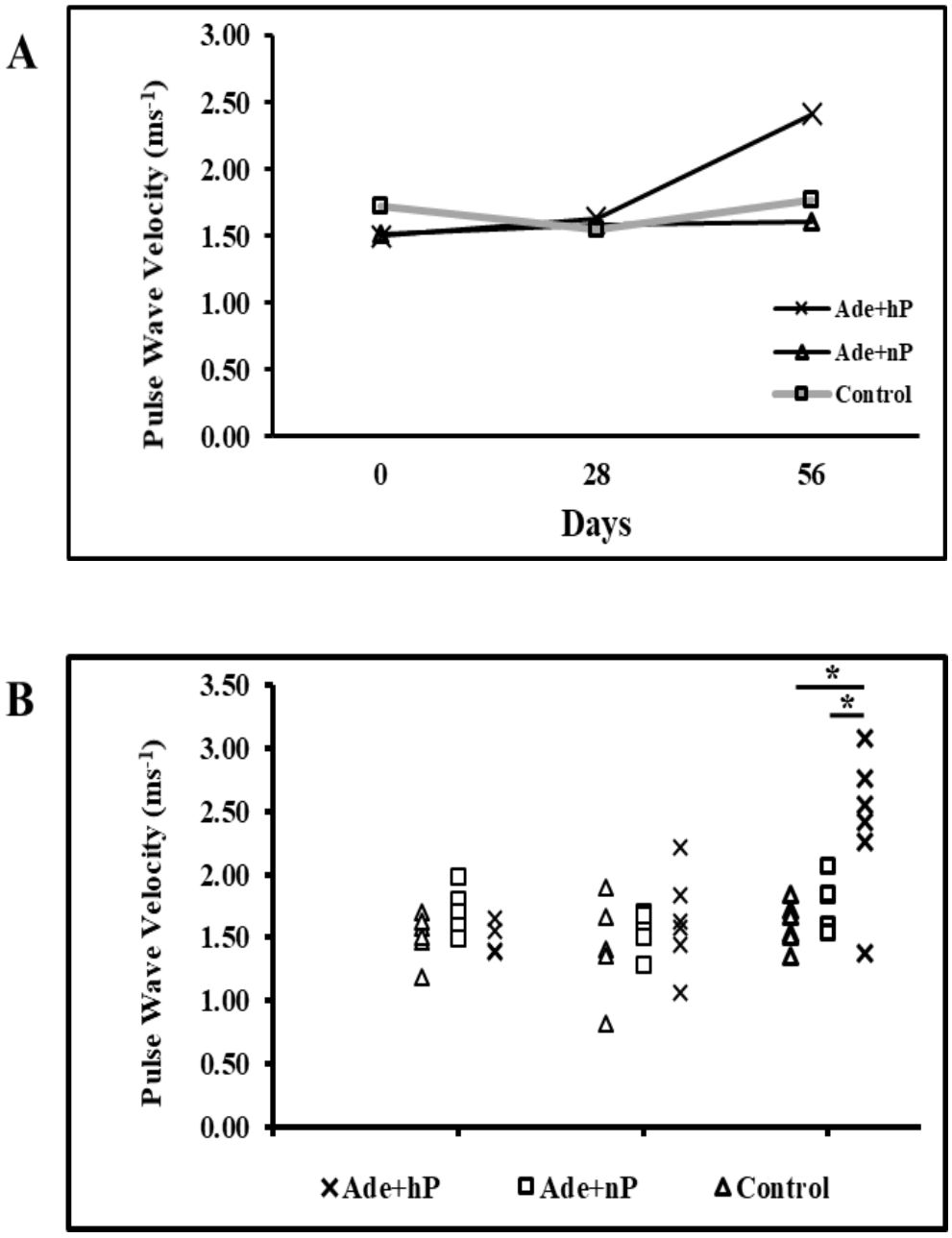

Figure 6-7: Local PWV in the abdominal aortas of the three groups of mice. (A) Mean Local PWV (ms^{-1}) of Ade+hP, Ade+nP and Control groups at 0, 28 and 56 days of feeding. (B) PWV (ms^{-1}) of all the mice from Ade+hP, Ade+Np, and Control groups at 0, 28, and 56day time points. (n=6 animals per group) (*, $p<0.05$, One –way ANOVA with Tukey's HSD).

6.3.4 Targeting of ELN-DiR-NPs to calcified regions of aortas

Elastin antibody conjugated and DiR dye loaded NPs (ELN-DiR-NPs) were injected through tail veins of mice at the end of customized diet feeding. The NPs targeted the calcified and degraded aortic elastic lamina sites within 24 hours while sparing the healthy regions of the aorta in 4 out of 6 mice in the Ade+hP fed group injected with ELN-DiR-NPs (Figure 6-8A a1), corresponding with the regions showing possible calcification in both the Micro CT and Ultrasound images. Mice that were fed Ade+nP and control diets did not show any targeting of the NPs to the aorta (Figure 6-8A a3, a5). Cross-sections of aortas from Ade+hP fed mice show positive signal for Cy7 fluorescence confirming that the ELN-DiR-NPs reached the calcified sites and targeted the degraded elastin fiber. No fluorescent signal could be detected in aortic cross-sections from the remaining groups of mice (Figure 6-8B).

6.3.5 Whole-mount aorta Alizarin Red staining

Images of whole mice aortas stained with alizarin red S and pictured on a stereomicroscope show bright red spots for calcium on the aortas from the Ade+hP diet group at the same regions where targeting was seen on the DiR fluorescence imaging (Figure 6-8A a2). This indicates that the elastin in these aortic regions was degraded and calcium was deposited, while the healthy regions did not show any staining for alizarin red. No such bright stain spots were seen in aortas from either the Ade+nP fed group of mice or control mice (Figure 6-8A a4, a6).

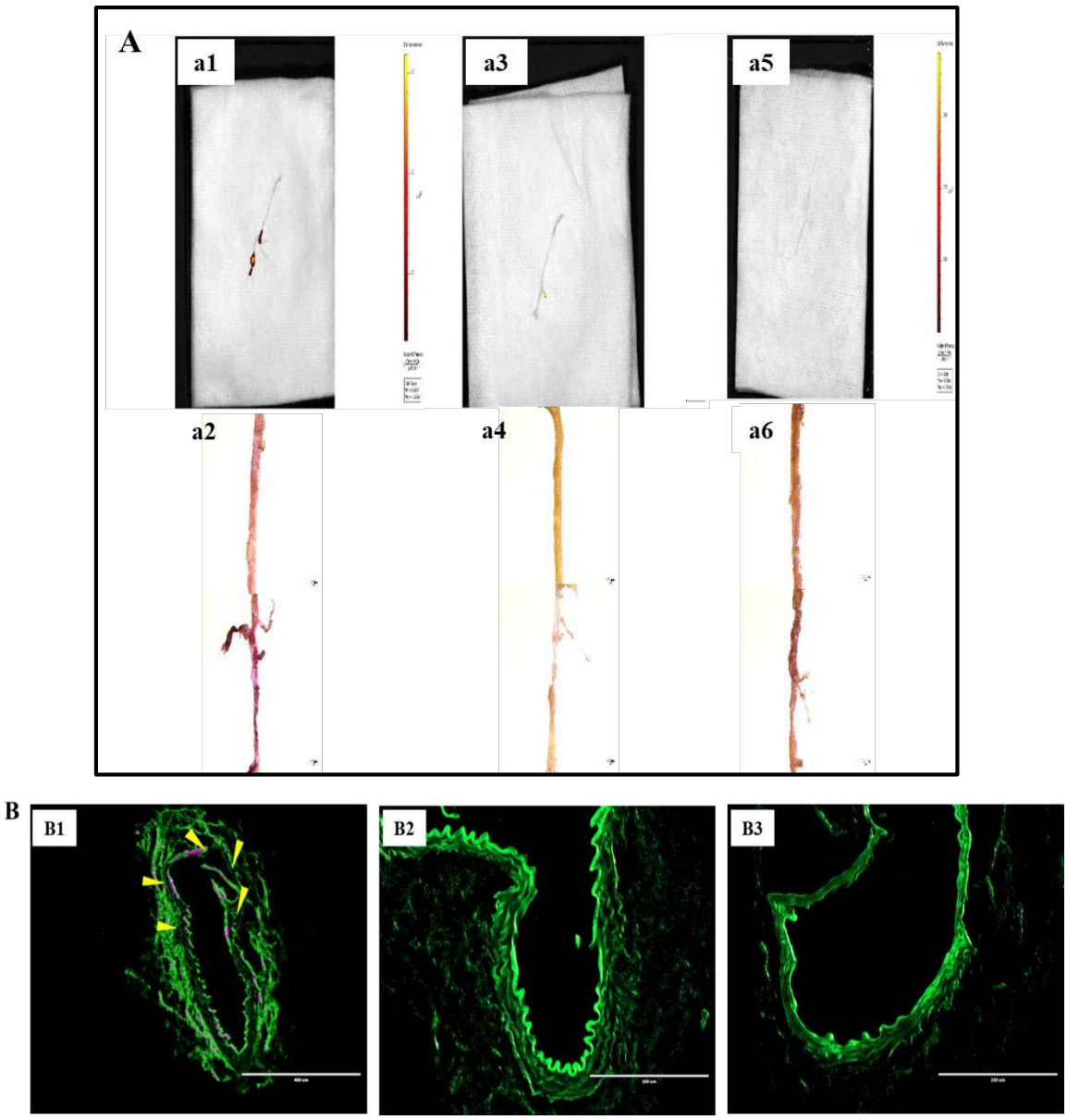

Figure 6-8: Targeting of ELN-DiR-NPs and accumulation around calcified sites of the aortas in Ade+hP mice. (A) DiR fluorescence as detected on iVIS Lumina imaging system and whole-mount aorta alizarin red staining to indicate calcification. (B) Cross-sections of aortas showing accumulation of ELN-DiR-NPs visualized by Cy7 fluorescence. (n=6 animals per group). *Scale bar = 400µm.*

6.3.6 Histological analysis of aortic cross-sections

Representative histological sections of the aortas showed the presence of calcification in the alizarin red-stained sections of Ade+hP fed mice (Figure 6-9 A). Black deposits of calcium were observed under von Kossa staining (Figure 6-9 D), and elastin fiber in the corresponding areas was damaged as shown by the VVG stain and Luna stain images (Figure 6–9 G, J). On the other hand, calcification was totally absent in the Ade+nP group (Figure 6-9 B, E, H, K) and control-diet fed mice aortic cross-sections. VVG and Luna stain images from these two groups of mice showed that the elastin fiber remained intact (Figure 6-9 C, F, I, L).

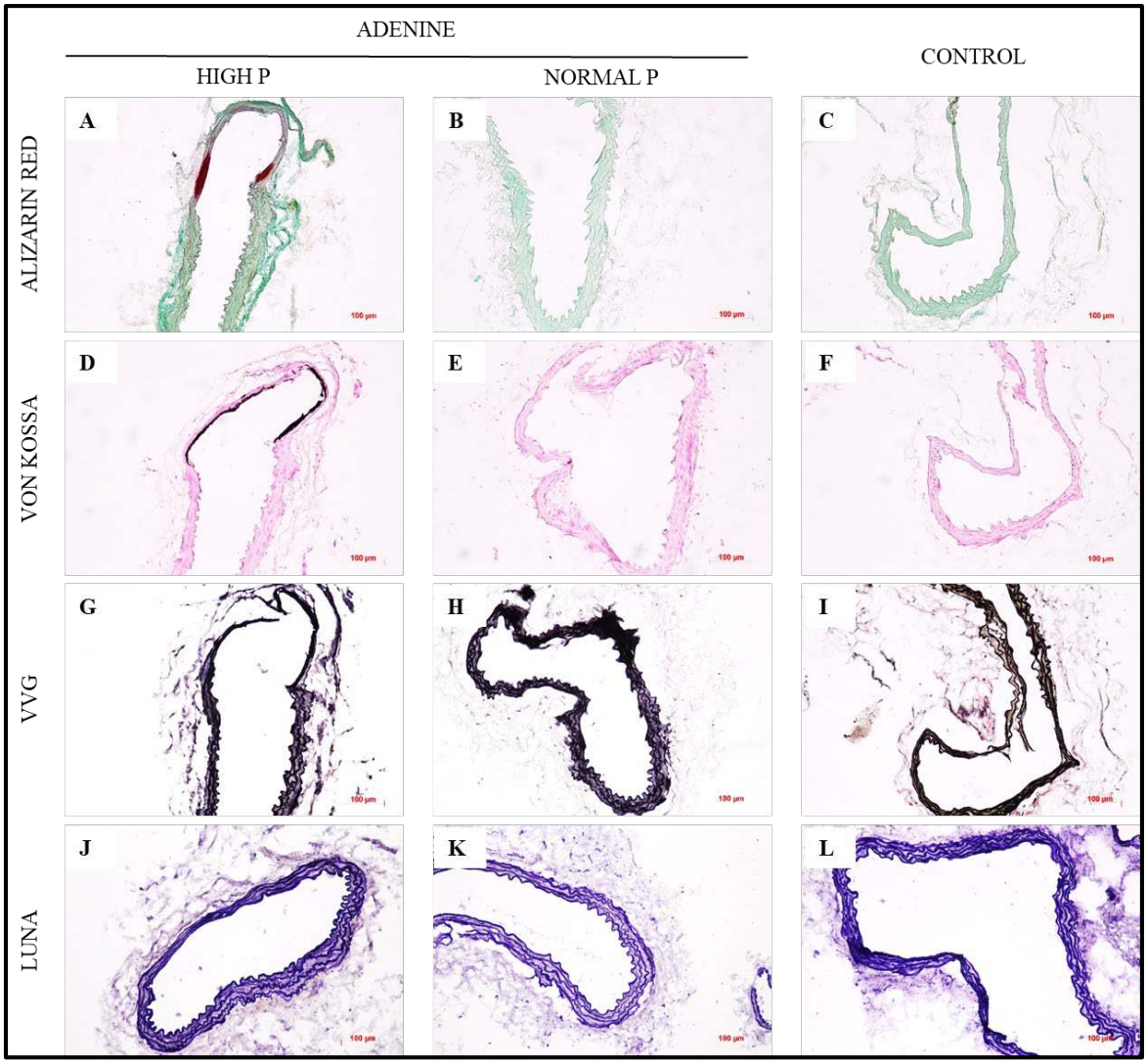

Figure 6-9: Representative histological images of aortic cross-sections from Ade+hP diet, Ade+nP diet and control diet-fed mice (n=6 per group). Alizarin Red S and von Kossa staining showing calcification and calcium deposition in the media layer of Ade+hP mice. Elastin fiber disruption and breakage as observed in VVG- and Luna- stained sections. (n=6 animals per group), *Scale bar = 100µm.*

6.3.7 Immunohistochemistry for VSMC-Osteogenic phenotypic switch

We performed immunohistochemistry to probe VSMC cell status after customized diet feeding. Comparisons were made between the three groups – Ade+hP, Ade+nP, and control – for expression of smooth muscle markers and osteogenic proteins. Staining for SMC Actin showed that its expression is more or less uniform across the three treatment groups, with somewhat lesser staining in Ade+hP and Ade+nP groups (Figure 6-10 A-C). IHC staining for another smooth muscle marker, Myosin heavy chain 11 (SMMHC) did not elicit any presence of the protein in both the adenine groups. However, its presence was detected in the control group (Figure 6-10 D-F).

In addition to smooth muscle markers, we wanted to observe possible expression of osteogenic markers in mice aortas. Specifically, we stained for RUNX-2 and BMP-2. RUNX-2 expression in greatest in Ade+hP group, while it was not detected in either the Ade+nP or control group (Figure 6-10 G-I). Similarly, the second osteogenic marker, BMP-2, was also clearly identified in the Ade+hP group. BMP-2 staining was completely absent in Ade+nP and control groups (Figure 6-10 J-L). Overall, IHC points towards the phenotypic transformation of VSMCs in mice aortas from the Ade+hP group, as is expected due to calcification.

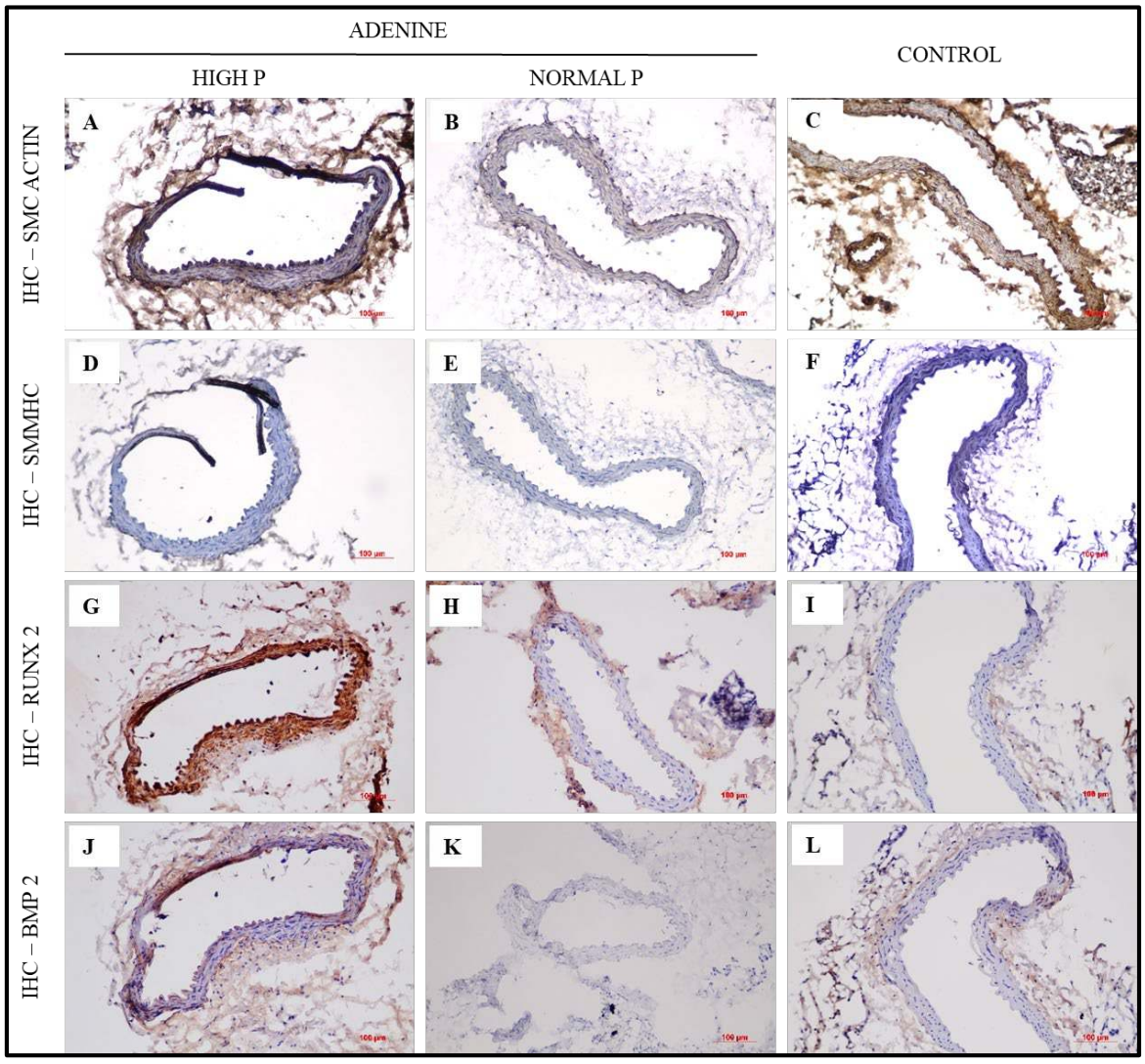

Figure 6-10: Immunohistochemistry for possible VSMC phenotypic transition to osteoblast-like cells. Expression of two smooth muscle markers, SMC Actin, and SMC Myosin is shown. Osteogenic markers RUNX-2 and BMP-2 are also shown in representative micrographs pictured from all three groups of mice. (n=6 per group). (Brown = DAB staining for SMC Actin and SMC Myosin, Red = NovaRed stain for RUNX-2 and BMP-2, Blue = nuclei). *Scale bar = 100 µm.*

6.3.8 Differential gene expression in isolated aortas

Among 22,206 analyzed gene expressions analyzed using the Mouse Clariom S Array, 273 genes showing differential expression between Ade+hP and control groups were identified with a cut-off fold change ≥ 2 or ≤ -2, and $p < 0.05$. Of the 273 genes with differential expression, 163 showed up-regulation and 110 genes were down-regulated in the Ade+hP group. Several genes known to be involved in calcification such as *ALPL, BMP2/4. Spp1, RUNX2, MSX2,* etc. showed upregulation in the adenine+hP group, but the fold change remained insignificant. VSMC-associated genes including Myh11, aSMA, Tagln were downregulated but without any statistical significance.

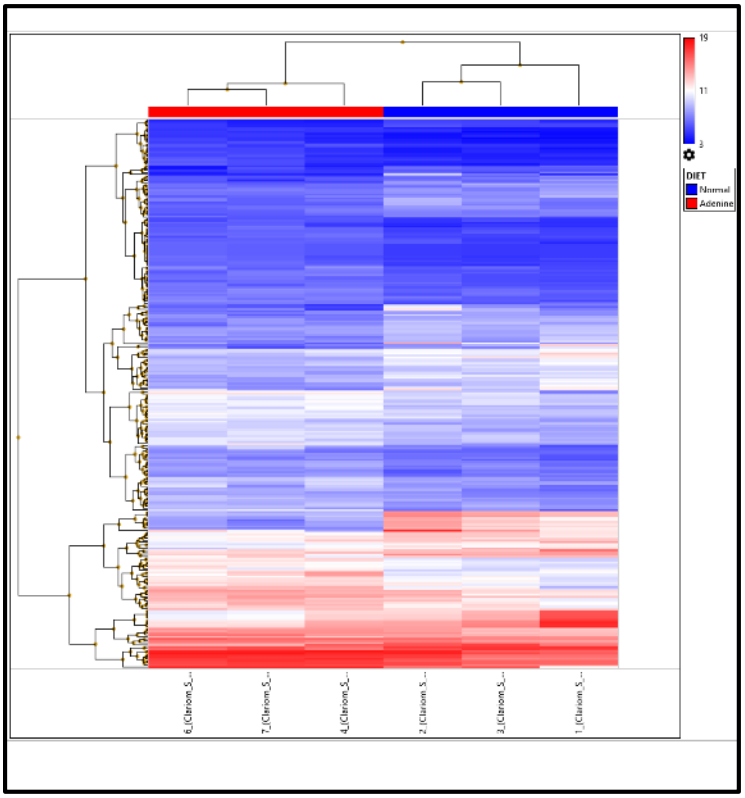

Figure 6-11: Heat map of gene-level whole-transcriptome differential expression profiling assay in Ade+hP diet- and control diet-fed groups of mice. (n=3 per group).

6.4 Discussion

In the present study, we wanted to establish and validate the adenine-CKD model in mice and achieve targeting of ELN-BSA-NPs to diseased (calcified) regions of the aorta for further usage in calcification reversal and vascular health studies. Although we have shown earlier that removal of elastin-specific vascular calcification by EDTA chelation therapy is achieved in rat models of $CaCl_2$ injury [259] and adenine model of CKD [281], it is unclear if this removal is permanent and restores vascular homeostasis.

As with rats, established techniques to induced renal failure and its complications in mice are mostly dependent on surgical intervention and/or transgenic manipulation [145, 162, 260, 282]. The adenine-induced CKD animal model again provides a viable alternative due to its easy relative ease in implementation. However, the adenine model does not consistently develop VC over time [262], owing partly due to the commonly used C57BL/6J strain being quite tolerant of ectopic calcification [283]. A similar dosage of adenine recommended in rats is next to impossible to implement in mice, as this level of dosage (0.75% w/w) or even lower can prove lethal to mice within days [277]. Based on some recent findings, 0.2% w/w seems to be a suitable dosage of adenine to induced CKD in mice of C57BL/6J strain [277, 279].

In agreement with multiple reports of a strong association between VC and phosphorus loading [275, 284-286], Tani et al. recently developed an adenine-based model of CKD capable of producing MAC, without any genetic manipulations, surgical interventions, or drug administration [287]. However, in our experience, reproducing their model of adenine-based CKD and VC proved moderately successful. We surmise that this

is due to inherent biological variation among animals themselves or the genetic strain used. Recently, Yoshida et al. reported DBA/2 mice to be a suitable mouse model for the study of MAC in CKD than C57BL/6J mice, which are thought to be calcification resistant [288]. Even so, during the course of this study, a few other studies have reported successful induction of MAC in C57BL/6 mice via modifications of their own, either by altering the route of adenine administration [289] or modification to the existing recommendations of adenine feeding [290]. Based on our understanding of this model, the consistency and severity of VC in this model still prove elusive. Further studies need to be pursued with appropriate modifications and improvements to this model to attain a robust and stable induction of MAC.

In our study with modifications to the model proposed by Tani et al., we investigated targeting of NPs conjugated with elastin antibody to sites of aortic calcification, developed *in vivo* imaging methodologies to monitor the onset and progress of VC and further validated the model by probing VSMC transdifferentation and their global gene expression profiles. A major hindrance of using noninvasive *in vivo* models of vascular VC is the difficulty in monitoring the onset and progress of the disease. In our study, we used high-resolution micro CT scanning and high-frequency ultrasound imaging to produce images that can be used to analyze and quantify VC in the adenine-model of CKD. Longitudinal micro CT scanning allowed us to detect the onset and presence of VC in Ade+hP mice without the extended use of radiation or without injecting any contrast agents. So far, studies to detect aortic calcium content using micro CT feature the use of

contrast agents [291, 292] or employ transgenic mice models that take as long as 6-12 months to develop quantifiable calcification in the aortic tree [293, 294].

We measured PWV of the infrarenal regions of the aorta non-invasively as a function of aortic distance and the transit time from Color-Doppler and Pulse-wave Doppler-mode view windows to determine local aortic stiffness [295, 296]. This method of PWV measurement is used ubiquitously in pre-clinical research, although it is used over a larger length typically between the carotid and femoral arteries [297, 298]. As it happens for carotid-femoral PWV evaluation in humans, this assessment is influenced by an error in distance measurement even more so in mice due to the distance being ~10 times smaller [299]. However, alternative methods to measure PWV are invasive with catheter-tip pressure transducers placed in two different arteries to measure intra-arterial pressure and transit times. An evident disadvantage with this approach is that the invasive procedure may result in the death of the animal, which, in most cases, has to be dissected for exact spatial distance measurement [299-301]. Our use of the simple, non-invasive method to measure regional PWV gave us values ~2 ms^{-1}, which are in agreement with literature [296, 302]. Green-LaGrange circumferential strain calculated from M-mode images serves to further corroborate aortic stiffness caused due to VC in mice.

We demonstrated the reproducibility of our targeted nanoparticle delivery system in this mouse model of adenine-CKD induced vascular calcification. Similar to our results with rats, we observed no fluorescence emanating from aortas of control-diet fed mice or in mice fed with 0.2% diet and normal levels of P (0.8%). When the P content in the 0.2% adenine diet was switched up to 1.8% after initial induction of renal failure, the aortas

clearly showed targeting of our NPs carrying DiR. Even in these mice, healthy regions of the aorta with uncalcified and undamaged elastin did not show any detectable fluorescence, confirming that the elastin antibody conjugated NPs only target diseased regions of the aortas. Cross-sections of these aortas further validate our findings by ratifying that the ELN-DiR-NPs infiltrate the medial layers of the diseased aorta through the vasa vasorum. Our targeted delivery system can, therefore, be used to deliver any therapeutic to damaged elastin and calcified sites in these mice.

Micrographs taken from histological staining of mouse aortas show clear evidence of MAC exclusively. Elastic fiber layers in these calcified areas appeared to be disrupted and broken around areas of calcium deposition, which is a characteristic feature of MAC. Immunohistochemical staining for presence of common smooth muscle markers, α-SMC actin, and SMMHC, was done to observe phenotypic alteration in VSMCs. α-SMC actin was found to be expressed evenly across the three groups, whereas SMMHC staining was lower in both the adenine-fed groups. Parallelly, we also detected positive staining for both osteogenic markers, RUNX-2 and BMP-2, in the Ade+hP group. No expression for either was seen in either the Ade+nP group or control group. This suggests a phenotypic switch of VSMCs associated with calcification in the Ade+hP group. Differential gene expression profiles obtained by Clariom S Arrays showed that 163 genes were upregulated in the Ade+hP group. Genes known to be involved in calcification and VSMC phenotypic switch to osteoblast-like phenotype such as *ALPL, BMP2/4, Spp1, Igf1, MSX2, RUNX2,* etc., although upregulated, did not show significant fold change difference. Genes associated with VSMCs namely Myh11, aSMA, Tagln, and others showed slight downregulated

compared to the control group. However, the increase or decrease in expression of both osteogenic- and VSMC-associated genes were not statistically significant. Further experiments with higher sample size and analyses are needed to draw more informative conclusions from gene expression profiles.

In conclusion, we were able to establish the adenine-induced CKD model of calcification in a commonly used C57BL/6J strain of mice. Usage of small animal imaging techniques viz., high-resolution microCT scanning, and high-frequency ultrasound imaging help us to monitor the progress of VC and gauge aortic stiffness parameters in these mice *in vivo.* We successfully demonstrated that our NP delivery system is able to target diseased regions in the aortas of mice with calcified aortas. Further validation of the model confirms that there is a transdifferentation of VSMCs to an osteogenic phenotype happening in the event of VC in the aorta. This model of adenine-induced CKD model of VC will allow us to test our targeted chelation therapy with EDTA NPs through monitoring and quantification of calcification *in vivo* and to investigate whether its reversal will result in restoration of healthy VSMC status, thus improving vascular function.

7 SPECIFIC AIM 4

TO DEVELOP AN *EX VIVO* PORCINE CAROTID ARTERY ORGAN CULTURE MODEL OF VASCULAR CALCIFICATION FOR EVALUATING WHETHER TREATMENT WITH EDTA LOADED NANOPARTICLES CONJUGATED WITH AN ANTI-ELASTIN ANTIBODY ELIMINATES CALCIFICATION AND REVERTS VSMCs TO THEIR NORMAL PHENOTYPE

7.1 Introduction

Vascular calcification (VC) is now considered an active and complex process resembling developmental skeletal formation. In addition to key events required for initiation and propagation of VC, such as loss of inhibitor function, upsurge of calcification promoters, development of calcifiable extracellular matrix (ECM) with degradation of elastin laminae due to inflammatory enzymes, and osteogenic differentiation of vascular smooth muscle cells (VSMCs) accompanying apoptosis and vesicle release. The latter two are key mechanisms that may occur simultaneously. There is a longstanding debate regarding which process occurs first, whether adoption of an osteoblast-like phenotype by VSMCs leads to or results from elastin damage and calcification [303]. We have evidence to believe that elastin degradation and mineralization occurs first, which triggers VSMC-osteoblast-like cell phenotypic shift [273, 274]. We further hypothesize that demineralization of calcified arteries promotes restoration of homeostasis.

Calcifying vascular cells have been known to share properties with bone, including higher alkaline phosphatase (ALP) activity, osteocalcin (OCN) and osteopontin (OPN) expression and increased presence of the bone morphogenic protein (BMP) family [304, 305]. A number of studies have focused on understanding the underlying process of VC

through *in vitro* models of primary cell lines from mice [306], bovine [307], and human cells [275, 308]. Usage of monocultures allows for better control of initial experimental conditions to improve detection accuracy. However, morphological variation has been noted at higher passage numbers, and beyond that, gene phenotype of VSMCs is altered. Moreover, a 2D cell culture cannot correctly examine the influence of cell-cell interaction.

Therefore, in this present aim, we hypothesize that an organ culture model would provide useful information to bridge the gap between monolayer cultures and animal models in vogue. Since our terminal goal is to transition our EDTA chelation therapy from present small animal models to human application, we presumed that an *ex vivo* organ culture from a larger animal would provide a feasible culture condition for assessment of VC, and VSMC cell status before and after demineralization. Here, we propose a porcine carotid artery organ culture model of VC under Pi-stimulation.

7.2 Materials and Methods

7.2.1 Isolation and collection of porcine carotid arteries

Fresh porcine carotid arteries were harvested from female domestic crossbred pigs with a Yorkshire background in Godley-Snell Research Center (Clemson, SC) for this study. All animals were 3-4 months old and weighed 35-45 kg. After the pigs were euthanized using commercial euthanasia solution, the thyroid cartilage was located. A 10 cm incision was made 3 cm laterally to the thyroid cartilage using a 10-blade scalpel, extending 5 cm superiorly to the thyroid cartilage and 5 cm inferiorly to the thyroid cartilage. Curved Mayo scissors were used to dissect through the underlying fascia and expose the sternocephalic muscle. The sternocephalic muscle was retracted to expose the internal and external jugular

veins, the common carotid artery, and the vagus nerve. The carotid sheath was dissected using a 10-blade scalpel, and the carotid artery was isolated and removed using surgical scissors. Following excision, the arteries were placed in sterile Moscona's solution (8 g NaCl, 0.2 g KCl, 1 g $NaHCO_3$, 1.7 g glucose, 0.005 g NaH_2PO_4 in 1 L DI water; pH 7.2) on ice and transported back to the lab.

7.2.2 Organ culture of porcine carotid arteries

A day before tissue collection, under sterile conditions, the bottom surface of each well in 12 well plates was coated with 2% agarose. Once the agarose hardened, sterile basal medium was added to each well (DMEM with 4500 mg/mL glucose), and well plates were incubated at 37°C overnight to equilibrate the agarose. On the day of tissue harvest, the old medium was replaced with fresh basal medium, and equilibration was continued until the tissues were ready. The collected carotid arteries were washed well in cold, sterile PBS supplemented with 1-3% Penicillin/Streptomycin, to remove remnants of blood, and the surrounding tissues were carefully cleaned with sterile, blunt forceps. Carotid arteries were then cut into rings of 1-2 mm in length and washed in cold, sterile PBS. Artery rings were placed individually in the pre-incubated and pre-equilibrated 12 well plates. Basal medium was now replaced with complete culture medium (DMEM with 4500 mg/mL glucose supplemented with 15% FBS, 1% Penicillin/Streptomycin). To induce calcification, Pi ($Na_2H_2PO_4$/NaH_2PO_4 at pH 7.4) was added the supplemented DMEM at a high concentration of 2.6mM in half of the total wells. The culture medium, both control and calcification media, was changed every 2 days. The culture went on for 1, 3, and 7 days followed by treatment with n=5 for each time point. An example well plate is outlined in

Figure 7-1. Tissues were cultured in individual well plates for histology, protein, and RNA isolation at each time point, respectively.

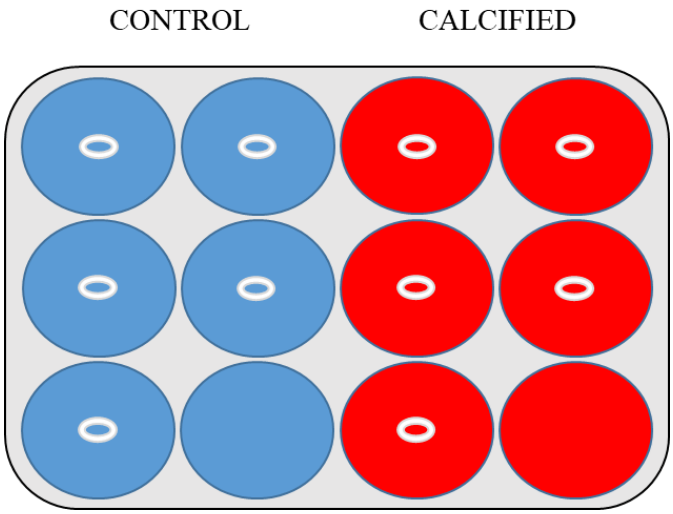

Figure 7-1: Sample well plate of porcine carotid artery organ culture. Blue designates wells with control culture medium. Wells containing medium supplemented with Pi to induce calcification are pictured in red. (n=5 per time point per study).

7.2.3 Treatment of porcine carotid rings with EDTA NPs for *ex vivo* chelation therapy

Following induction of calcification at Day 7, carotid artery rings were treated with nanoparticles (NPs) loaded with EDTA and conjugated with an anti-elastin antibody (ELN-EDTA-NPs) to examine for possible reversal of calcification. After aspirating media and washing the tissues with sterile PBS, NPs were applied directly on the tissue rings (at a final concentration of 10 mg EDTA per well) using a micropipette and allowed to conjugate for a short time. Media was replenished immediately afterwards to continue the culture. NPs without any EDTA loaded, but conjugated with the anti-elastin antibody were used

for non-EDTA control group (ELN-Blank-NPs). A third of group of wells were not treated with any NPs to act as non-treatment controls. The tissues were treated as described above for two times every 3 days over one week.

7.2.4 Histological staining of carotid artery rings

At Day 1, 3 and 7, the carotid artery rings consigned to undergo histological analyses were taken out from their respective well plates and fixed in 10% neutral buffered formalin for 24 hours. Following processing for removal of formalin, the rings were embedded in paraffin and sectioned at 6μm thickness and stained with the following histological stains for tissue morphology – Hematoxylin & Eosin (H&E), Verhoeff von Geison (VVG), Alizarin Red S, von Kossa, Luna staining for elastin fibers.

7.2.5 Immunohistochemical analyses for expression of osteogenic markers

Briefly, rehydrated paraffin sections (5 μm) were exposed to a boiling water bath in a pressure cooker for 10 minutes with citrate buffer (10 mM Sodium Citrate, 0.05% Tween 20, pH 6.0) for heat-induced unmasking of antigens. Endogenous peroxidases were quenched with 3% hydrogen peroxide. Tissue sections were incubated in normal serum for 1hr at RT to block out non-specific binding. Primary Antibodies against were applied overnight at 4°C against Alpha smooth muscle actin (ACTA2, or SMC actin) (Novus Biologicals, Centennial, CO), Smooth Muscle Myosin Heavy Chain (MYH11, or SMMHC), Runt-related transcription factor (RUNX-2) (Santa Cruz Biotechnology, Inc., Dallas, TX), Bone morphogenic factor-2 (BMP-2). Following primary antibody incubation, relevant secondary antibodies were applied, and signal was enhanced by ABC method (Vector, Burlingame, CA). Slides were visualized by either 3,3′-Diaminobenzidine

(DAB) or NovaRed peroxidase substrate chromogens (Vector, Burlingame, CA) followed by a light hematoxylin counterstaining prior to mounting.

7.2.6 Quantification of calcium in tissue rings

Following being harvested and washed with PBS, the aortic rings were treated with 0.6 N HCl overnight at 4°C to decalcify and release bound Ca into the supernatant. Dissolve calcium in the supernatants was determined by the o-Cresolphthalein method using a commercially available kit (Abcam Inc., Cambridge, MA). This method is based on Ca reacting with o-Cresolphthalein complexone in an alkaline solution. Ca concentrations were reported after being normalized to dry weights.

7.2.7 Total protein extraction from carotid cultures

Carotid artery rings were collected at each time point for protein extraction, snap-frozen, and stored at -80°C until extraction. Frozen tissue rings were pulverized with pre-cooled mortar and pestle and placed in pre-cooled 1.5mL centrifuge tubes containing 600µL RIPA buffer (23 mM Tris-HCl pH 7.6, 150 mM NaCl, 5 mM EDTA, 1% Triton X-100, 1% sodium deoxycholate, 0.1% SDS substituted with protease inhibitors at the time of use). Vortex well and homogenize the tissue completely using probe sonication. The tubes were then shaken on ice for approximately 3 hours, and proteins were extracted by centrifugation @12000rpm at 4°C for 20 minutes. The resulting supernatants were carefully transferred to fresh, precooled 1.5mL tubes using a micropipette and stored at -20°C for further analyses. BCA protein assay was performed on the final samples to determine the protein concentration.

7.2.8 Western Blotting

Samples containing equal amounts of protein, as measured from protein quantification, were mixed with 4X reducing buffer containing β-mercaptoethanol, boiled down 5 minutes and cooled. They were then subjected to sodium dodecyl sulfate-polyacrylamide electrophoresis with Tris/Glycine denaturing running buffer (25 mM Tris, 192 mM Glycine, 0.1% SDS) for 50 minutes at 200V on 4-15% Mini-Protean TGX precast gels (BioRad Laboratories Inc., Herculus, CA). The gels were subsequently transferred to pre-conditioned polyvinyl fluoride (PVDF) membrane. The transfer lasted for 50 minutes at 100V in a tank system on ice, using Tris/Glycine transfer buffer (25 mM Tris, 192 mM Glycine, 20% methanol). After washing with TBS and blocking for 1 hour at RT using 10% non-fat dry milk in TBS, the membrane was washed in TBST (0.05% Tween in TBS) 3 times for 5 minutes each. The membrane was then incubated overnight at 4°C with primary antibodies in 2% dry milk in TBST. The following primary antibodies were used: Alpha smooth muscle actin (ACTA2, or SMC actin, 1:10000) (Novus Biologicals, Centennial, CO), Smooth Muscle Myosin Heavy Chain (MYH11, or SMMHC, 1:3000) (Proteintech Group Inc., Rosemont, IL), Runt-related transcription factor (RUNX-2, 1:500) (Santa Cruz Biotechnology Inc., Dallas, TX), and Bone morphogenic factor-2 (BMP-2, 1:2000) (Proteintech Group Inc., Rosemont, IL). GAPDH (1:1500) (Proteintech Group Inc., Rosemont, IL) and β-actin (1:1000) (Santa Cruz Biotechnology Inc., Dallas, TX). The next day, the membrane was washed 5 times for 10 minutes in TBST to remove the unbound primary antibody and incubated with an appropriate HRP-conjugated secondary antibody (1:20000) in 2% dry milk in TBST for 1 hr at RT. After washing with TBST for

3 times 10 minutes each time, the membrane was developing using Clarity Western ECL Substrate (BioRad Laboratories Inc., Herculus, CA) for 5 minutes. Membranes were then imaged using Chemi Doc It2 imaging system (UVP) at different exposure times for individual proteins. Densitometry analysis was performed using Image J software for quantification.

7.3 Results

7.3.1 Histology of porcine carotid artery rings

Hematoxylin & Eosin staining of formalin-fixed and paraffin-embedded carotid ring sections show appreciable staining for nuclei until Day 3 of the organ culture in the calcified group alluding to cellular presence. Only on Day 7, there is a noticeable decrease in nuclear staining (Figure 7-2 B-D). Images from the control group suggest that the cells are thriving throughout the duration (Figure 7-2 A). Luna stain and VVG stain were used to observe elastin fiber morphology. There is no discernible damage to elastin seen in the calcified group in any of the Day 1, Day 3 or Day 7-time points, either on the Luna stained sections (Figure 7-2 F-H) or VVG sections (Figure 7-2 J-L). As expected, intact elastin fiber was identified in the control group (Figure 7-2 E, I).

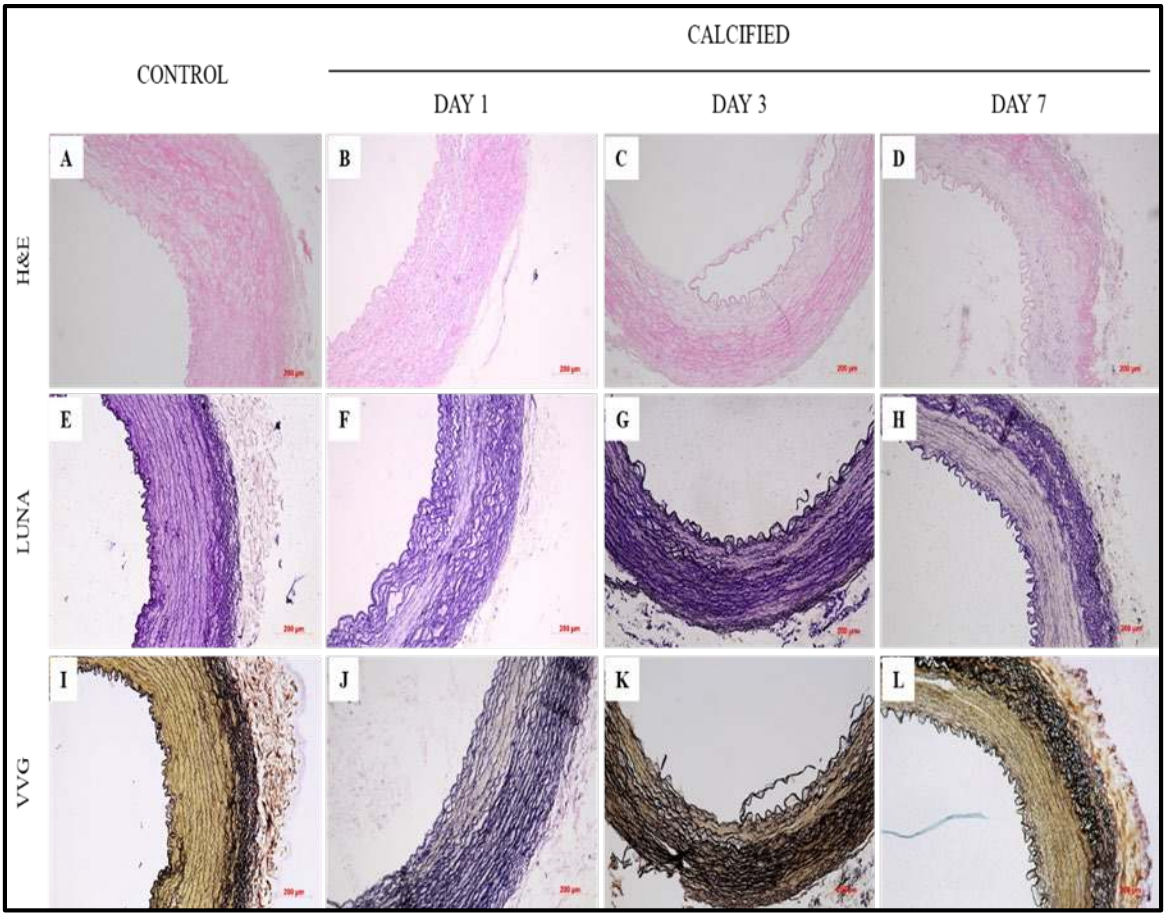

Figure 7-2: Digital micrographs of H&E, Luna, and VVG staining on porcine carotid rings. (A-D) H&E staining shows. (E-H) Luna stain illustrates intact elastin fiber structure with no obvious damage. (I-L) VVG Stain for elastin fiber confirms observations made on Luna stain images. (n=5 per time point per group). *Scale bar = 200 μm.*

7.3.2 Evaluation of calcification of the carotid arteries

Alizarin Red S staining was performed to evaluate calcium deposition. Following incubation of the carotid arteries with calcification medium, faint deposition of calcium is observed as early as Day 1 of the organ culture (Figure 7-3 B).

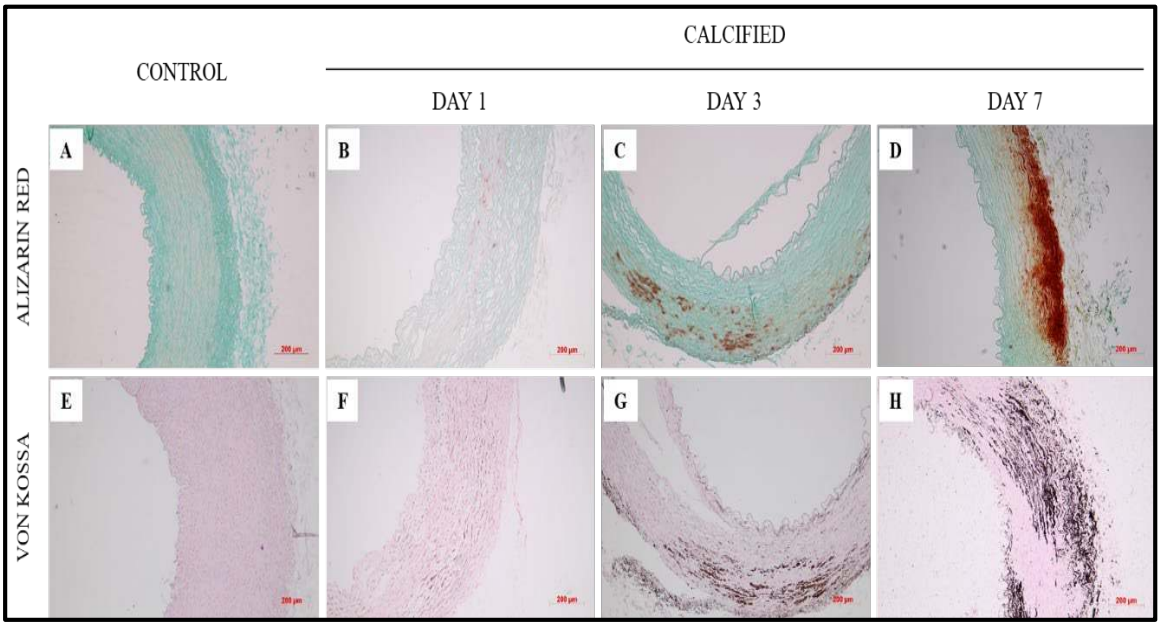

Figure 7-3: Evaluation of calcification by histological staining of carotid artery rings. Representative images of calcification in porcine carotid artery cross-sections as pictured by Alizarin Red S stain (A-D) and von Kossa Stain (E-G) (n=5 per time point per group). *Scale bar = 200 µm.*

Calcium deposition increases as the culture progresses at Day 3, and by Day 7, heavy calcification of the carotids was seen microscopically (Figure 7-3 C-D). von Kossa staining confirms the presence of calcium deposits with increasing deposition from Day 1 through Day 7 (Figure 7-3 F-H). No calcification or calcium deposits are observed in the carotid arteries incubated with control medium (Figure 7-3 A, E).

7.3.3 Immunohistochemistry for smooth muscle cell apoptosis and smooth muscle marker expression

Immunohistochemistry for Caspase-3 shows considerable expression of the apoptotic protein across control and calcified groups. At Day 1, 3, and 7 in the calcified arteries, Caspase-3 is present in all the three layers of the arterial wall (Figure 7-4 A-D). Staining for SMC actin is comparable in the control group, and at all the three-time points in calcified arteries, indicating that there may not be a reduced expression, as expected, with increasing calcification (Figure 7-4 E-H). SMMHC was fairly well expressed in the control group. Calcified group shows a negligible signal for SMMHC on Day 1 and 3, whereas its expression was detected at Day 7 (Figure 7-4 I-L). Overall, smooth muscle cell apoptosis is consistent in both control and calcified arteries; Expression of SMC actin was not found to decrease over time with increased deposition of Ca in the calcified arteries.

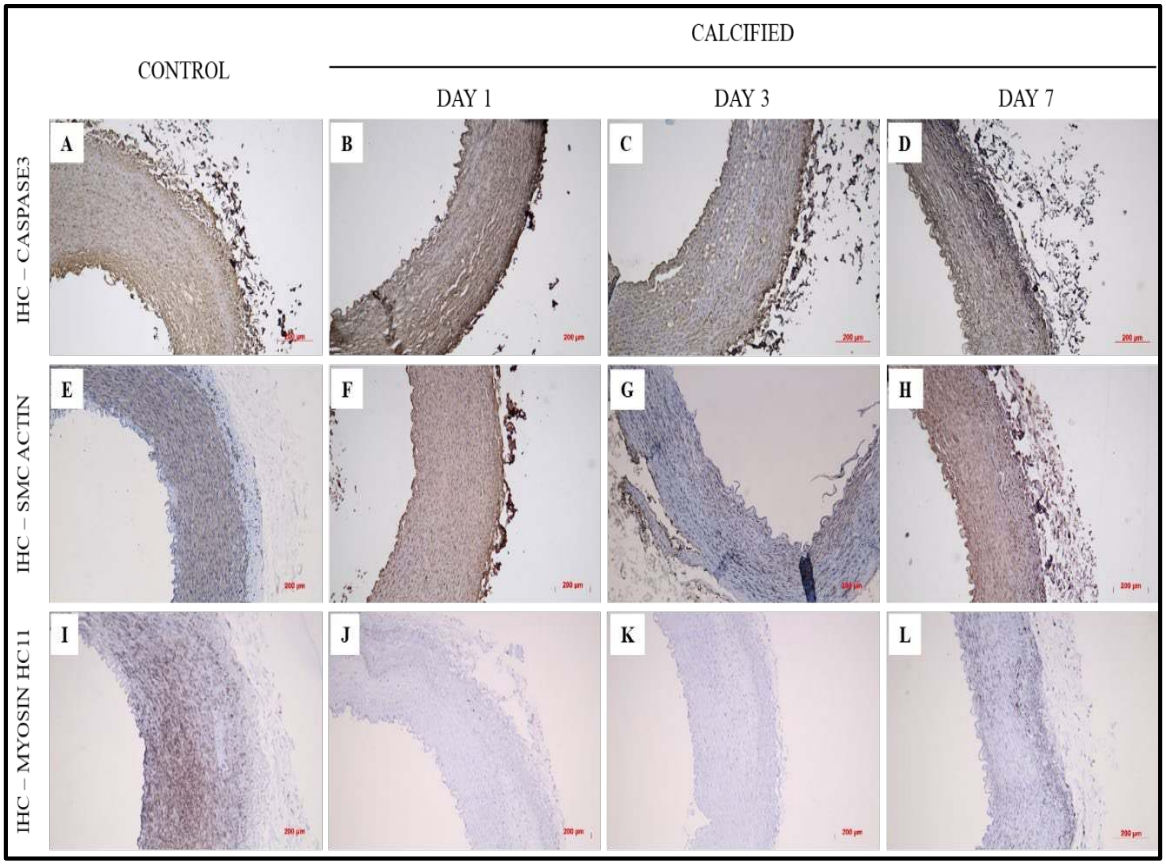

Figure 7-4: Immunohistochemical staining for smooth muscle apoptosis and expression of smooth muscle markers. Representative images of calcification in porcine carotid artery cross-sections from Caspase-3 (A-D), ACTA2 (E-H), and SMMHC (I-L) staining. (n=5 per time point per group). *(Brown = DAB, purple = nuclei). Scale bar = 200 µm.*

7.3.4 Immunohistochemistry for expression of osteogenic cell markers

Following analysis of smooth muscle cell apoptosis and expression of smooth muscle cell markers, we wanted to observe for possible upregulation in osteogenic cell markers. As seen in Figure 7-5, there was very sparse, if any, expression of both RUNX-2 (B-D) and BMP-2 (F-H) in the calcified group at Day 1, 3 and 7-time points. Only on Day 7, RUNX-2 could be detected in calcified group. Control group did not show any staining for the two osteogenic markers, which was expected (A-E).

Based on observations made with IHC staining, VSMCs in the carotid artery cultures seem to undergo apoptosis both in the control and calcified groups. There was no significant reduction of smooth muscle cell marker expression or upturn in osteogenic marker expression in the calcified group.

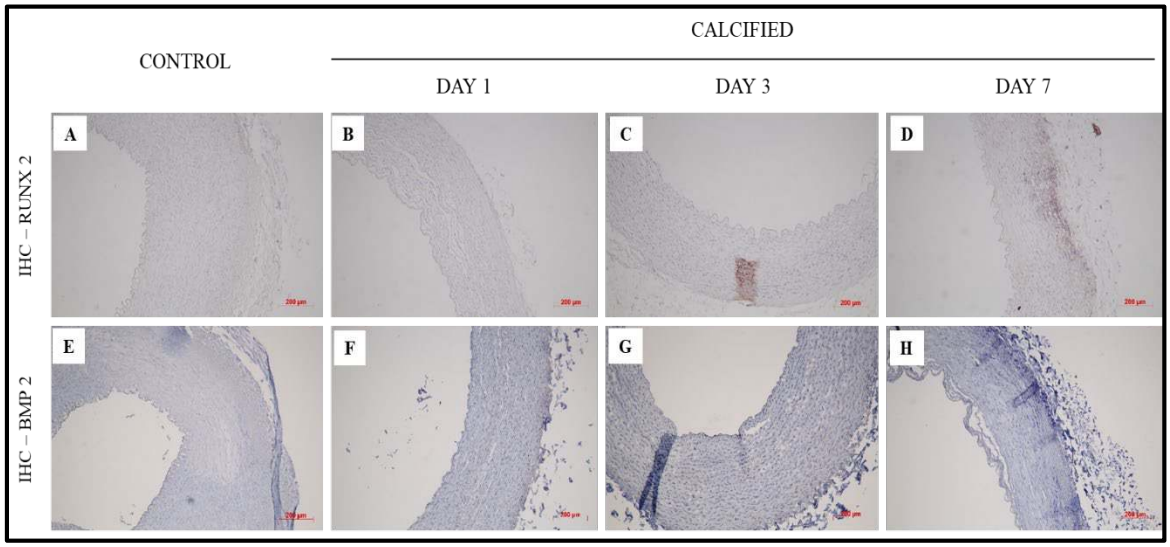

Figure 7-5: Immunohistochemical staining for osteogenic markers – RUNX2 and BMP2. Representative micrographs of IHC staining for RUNX-2 (A-D), and BMP-2 (E-H) in control and calcified groups. (n=5 per time point per group). *(Red = NovaRed, purple = nuclei). Scale bar = 200 µm.*

7.3.5 Western blot analysis for smooth muscle and osteogenic markers

Western blotting was used to check for expression of smooth muscle- and osteogenic- markers on total protein isolated from both the groups of carotid artery rings. α-SMA expression was normalized to GADPH housekeeping gene, and β-actin was used to show relative SM-MHC expression. At Day 1 and Day 7-time points of culture, no significant increase or decrease was observed in the expression of the two smooth muscle

proteins in the calcified group when compared to controls (Figure 7-6), consolidating the observations made with immunohistochemistry. At any of the time points, no bands could be detected for either of the two osteogenic markers. Both RUNX-2 and BMP-2 did not show any expression in control and calcified groups (Figure 7-7).

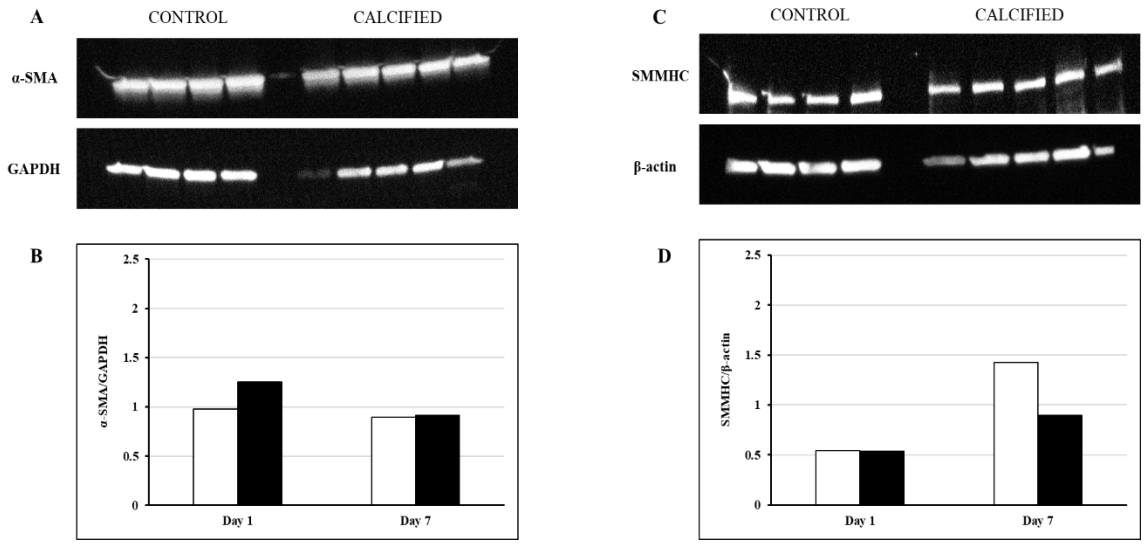

Figure 7-6: Western blots for smooth muscle cell markers in control and calcified carotid artery rings. (A, B) α-SMA expression in control and calcified carotid aortic rings. No significant difference is seen in expression at either Day 1 or Day 7-time points. (C, D) SM-MYH expression in control and calcified carotids. As with α-SMA, there was no statistically significant difference in expression at both time points. (n=4 per group per time point) (White columns: control group, black columns: calcified group).

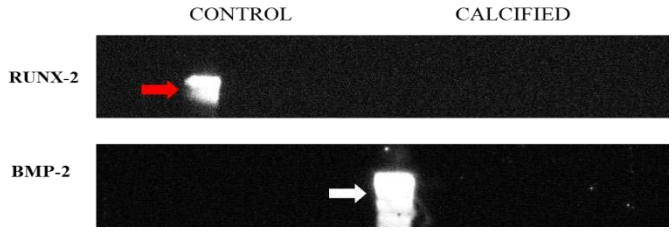

Figure 7-7: Images taken after western blotting for osteogenic markers in control and calcified groups. No expression could be detected for the two osteogenic markers tested – RUNX-2 and BMP-2 – at any time point in either control or calcified carotid rings. (n=4 per time point per group). (Red arrow indicates positive control for RUNX-2; white arrow shows protein ladder).

7.3.6 Reversal of Pi-induced calcification with EDTA-loaded NP treatment

Treatment with ELN-EDTA-NPs moderately reversed calcification induced by supplementation with Pi. Alizarin red staining of carotid artery rings following treatment shows modest reversal of calcification in the ELN-EDTA-NPs group while bright red calcified areas persevered in the ELN-Blank-NPs group and the untreated group (Figure 7-8 A-C). Similar results were witnessed with von Kossa staining, with ELN-EDTA-NPs staining least for Ca deposits where as both the ELN-Blank-NPs group and untreated groups had extensive staining (Figure 7-8 D-F). Tissue rings were decalcified by incubation in 0.6N HCl and Ca in the supernatants was quantified using o-Cresolphthalein complexone method for detection of Ca. Quantified Ca was normalized to dry weights of the tissues with ELN-EDTA-NPs group having mean quantified Ca values of 0.97±0.30 µg/mg of dry weight. Ca values in ELN-Blank-NPs and untreated groups remained at 1.39±0.09 and 1.42±0.34 µg/mg of dry weight of tissue respectively. It is pertinent to note here that not all the tissues in ELN-EDTA-NPs showed reversal of calcification and the

difference remained statistically insignificant (Figure 7-9), probably due to the small number of samples tested (n=3).

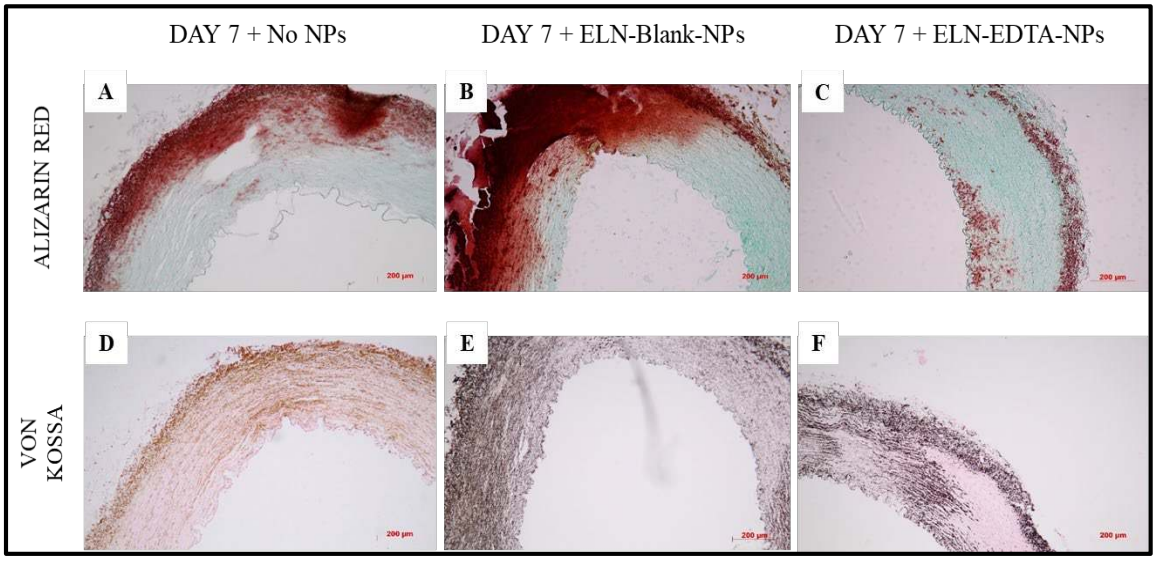

Figure 7-8: Representative histological images of carotid artery rings depicting calcification after treatment. ELN-EDTA-NPs show reasonable reversal of calcification while persisting in ELN-Blank-NPs and untreated groups. (n=3 per group) *Scale bar = 200 μm*.

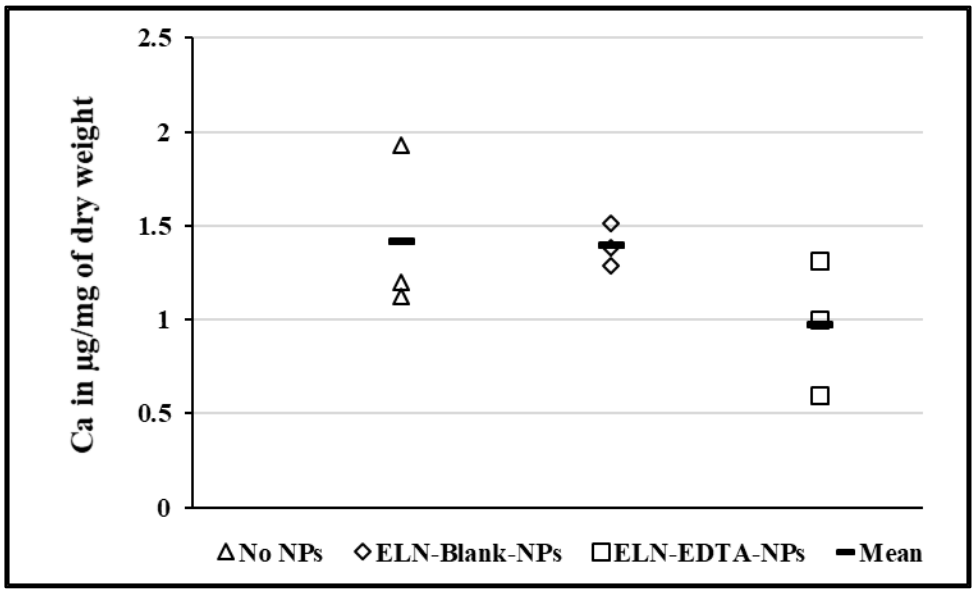

Figure 7-9: Quantification of Ca by o-Cresolphthalein complexone method following treatment. ELN-EDTA-NPs suggest removal of calcification in 2 out of 3 tissue samples used. ELN-Blank-NPs and untreated groups have comparatively higher levels of Ca. (n=3 per group).

7.4 Discussion

In the present study, we utilized the well-known Pi-induced model of calcification in organ culture of porcine carotid arteries for the first time. This experimental model of carotid artery culture is relatively simple and easy and cuts down the time to thoroughly evaluate the process of induction and reversal of VC.

We followed an *ex vivo* organ culture model described in previous reports [309] to generate a high-phosphorus-induced VC [310-313]. Many such studies report that a concentration of 2.6-3.0 mM Pi in the culture media as it produces a degree of calcification easy to detect through examination under microscopy. However, these studies utilize VSMCs from humans, rats, and mice and aortic rings from rats and mice for their culture

studies. For our study, we used porcine carotid arteries harvested fresh from swines at the local animal research facility. Pi-induced calcification has not been studied in porcine artery cultures hitherto, and we believe this will serve as an ideal model to explore VC and chelation therapy, towards larger animal studies *in vivo.*

Following exposure to extracellular Pi in the media, carotid artery rings undergo time-dependent calcific deposition with increasing deposition up to 7 days in culture, as reported in similar studies with other tissues mentioned above. Though, no accompanying elastin fiber degradation or destruction was readily apparent in either Luna stained sections or VVG staining [314, 315]. Beyond 7 days, there was no apparent increase in calcification under microscopic observations on histological stains (data not shown). Hence, we chose the Day 7-time point for our reversal experiments.

Next, evaluated VSMCs for possible reprogramming into osteoblast-like cells through immunohistochemistry, western blotting, and gene expression analyses. Cultured SMCs have long been known to be capable of calcifying and expressing osteogenic phenotypes when exposed to high levels of Pi [95, 309, 316, 317]. In our assessment for phenotypic change of VSMCs into osteoblast-like cells, we found no upregulation of RUNX-2 and BMP-2, both markers are known to be expressed by calcifying vascular cells. IHC staining for the two osteogenic markers does not show any enhanced staining in calcified carotid rings. While VSMCs in cultured rings show expression of the apoptotic marker Caspase-3 [318], its presence is universal amongst control and calcified groups. Simultaneously, there is no loss of smooth muscle cell markers, α-SMC actin, and SMMHC, with time-dependent increase in calcium deposition.

Immunoblot analyses for increased protein expression of RUNX-2 and BMP-2 showed no detection for either of the two osteogenic markers in the calcified group, on Day 1 or Day 7-time points. Even after repeated experiments with different concentrations of primary antibodies and higher quantities of total proteins loaded for gel electrophoresis, no bands could be visualized. Concomitantly, expression of α-SMC actin and SMMHC remained fairly constant over the 7-day time period with no statistically significant difference between the control and calcified groups. Put together, our data with IHC and WB reveals that calcification of the carotid artery rings in this setting maybe due to passive mineralization and does not involve any cellular responses.

We further assessed whether treatment with EDTA-loaded NPs conjugated with an anti-elastin antibody could reverse the Pi-induced calcification in carotid tissue rings. We applied EDTA-loaded NPs at a final dosage of 10 mg EDTA/well, twice over a period of one week. Histological staining with alizarin red and von Kossa stains to spot calcification following treatment suggest that there is some degree of reversal of calcification with ELN-EDTA-NPs, while calcification persisted in the tissue sections from ELN-Blank-NPs and untreated groups. To measure the Ca present in tissues after treatment, we decalcified the carotid rings by placing them in 0.6N HCl [319] and determined the Ca released into the supernatant using the o-Cresolphthalein method. The observations we made with histology were corroborated with quantified Ca values being noticeably lower in the ELN-EDTA-NPs group compared to the others. However, out of the three tissue samples used to analyze reversal of calcification, only two show lessened calcium. ELN-EDTA-NPs show promising results, but the change is not significant. This observation could have been due

to the small number of samples used (n=3), and the results did not reach statistical significance. To substantiate this hypothesis, a pilot study with increasing amounts of EDTA directly added to the media yielded no removal of calcification. Further, the dosage of ELN-EDTA-NPs at 10mg/well may not have been sufficient to achieve complete reversal. Higher magnitudes of EDTA targeted to calcific deposits may be needed to achieve better removal, although EDTA is known to be cytotoxic.

We conclude that exposure to excess Pi concentrations in the culture media resulted in time-dependent increase in mineralization of calcium deposits in porcine carotid artery rings. Evidence from immunohistochemical staining and western blot analysis for smooth muscle and osteogenic markers reveals that there was no significant reduction in expression of the former, combined with no increase in bone protein expression at any of the three-time points. Treatment with ELN-EDTA-NPs moderately removed mineralization from calcified tissue rings. At this point, the *ex vivo* porcine carotid artery organ culture of Pi-induced VC is not optimized for use in studies to assess effects of EDTA chelation therapy on VSMC calcification and transdifferentiation. Further experiments are necessary to improve the model to represent the process of active calcification that occurs *in vivo.*

8 CONCLUSIONS AND FUTURE RECOMMENDATIONS

8.1 Conclusions

Vascular calcification (VC) is a key pathological feature observed in various forms of cardiovascular diseases. It is commonly seen in aging, diabetes, and chronic kidney disease (CKD). Elastin-specific medial arterial calcification (MAC) is more commonly seen in CKD, and patients with CKD are more prone to die of a cardiovascular event due to MAC than fully progress to complete renal failure. Majority of the current treatment methods are focused on curtailing the causative factors and preventing calcification. A novel therapeutic strategy that stabilizes and eventually reverses calcification is an urgent health care need and is of immense value to patients with CKD. We have developed nanoparticles that can be targeted to the sites of arterial calcification by using an antibody that exclusively recognizes and binds to degraded elastin, a common appearance in calcification. Our goal is to load these nanoparticles (NPs) with Ethylene diamine tetraacetic acid (EDTA), a well-known chelating agent and deliver EDTA to the calcified sites on the aorta to facilitate reversal of mineralization without causing any unpleasant side effects.

In the first part of this project, we set out to test our targeted EDTA chelation therapy in a clinically relevant systemic model of CKD-related calcification. For this, we used the well-known rat adenine-induced CKD model of medial calcification. We established this model without unexpected mortality, as is usually seen, and fairly evenly produced calcification across all animals. Then, we demonstrated the ability of our NPs to

target calcified sites on the aortas of these rats. We were able to successfully reverse mineralized calcium *in vivo* by site-specifically delivering EDTA at a dosage ~twenty-fold lower than systemic chelation therapies currently in use. This was achieved without causing any unwanted side effects, and the animals showed signs of improvement in vascular function.

Subsequently, we replicated targeting of NPs to calcified sites in a murine model of CKD-related calcification. This was accomplished in adenine plus high phosphate induced model of CKD and medial calcification. We further wanted to establish ways to monitor disease progression *in vivo* for forthcoming investigations on reversal of calcification and its effect on disease outcomes and vascular health. For this, we used small animal imaging techniques such as ion micro CT and ultrasound to visualize onset and development of calcification. One of our eventual objectives is to explore phenotypic changes in VSMCs prior to and after reversal of calcification *in vivo.* Stringent cell lineage tracing studies on VSMCs will be required to probe their fate, and we laid down the first step by profiling global gene expression of VSMCs in calcified aortas of the adenine-diet fed mice.

8.2 Recommendations for future work

1) Despite the successful use of adenine model to evaluate chelation therapy in reversal of MAC, this model presents high biological variability with regards to development of robust calcification. In humans, calcification is seen throughout the length of the aortic tree, and in heart valves as well. In our experience with the adenine model, both in rats and mice, calcification in these animals was restricted to infrarenal region of the aorta. Keeping in consideration studies showing calcification at various loci on the aorta, we have only had moderate success in establishing severe MAC at different sites on the vasculature. Additionally, all the animals used in this model do not show calcified deposits; only as many as 60% of the animals develop MAC. Put together; it would require an unusually high number of animals to investigate and compare treatment regimens with acceptable statistical power. It is essential to make further adjustments to the model we used, not restricted to dietary alterations, and usage of a genetic strain of mice more prone to calcification.
2) At this time, we do not know if the VSMCs return to their original phenotype after reversal of calcification *in vivo*, or if they undergo apoptosis and are repopulated by new SMCs recruited from surrounding cells, pericytes, endothelial-mesenchymal transition (EndoMT), or hematopoietic stem cells (HSC). Lineage tracing studies need to be performed with tamoxifen-induced Cre recombinase mice with dual fluorescence indicator/reporter for SMC, EndoMT, HSC, or pericyte origin.

3) The groundbreaking nanoparticle delivery system alone could be used to deliver not just chelating agents, but other specific drugs, proteins, or imaging agents to the calcified sites, and could open a host of possibilities. For example, the targeted delivery system could be utilized to deliver pentagalloyl glucose (PGG) to the damaged elastin sites. PGG tightly binds to elastin and blocks its calcium-binding sites, while also helping in reduced expression of matrix-degrading enzymes and osteogenic proteins, in addition to replenishing elastin fiber deposition.
4) Patients with CKD need dialysis as their kidney function worsens and GFR falls below 15. As mentioned, the long term goal of this project is to translate our targeted EDTA chelation to individuals suffering from kidney disease and improve their cardiovascular outcomes. It would, therefore, be judicious to administer targeted EDTA chelation to the patients at the time of dialysis as a co-therapy, to avoid repeated incisions. Currently, each dialysis treatment lasts about four hours and is done three times per week. At this stage, our NPs are designed to release EDTA in a burst release manner over a period of 72 hours. This would mean that patients need to be given intravenous injections at a rate of two times per week if the targeted EDTA chelation regimen is endorsed. Accordingly, it is recommended that further tailoring of the NPs is necessary to ensure that the chelating agent is released quicker, within 48-72 hours, to ensure that co-therapy with dialysis remains a possibility.
5) Different mineral phases arise during uremic MAC due to the result of different pathological mechanisms involved in their precipitation. Hydroxyapatite

[$Ca_{10}(PO_4)_6OH_2$], a common skeletal mineral was reported in uremic arterial calcifications in some studies [320, 321]. In another study, a combination of brushite and hydroxyapatite were observed in calcifications of stenotic arteriovenous fistulas [322]. A study of uremic calcification in rodents detected the presence of whitlockite [$(Ca, Mg)_3(PO_4)_2$], along with hydroxyapatite [323]. Recently, whitlockite was identified in human uremic arterial calcifications. This is in contrast to most studies, which so far have reported only hydroxyapatite or carbonated apatite in uremic vascular calcifications [322]. It would then be imperative to properly characterize the kind of mineral deposition present in the calcified aortas of patients with CKD as this would affect the choice of chelating agents for dissolution of mineral.

6) Considering the value of *in vivo* imaging and monitoring of disease progression in impending studies in mice, it would be useful to have another diagnostic tool using CT imaging with gold as X-ray contrast. Currently, we relied on CT scanning without the use of any contrast agents for improved visibility of calcification. Recently, our lab has evinced that gold NPs, combined with the elastin targeting approach, can be used to predict the degree of elastin damage and rupture potential in AAAs [324]. A quantitative relationship may thus be established to correlate elastin damage at calcified sites and corresponding gold nanoparticle binding, providing us an additional remarkable visual tool to track development of calcification in mice before, and after EDTA chelation therapy.

7) Arterial calcification is augmented in metabolic syndrome, type 2, and type 1 diabetes mellitus, resulting in impaired vessel compliance and function. Consequences of MAC in diabetes are impaired hemodynamic regulation and increased cardiac post-load; it is a strong predictor of lower-extremity amputation and mortality. Patients with type 2 diabetes were at a four-fold increased risk for lower-extremity amputation and two-fold enhancement of cardiovascular mortality [325, 326]. Use of site-specific chelation therapy for reversal of diabetic MAC and improvement in arterial health is thus an attractive prospect.
8) Our nanoparticle targeting system is a product of several years of successful substantiation in various *ex vivo* and *in vivo* small animal models. To utilize this approach for targeting of damaged elastin in other pathologies such as Marfan syndrome, varicose veins, deep vein thrombosis, cutis laxa, Pseudoxanthoma elasticum (PXE), etc. can result in fresh drug delivery strategies. Additionally, nanoparticle surfaces could be modified to target established markers to specific cancers [327, 328].

BIBLIOGRAPHY

1. Benjamin, E.J., et al., *Heart Disease and Stroke Statistics-2019 Update: A Report From the American Heart Association.* Circulation, 2019. **139**(10): p. e56-e528.

2. World Health Organization. *Cardiovascular diseases (CVDs)*. 2017, May 17; Available from: https://www.who.int/en/news-room/fact-sheets/detail/cardiovascular-diseases-(cvds).

3. Fryar, C.D., T.C. Chen, and X. Li, *Prevalence of uncontrolled risk factors for cardiovascular disease: United States, 1999-2010.* NCHS Data Brief, 2012(103): p. 1-8.

4. O'Donnell, C.J. and R. Elosua, *[Cardiovascular risk factors. Insights from Framingham Heart Study].* Rev Esp Cardiol, 2008. **61**(3): p. 299-310.

5. Sarnak, M.J., et al., *Kidney disease as a risk factor for development of cardiovascular disease - A statement from the American Heart Association Councils on kidney in cardiovascular disease, high blood pressure research, clinical cardiology, and epidemiology and prevention.* Hypertension, 2003. **42**(5): p. 1050-1065.

6. *Diet, Exercise, and Chronic Disease: The Biological Basis of Prevention.* Diet, Exercise, and Chronic Disease: The Biological Basis of Prevention, 2014: p. 1-423.

7. MacIsaac, A.I., et al., *High speed rotational atherectomy: outcome in calcified and noncalcified coronary artery lesions.* J Am Coll Cardiol, 1995. **26**(3): p. 731-6.

8. Coselli, J.S., L.D. Conklin, and S.A. LeMaire, *Thoracoabdominal aortic aneurysm repair: review and update of current strategies.* Ann Thorac Surg, 2002. **74**(5): p. S1881-4; discussion S1892-8.

9. Lamas, G.A. and S.J. Hussein, *EDTA chelation therapy meets evidence-based medicine.* Complement Ther Clin Pract, 2006. **12**(3): p. 213-5.

10. Atwood, K.C., et al., *Why the NIH Trial to Assess Chelation Therapy (TACT) should be abandoned.* Medscape J Med, 2008. **10**(5): p. 115.

11. Jackson, G., *Chelation therapy is TACT-less.* Int J Clin Pract, 2008. **62**(12): p. 1821-2.

12. American College of Cardiology. *AHA 2019 Heart Disease and Stroke Statistics*. 2019, February 19]; Available from: https://www.acc.org/latest-in-cardiology/ten-points-to-remember/2019/02/15/14/39/aha-2019-heart-disease-and-stroke-statistics.

13. Roth, G.A., et al., *Global, Regional, and National Burden of Cardiovascular Diseases for 10 Causes, 1990 to 2015.* J Am Coll Cardiol, 2017. **70**(1): p. 1-25.

14. Centers for Disease Control and Prevention (CDC). *Heart Disease Death Rates, Total Population Ages 35+*. 2018, May 21; Available from: https://www.cdc.gov/dhdsp/maps/national_maps/hd_all.htm.

15. Clipground. *https://clipground.com/coronary-clipart.html*. Available from: https://clipground.com/coronary-clipart.html.

16. D'Agostino, R.B., Sr., et al., *Cardiovascular Disease Risk Assessment: Insights from Framingham.* Glob Heart, 2013. **8**(1): p. 11-23.

17. in *Chronic Heart Failure: National Clinical Guideline for Diagnosis and Management in Primary and Secondary Care: Partial Update*. 2010: London.

18. Encyclopædia Britannica. *Human cardiovascular system*. 2018, July 13; Available from: https://www.britannica.com/science/human-cardiovascular-system.

19. Michigan Medical School. *Michigan Histology and Virtual Microscopy Learning Resources*. Available from: http://histology.medicine.umich.edu/full-slide-list.

20. Shapiro, S.D., et al., *Marked longevity of human lung parenchymal elastic fibers deduced from prevalence of D-aspartate and nuclear weapons-related radiocarbon.* J Clin Invest, 1991. **87**(5): p. 1828-34.

21. Cleary, E.G., L.B. Sandberg, and D.S. Jackson, *The changes in chemical composition during development of the bovine nuchal ligament.* J Cell Biol, 1967. **33**(3): p. 469-79.

22. Mecham, R.P., et al., *Elastin synthesis by ligamentum nuchae fibroblasts: effects of culture conditions and extracellular matrix on elastin production.* J Cell Biol, 1981. **90**(2): p. 332-8.

23. Burke, J.M. and R. Ross, *Synthesis of connective tissue macromolecules by smooth muscle.* Int Rev Connect Tissue Res, 1979. **8**: p. 119-57.

24. Quintarelli, G., et al., *Fibrogenesis and biosynthesis of elastin in cartilage.* Connect Tissue Res, 1979. **7**(1): p. 1-19.

25. Cantor, J.O., et al., *Synthesis of crosslinked elastin by an endothelial cell culture.* Biochem Biophys Res Commun, 1980. **95**(4): p. 1381-6.

26. Vrhovski, B. and A.S. Weiss, *Biochemistry of tropoelastin.* Eur J Biochem, 1998. **258**(1): p. 1-18.

27. Rosenbloom, J., W.R. Abrams, and R. Mecham, *Extracellular matrix 4: the elastic fiber.* FASEB J, 1993. **7**(13): p. 1208-18.

28. Shifren, A. and R.P. Mecham, *The stumbling block in lung repair of emphysema: elastic fiber assembly.* Proc Am Thorac Soc, 2006. **3**(5): p. 428-33.

29. Dietz, H.C. and R.E. Pyeritz, *Mutations in the human gene for fibrillin-1 (FBN1) in the Marfan syndrome and related disorders.* Hum Mol Genet, 1995. **4 Spec No**: p. 1799-809.

30. Ramamurthi, A. and I. Vesely, *Evaluation of the matrix-synthesis potential of crosslinked hyaluronan gels for tissue engineering of aortic heart valves.* Biomaterials, 2005. **26**(9): p. 999-1010.

31. Mithieux, S.M. and A.S. Weiss, *Elastin.* Adv Protein Chem, 2005. **70**: p. 437-61.

32. Li, B. and V. Daggett, *Molecular basis for the extensibility of elastin.* J Muscle Res Cell Motil, 2002. **23**(5-6): p. 561-73.

33. Fazio, M.J., et al., *Human elastin gene: new evidence for localization to the long arm of chromosome 7.* Am J Hum Genet, 1991. **48**(4): p. 696-703.

34. Fritze, O., et al., *Age-related changes in the elastic tissue of the human aorta.* J Vasc Res, 2012. **49**(1): p. 77-86.

35. Xu, J. and G.-P. Shi, *Vascular wall extracellular matrix proteins and vascular diseases.* Biochimica et Biophysica Acta (BBA)-Molecular Basis of Disease, 2014. **1842**(11): p. 2106-2119.

36. Clarke, A.W., et al., *Tropoelastin massively associates during coacervation to form quantized protein spheres.* Biochemistry, 2006. **45**(33): p. 9989-96.

37. Mecham, R.P., *Elastin synthesis and fiber assembly.* Ann N Y Acad Sci, 1991. **624**: p. 137-46.

38. Clarke, A.W., et al., *Coacervation is promoted by molecular interactions between the PF2 segment of fibrillin-1 and the domain 4 region of tropoelastin.* Biochemistry, 2005. **44**(30): p. 10271-81.

39. Hirai, M., et al., *Fibulin-5/DANCE has an elastogenic organizer activity that is abrogated by proteolytic cleavage in vivo.* J Cell Biol, 2007. **176**(7): p. 1061-71.

40. Kagan, H.M. and K.A. Sullivan, *Lysyl oxidase: preparation and role in elastin biosynthesis.* Methods Enzymol, 1982. **82 Pt A**: p. 637-50.

41. Nivison-Smith, L. and A. Weiss, *Elastin based constructs*, in *Regenerative Medicine and Tissue Engineering-Cells and Biomaterials*. 2011, IntechOpen.

42. Alberts, B., et al., *Essential cell biology*. 2014.

43. Pai, A.S. and C.M. Giachelli, *Matrix remodeling in vascular calcification associated with chronic kidney disease.* Journal of the American Society of Nephrology, 2010. **21**(10): p. 1637-1640.

44. Dao, H.H., et al., *Evolution and modulation of age-related medial elastocalcinosis: impact on large artery stiffness and isolated systolic hypertension.* Cardiovascular research, 2005. **66**(2): p. 307-317.

45. Edmonds, M., *Medial arterial calcification and diabetes mellitus.* Zeitschrift für Kardiologie, 2000. **89**(2): p. S101-S104.

46. Salusky, I.B. and W.G. Goodman, *Cardiovascular calcification in end-stage renal disease.* Nephrology Dialysis Transplantation, 2002. **17**(2): p. 336-339.

47. Aikawa, E., et al., *561 ARTERIAL AND AORTIC VALVE CALCIFICATION ABOLISHED BY ELASTOLYTIC CATHEPSIN S DEFICIENCY IN CHRONIC RENAL DISEASE.* Atherosclerosis Supplements, 2009. **10**(2): p. e329.

48. Sun, J., et al., *Mast cells modulate the pathogenesis of elastase-induced abdominal aortic aneurysms in mice.* The Journal of clinical investigation, 2007. **117**(11): p. 3359-3368.

49. Libby, P., P.M. Ridker, and A. Maseri, *Inflammation and atherosclerosis.* Circulation, 2002. **105**(9): p. 1135-1143.

50. Sims, F.H., *The initiation of intimal thickening in human arteries.* Pathology, 2000. **32**(3): p. 171-175.

51. Hoerger, T.J., et al., *The future burden of CKD in the United States: a simulation model for the CDC CKD Initiative.* American Journal of Kidney Diseases, 2015. **65**(3): p. 403-411.

52. The Lancet. *Chronic Kidney Disease*. 2017, March 25; Available from: https://www.thelancet.com/journals/lancet/article/PIIS0140-6736(16)32064-5/fulltext.

53. Webster, A.C., et al., *Chronic kidney disease.* The Lancet, 2017. **389**(10075): p. 1238-1252.

54. National Institute Of Diabetes and Digestive and Kidney Diseases. *Kidney Disease Statistics for the United States*. December 1, 2016; Available from: https://www.niddk.nih.gov/health-information/health-statistics/kidney-disease.

55. Kearney, P.M., et al., *Global burden of hypertension: analysis of worldwide data.* The lancet, 2005. **365**(9455): p. 217-223.

56. Jha, V., et al., *Chronic kidney disease: global dimension and perspectives.* The Lancet, 2013. **382**(9888): p. 260-272.

57. Levey, A.S. and J. Coresh, *Chronic kidney disease.* Lancet, 2012. **379**(9811): p. 165-80.

58. Hsu, C.Y., et al., *The risk of acute renal failure in patients with chronic kidney disease.* Kidney Int, 2008. **74**(1): p. 101-7.

59. James, M.T., et al., *Glomerular filtration rate, proteinuria, and the incidence and consequences of acute kidney injury: a cohort study.* Lancet, 2010. **376**(9758): p. 2096-103.

60. James, M.T., et al., *CKD and risk of hospitalization and death with pneumonia.* Am J Kidney Dis, 2009. **54**(1): p. 24-32.

61. Hailpern, S.M., et al., *Moderate chronic kidney disease and cognitive function in adults 20 to 59 years of age: Third National Health and Nutrition Examination Survey (NHANES III).* J Am Soc Nephrol, 2007. **18**(7): p. 2205-13.

62. Kittiskulnam, P., A. Sheshadri, and K.L. Johansen, *Consequences of CKD on Functioning.* Semin Nephrol, 2016. **36**(4): p. 305-18.

63. Wilhelm-Leen, E.R., et al., *Frailty and chronic kidney disease: the Third National Health and Nutrition Evaluation Survey.* Am J Med, 2009. **122**(7): p. 664-71 e2.

64. Matsushita, K., et al., *Association of estimated glomerular filtration rate and albuminuria with all-cause and cardiovascular mortality in general population cohorts: a collaborative meta-analysis.* Lancet, 2010. **375**(9731): p. 2073-2081.

65. Tonelli, M., et al., *Chronic kidney disease and mortality risk: A systematic review.* Journal of the American Society of Nephrology, 2006. **17**(7): p. 2034-2047.

66. Fox, C.S., et al., *Associations of kidney disease measures with mortality and end-stage renal disease in individuals with and without diabetes: a meta-analysis.* Lancet, 2012. **380**(9854): p. 1662-73.

67. Go, A.S., et al., *Chronic kidney disease and the risks of death, cardiovascular events, and hospitalization.* New England Journal of Medicine, 2004. **351**(13): p. 1296-1305.

68. Kendrick, J. and M.B. Chonchol, *Nontraditional risk factors for cardiovascular disease in patients with chronic kidney disease.* Nature Reviews Nephrology, 2008. **4**(12): p. 672.

69. Weiner, D.E., et al., *The relationship between nontraditional risk factors and outcomes in individuals with stage 3 to 4 CKD.* American Journal of Kidney Diseases, 2008. **51**(2): p. 212-223.

70. Muntner, P., et al., *Traditional and nontraditional risk factors predict coronary heart disease in chronic kidney disease: results from the atherosclerosis risk in communities study.* Journal of the American Society of Nephrology, 2005. **16**(2): p. 529-538.

71. Ketteler, M., G. Schlieper, and J. Floege, *Calcification and cardiovascular health - New insights into an old phenomenon.* Hypertension, 2006. **47**(6): p. 1027-1034.

72. London, G.M., et al., *Arterial media calcification in end-stage renal disease: impact on all-cause and cardiovascular mortality.* Nephrol Dial Transplant, 2003. **18**(9): p. 1731-40.

73. Lanzer, P., et al., *Medial vascular calcification revisited: review and perspectives.* European Heart Journal, 2014. **35**(23): p. 1515-U24.

74. Brandenburg, V.M., et al., *Calcific uraemic arteriolopathy: a rare disease with a potentially high impact on chronic kidney disease-mineral and bone disorder.* Pediatr Nephrol, 2014. **29**(12): p. 2289-98.

75. Johnson, R.C., J.A. Leopold, and J. Loscalzo, *Vascular calcification: pathobiological mechanisms and clinical implications.* Circ Res, 2006. **99**(10): p. 1044-59.

76. Blacher, J., et al., *Arterial calcifications, arterial stiffness, and cardiovascular risk in end-stage renal disease.* Hypertension, 2001. **38**(4): p. 938-42.

77. Schlieper, G., et al., *Vascular calcification in chronic kidney disease: an update.* Nephrol Dial Transplant, 2015.

78. Schlieper, G., et al., *The vulnerable patient with chronic kidney disease.* Nephrol Dial Transplant, 2015.

79. Moe, S.M. and N.X. Chen, *Mechanisms of vascular calcification in chronic kidney disease.* J Am Soc Nephrol, 2008. **19**(2): p. 213-6.

80. Thompson, B. and D.A. Towler, *Arterial calcification and bone physiology: role of the bone-vascular axis.* Nat Rev Endocrinol, 2012. **8**(9): p. 529-43.

81. Mizobuchi, M., D. Towler, and E. Slatopolsky, *Vascular Calcification: The Killer of Patients with Chronic Kidney Disease.* Journal of the American Society of Nephrology, 2009. **20**(7): p. 1453-1464.

82. Savage, T., et al., *Calcified plaque is common in the carotid and femoral arteries of dialysis patients without clinical vascular disease.* Nephrol Dial Transplant, 1998. **13**(8): p. 2004-12.

83. London, G.M., *Cardiovascular disease in chronic renal failure: Pathophysiologic aspects.* Seminars in Dialysis, 2003. **16**(2): p. 85-94.

84. Luo, G.B., et al., *Spontaneous calcification of arteries and cartilage in mice lacking matrix GLA protein.* Nature, 1997. **386**(6620): p. 78-81.

85. Westenfeld, R., et al., *Fetuin-A protects against atherosclerotic calcification in CKD.* J Am Soc Nephrol, 2009. **20**(6): p. 1264-74.

86. Hu, M.C., et al., *Klotho deficiency causes vascular calcification in chronic kidney disease.* Journal of the American Society of Nephrology, 2011. **22**(1): p. 124-136.

87. O'Neill, W.C., M.K. Sigrist, and C.W. McIntyre, *Plasma pyrophosphate and vascular calcification in chronic kidney disease.* Nephrology Dialysis Transplantation, 2010. **25**(1): p. 187-191.

88. Speer, M.Y., et al., *Inactivation of the osteopontin gene enhances vascular calcification of matrix Gla protein-deficient mice: Evidence for osteopontin as an inducible inhibitor of vascular calcification in vivo.* Journal of Experimental Medicine, 2002. **196**(8): p. 1047-1055.

89. Bucay, N., et al., *osteoprotegerin-deficient mice develop early onset osteoporosis and arterial calcification.* Genes & Development, 1998. **12**(9): p. 1260-1268.

90. Speer, M.Y., et al., *Runx2/Cbfa1, but not loss of myocardin, is required for smooth muscle cell lineage reprogramming toward osteochondrogenesis.* Journal of cellular biochemistry, 2010. **110**(4): p. 935-947.

91. Moe, S.M., et al., *Medial artery calcification in ESRD patients is associated with deposition of bone matrix proteins.* Kidney international, 2002. **61**(2): p. 638-647.

92. Jono, S., C. Peinado, and C.M. Giachelli, *Phosphorylation of osteopontin is required for inhibition of vascular smooth muscle cell calcification.* Journal of Biological Chemistry, 2000. **275**(26): p. 20197-20203.

93. Tyson, K.L., et al., *Osteo/chondrocytic transcription factors and their target genes exhibit distinct patterns of expression in human arterial calcification.* Arteriosclerosis, thrombosis, and vascular biology, 2003. **23**(3): p. 489-494.

94. Shanahan, C.M., et al., *Arterial Calcification in Chronic Kidney Disease: Key Roles for Calcium and Phosphate.* Circulation Research, 2011. **109**(6): p. 697-711.

95. Steitz, S.A., et al., *Smooth muscle cell phenotypic transition associated with calcification: upregulation of Cbfa1 and downregulation of smooth muscle lineage markers.* Circulation research, 2001. **89**(12): p. 1147-1154.

96. Bouvet, C., et al., *Sequential activation of matrix metalloproteinase 9 and transforming growth factor β in arterial elastocalcinosis.* Arteriosclerosis, thrombosis, and vascular biology, 2008. **28**(5): p. 856-862.

97. Chen, N.X., et al., *Activation of arterial matrix metalloproteinases leads to vascular calcification in chronic kidney disease.* American journal of nephrology, 2011. **34**(3): p. 211-219.

98. Basalyga, D.M., et al., *Elastin degradation and calcification in an abdominal aorta injury model: role of matrix metalloproteinases.* Circulation, 2004. **110**(22): p. 3480-3487.

99. Chung, A.W., et al., *Upregulation of matrix metalloproteinase-2 in the arterial vasculature contributes to stiffening and vasomotor dysfunction in patients with chronic kidney disease.* Circulation, 2009. **120**(9): p. 792.

100. Chung, A.W., et al., *Matrix metalloproteinase-2 and-9 exacerbate arterial stiffening and angiogenesis in diabetes and chronic kidney disease.* Cardiovascular research, 2009. **84**(3): p. 494-504.

101. Dudenbostel, T. and S.P. Glasser, *Effects of antihypertensive drugs on arterial stiffness.* Cardiology in review, 2012. **20**(5).

102. Rattazzi, M., et al., *Hypertension and vascular calcification: a vicious cycle?* Journal of hypertension, 2012. **30**(10): p. 1885-1893.

103. Motro, M. and J. Shemesh, *Calcium channel blocker nifedipine slows down progression of coronary calcification in hypertensive patients compared with diuretics.* Hypertension, 2001. **37**(6): p. 1410-3.

104. London, G.M., et al., *Cardiac hypertrophy, aortic compliance, peripheral resistance, and wave reflection in end-stage renal disease. Comparative effects of ACE inhibition and calcium channel blockade.* Circulation, 1994. **90**(6): p. 2786-96.

105. Deary, A.J., et al., *Double-blind, placebo-controlled crossover comparison of five classes of antihypertensive drugs.* J Hypertens, 2002. **20**(4): p. 771-7.

106. Bruining, N., et al., *Coronary calcium significantly affects quantitative analysis of coronary ultrasound: importance for atherosclerosis progression/regression studies.* Coron Artery Dis, 2009. **20**(6): p. 409-14.

107. Maahs, D.M., et al., *ACE-I/ARB treatment in type 1 diabetes patients with albuminuria is associated with lower odds of progression of coronary artery calcification.* J Diabetes Complications, 2007. **21**(5): p. 273-9.

108. Frimodt-Moller, M., et al., *Beneficial effects on arterial stiffness and pulse-wave reflection of combined enalapril and candesartan in chronic kidney disease--a randomized trial.* PLoS One, 2012. **7**(7): p. e41757.

109. Isakova, T., et al., *Pilot study of dietary phosphorus restriction and phosphorus binders to target fibroblast growth factor 23 in patients with chronic kidney disease.* Nephrol Dial Transplant, 2011. **26**(2): p. 584-91.

110. Hutchison, A.J., C.P. Smith, and P.E. Brenchley, *Pharmacology, efficacy and safety of oral phosphate binders.* Nat Rev Nephrol, 2011. **7**(10): p. 578-89.

111. Chertow, G.M., et al., *Sevelamer attenuates the progression of coronary and aortic calcification in hemodialysis patients.* Kidney Int, 2002. **62**(1): p. 245-52.

112. Block, G.A., et al., *Effects of sevelamer and calcium on coronary artery calcification in patients new to hemodialysis.* Kidney Int, 2005. **68**(4): p. 1815-24.

113. Russo, D., et al., *The progression of coronary artery calcification in predialysis patients on calcium carbonate or sevelamer.* Kidney Int, 2007. **72**(10): p. 1255-61.

114. Teng, M., et al., *Survival of patients undergoing hemodialysis with paricalcitol or calcitriol therapy.* N Engl J Med, 2003. **349**(5): p. 446-56.

115. Tentori, F., et al., *Mortality risk among hemodialysis patients receiving different vitamin D analogs.* Kidney Int, 2006. **70**(10): p. 1858-65.

116. Ogawa, T., et al., *Relation of oral 1alpha-hydroxy vitamin D3 to the progression of aortic arch calcification in hemodialysis patients.* Heart Vessels, 2010. **25**(1): p. 1-6.

117. Sprague, S.M., et al., *Paricalcitol versus calcitriol in the treatment of secondary hyperparathyroidism.* Kidney Int, 2003. **63**(4): p. 1483-90.

118. Raggi, P., et al., *The ADVANCE study: a randomized study to evaluate the effects of cinacalcet plus low-dose vitamin D on vascular calcification in patients on hemodialysis.* Nephrol Dial Transplant, 2011. **26**(4): p. 1327-39.

119. Investigators, E.T., et al., *Effect of cinacalcet on cardiovascular disease in patients undergoing dialysis.* N Engl J Med, 2012. **367**(26): p. 2482-94.

120. Bleyer, A.J., et al., *Changes in cardiovascular calcification after parathyroidectomy in patients with ESRD.* Am J Kidney Dis, 2005. **46**(3): p. 464-9.

121. Iwamoto, N., et al., *Total parathyroidectomy improves survival of hemodialysis patients with secondary hyperparathyroidism.* J Nephrol, 2012. **25**(5): p. 755-63.

122. Nitta, K., et al., *Effects of cyclic intermittent etidronate therapy on coronary artery calcification in patients receiving long-term hemodialysis.* Am J Kidney Dis, 2004. **44**(4): p. 680-8.

123. Hashiba, H., et al., *Inhibition of the progression of aortic calcification by etidronate treatment in hemodialysis patients: long-term effects.* Ther Apher Dial, 2006. **10**(1): p. 59-64.

124. Ariyoshi, T., et al., *Effect of etidronic acid on arterial calcification in dialysis patients.* Clin Drug Investig, 2006. **26**(4): p. 215-22.

125. Toussaint, N.D., et al., *Effect of alendronate on vascular calcification in CKD stages 3 and 4: a pilot randomized controlled trial.* Am J Kidney Dis, 2010. **56**(1): p. 57-68.

126. Araya, C.E., et al., *Sodium thiosulfate treatment for calcific uremic arteriolopathy in children and young adults.* Clin J Am Soc Nephrol, 2006. **1**(6): p. 1161-6.

127. Mataic, D. and B. Bastani, *Intraperitoneal sodium thiosulfate for the treatment of calciphylaxis.* Ren Fail, 2006. **28**(4): p. 361-3.

128. Adirekkiat, S., et al., *Sodium thiosulfate delays the progression of coronary artery calcification in haemodialysis patients.* Nephrol Dial Transplant, 2010. **25**(6): p. 1923-9.

129. Mathews, S.J., et al., *Effects of sodium thiosulfate on vascular calcification in end-stage renal disease: a pilot study of feasibility, safety and efficacy.* Am J Nephrol, 2011. **33**(2): p. 131-8.

130. Simpson, C.L., et al., *Toward cell therapy for vascular calcification: osteoclast-mediated demineralization of calcified elastin.* Cardiovasc Pathol, 2007. **16**(1): p. 29-37.

131. Basalyga, D.M., et al., *Elastin degradation and calcification in an abdominal aorta injury model: role of matrix metalloproteinases.* Circulation, 2004. **110**(22): p. 3480-7.

132. Ikonomidis, J.S., et al., *A murine model of thoracic aortic aneurysms.* J Surg Res, 2003. **115**(1): p. 157-63.

133. Lai, C.H., et al., *Recombinant human thrombomodulin suppresses experimental abdominal aortic aneurysms induced by calcium chloride in mice.* Ann Surg, 2013. **258**(6): p. 1103-10.

134. Price, P.A., S.A. Faus, and M.K. Williamson, *Warfarin causes rapid calcification of the elastic lamellae in rat arteries and heart valves.* Arterioscler Thromb Vasc Biol, 1998. **18**(9): p. 1400-7.

135. Bouvet, C., et al., *A new rat model of diabetic macrovascular complication.* Cardiovasc Res, 2007. **73**(3): p. 504-11.

136. Bostrom, K. and L.L. Demer, *Regulatory mechanisms in vascular calcification.* Crit Rev Eukaryot Gene Expr, 2000. **10**(2): p. 151-8.

137. Price, P.A., et al., *Osteoprotegerin inhibits artery calcification induced by warfarin and by vitamin D.* Arterioscler Thromb Vasc Biol, 2001. **21**(10): p. 1610-6.

138. Bas, A., et al., *Reversibility of calcitriol-induced medial artery calcification in rats with intact renal function.* J Bone Miner Res, 2006. **21**(3): p. 484-90.

139. Niederhoffer, N., et al., *Aortic calcification produced by vitamin D3 plus nicotine.* J Vasc Res, 1997. **34**(5): p. 386-98.

140. Adijiang, A., et al., *Indoxyl sulphate promotes aortic calcification with expression of osteoblast-specific proteins in hypertensive rats.* Nephrol Dial Transplant, 2008. **23**(6): p. 1892-901.

141. Ding, Y.H., et al., *Modified technique to create morphologically reproducible elastase-induced aneurysms in rabbits.* Neuroradiology, 2006. **48**(8): p. 528-32.

142. Trollope, A., et al., *Animal models of abdominal aortic aneurysm and their role in furthering management of human disease.* Cardiovascular Pathology, 2011. **20**(2): p. 114-123.

143. Razzaque, M.S., et al., *Premature aging-like phenotype in fibroblast growth factor 23 null mice is a vitamin D-mediated process.* Faseb Journal, 2006. **20**(1): p. 720-+.

144. Kuro-o, M., et al., *Mutation of the mouse klotho gene leads to a syndrome resembling ageing.* Nature, 1997. **390**(6655): p. 45-51.

145. Westenfeld, R., et al., *Fetuin-A (AHSG) prevents extraosseous calcification induced by uraemia and phosphate challenge in mice.* Nephrol Dial Transplant, 2007. **22**(6): p. 1537-46.

146. Paigen, B., et al., *Variation in Susceptibility to Atherosclerosis among Inbred Strains of Mice.* Atherosclerosis, 1985. **57**(1): p. 65-73.

147. Reddick, R.L., S.H. Zhang, and N. Maeda, *Atherosclerosis in mice lacking apo E. Evaluation of lesional development and progression.* Arterioscler Thromb, 1994. **14**(1): p. 141-7.

148. Bro, S., et al., *Chronic renal failure accelerates atherogenesis in apolipoprotein E-deficient mice.* J Am Soc Nephrol, 2003. **14**(10): p. 2466-74.

149. Ishibashi, S., et al., *Massive xanthomatosis and atherosclerosis in cholesterol-fed low density lipoprotein receptor-negative mice.* J Clin Invest, 1994. **93**(5): p. 1885-93.

150. Davies, M.R., R.J. Lund, and K.A. Hruska, *BMP-7 is an efficacious treatment of vascular calcification in a murine model of atherosclerosis and chronic renal failure.* Journal of the American Society of Nephrology, 2003. **14**(6): p. 1559-1567.

151. Schafer, C., et al., *The serum protein alpha(2)-Heremans-Schmid glycoprotein/fetuin-A is a systemically acting inhibitor of ectopic calcification.* Journal of Clinical Investigation, 2003. **112**(3): p. 357-366.

152. Stubbs, J.R., et al., *Role of hyperphosphatemia and 1,25-dihydroxyvitamin D in vascular calcification and mortality in fibroblastic growth factor 23 null mice.* Journal of the American Society of Nephrology, 2007. **18**(7): p. 2116-2124.

153. Haffner, D., et al., *Systemic cardiovascular disease in uremic rats induced by 1,25(OH)2D3.* J Hypertens, 2005. **23**(5): p. 1067-75.

154. Kawata, T., et al., *Cinacalcet suppresses calcification of the aorta and heart in uremic rats.* Kidney Int, 2008. **74**(10): p. 1270-7.

155. Neves, K.R., et al., *Vascular calcification: contribution of parathyroid hormone in renal failure.* Kidney Int, 2007. **71**(12): p. 1262-70.

156. Katsumata, K., et al., *Sevelamer hydrochloride prevents ectopic calcification and renal osteodystrophy in chronic renal failure rats.* Kidney International, 2003. **64**(2): p. 441-450.

157. Price, P.A., A.M. Roublick, and M.K. Williamson, *Artery calcification in uremic rats is increased by a low protein diet and prevented by treatment with ibandronate.* Kidney International, 2006. **70**(9): p. 1577-1583.

158. Terai, K., et al., *Vascular calcification and secondary hyperparathyroidism of severe chronic kidney disease and its relation to serum phosphate and calcium levels.* British Journal of Pharmacology, 2009. **156**(8): p. 1267-1278.

159. Neven, E., et al., *Adequate phosphate binding with lanthanum carbonate attenuates arterial calcification in chronic renal failure rats.* Nephrology Dialysis Transplantation, 2009. **24**(6): p. 1790-1799.

160. Chanutin, A. and E.B. FERRIS, *Experimental renal insufficiency produced by partial nephrectomy: I. Control diet.* Archives of Internal Medicine, 1932. **49**(5): p. 767-787.

161. Ejerblad, S., I. Eriksson, and H. Johansson, *Uræmic arterial disease: an experimental study with special reference to the effect of parathyroidectomy.* Scandinavian journal of urology and nephrology, 1979. **13**(2): p. 161-169.

162. Gagnon, R.F. and W.P. Duguid, *A reproducible model for chronic renal failure in the mouse.* Urol Res, 1983. **11**(1): p. 11-4.

163. Shobeiri, N., M.A. Adams, and R.M. Holden, *Vascular calcification in animal models of CKD: a review.* American journal of nephrology, 2010. **31**(6): p. 471-481.

164. Kaspareit-Rittinghausen, J., F. Deerberg, and A. Wcislo, *Hereditary polycystic kidney disease. Adult polycystic kidney disease associated with renal hypertension, renal osteodystrophy, and uremic enteritis in SPRD rats.* Am J Pathol, 1991. **139**(3): p. 693-6.

165. Brown, J.H., et al., *Missense mutation in sterile alpha motif of novel protein SamCystin is associated with polycystic kidney disease in (cy/+) rat.* J Am Soc Nephrol, 2005. **16**(12): p. 3517-26.

166. Moe, S.M., et al., *A rat model of chronic kidney disease-mineral bone disorder.* Kidney Int, 2009. **75**(2): p. 176-84.

167. de Vries, A. and O. Sperling, *Implications of disorders of purine metabolism for the kidney and the urinary tract.* Ciba Found Symp, 1977(48): p. 179-206.

168. Fye, K.H., et al., *Adenine phosphoribosyltransferase deficiency with renal deposition of 2,8-dihydroxyadenine leading to nephrolithiasis and chronic renal failure.* Arch Intern Med, 1993. **153**(6): p. 767-70.

169. Yokozawa, T., et al., *Animal model of adenine-induced chronic renal failure in rats.* Nephron, 1986. **44**(3): p. 230-4.

170. Okada, H., et al., *Reversibility of adenine-induced renal failure in rats.* Clinical and Experimental Nephrology, 1999. **3**(2): p. 82-88.

171. Henley, C., et al., *The calcimimetic AMG 641 abrogates parathyroid hyperplasia, bone and vascular calcification abnormalities in uremic rats.* Eur J Pharmacol, 2009. **616**(1-3): p. 306-13.

172. Matsui, I., et al., *Fully phosphorylated fetuin-A forms a mineral complex in the serum of rats with adenine-induced renal failure.* Kidney Int, 2009. **75**(9): p. 915-28.

173. Tamagaki, K., et al., *Severe hyperparathyroidism with bone abnormalities and metastatic calcification in rats with adenine-induced uraemia.* Nephrol Dial Transplant, 2006. **21**(3): p. 651-9.

174. Neven, E., et al., *Endochondral bone formation is involved in media calcification in rats and in men.* Kidney Int, 2007. **72**(5): p. 574-81.

175. Lomashvili, K.A., et al., *Effect of bisphosphonates on vascular calcification and bone metabolism in experimental renal failure.* Kidney Int, 2009. **75**(6): p. 617-25.

176. Neven, E. and P.C. D'Haese, *Vascular calcification in chronic renal failure: what have we learned from animal studies?* Circ Res, 2011. **108**(2): p. 249-64.

177. Lomashvili, K.A., et al., *Effect of bisphosphonates on vascular calcification and bone metabolism in experimental renal failure.* Kidney International, 2009. **75**(6): p. 617-625.

178. Yamada, S., et al., *The antioxidant tempol ameliorates arterial medial calcification in uremic rats: important role of oxidative stress in the pathogenesis of vascular calcification in chronic kidney disease.* J Bone Miner Res, 2012. **27**(2): p. 474-85.

179. Pasch, A., et al., *Sodium thiosulfate prevents vascular calcifications in uremic rats.* Kidney International, 2008. **74**(11): p. 1444-1453.

180. Morgan, G.T. and H.D.K. Drew, *CLXII.—Researches on residual affinity and co-ordination. Part II. Acetylacetones of selenium and tellurium.* Journal of the Chemical Society, Transactions, 1920. **117**: p. 1456-1465.

181. *Stability, Chelation and the Chelate Effect*. 1995, May Available from: http://wwwchem.uwimona.edu.jm/courses/chelate.html.

182. Paolieri, M., *Ferdinand Münz: EDTA and 40 years of inventions.* Bulletin for the History of Chemistry, 2017. **42**: p. 133-140.

183. Peters, R.A., L.A. Stocken, and R. Thompson, *British anti-lewisite (BAL).* Nature, 1945. **156**(3969): p. 616.

184. Flora, S.J. and V. Pachauri, *Chelation in metal intoxication.* International journal of environmental research and public health, 2010. **7**(7): p. 2745-2788.

185. Wax, P.M. *Current use of chelation in American health care*. in *Journal of Medical Toxicology*. 2013. Springer.

186. Aaseth, J., et al., *Chelation in metal intoxication—principles and paradigms.* Journal of Trace Elements in medicine and Biology, 2015. **31**: p. 260-266.

187. Seely, D.M., P. Wu, and E.J. Mills, *EDTA chelation therapy for cardiovascular disease: a systematic review.* BMC Cardiovasc Disord, 2005. **5**: p. 32.

188. Clarke, C.N., N.E. Clarke, and R.E. Mosher, *Treatment of angina pectoris with disodium ethylene diamine tetraacetic acid.* Am J Med Sci, 1956. **232**(6): p. 654-66.

189. Sucu, N., et al., *Two stage EDTA anti-calcification method for bioprosthetic heart valve materials.* Med Sci Monit, 2006. **12**(6): p. MT33-8.

190. Lamas, G.A., et al., *Effect of disodium EDTA chelation regimen on cardiovascular events in patients with previous myocardial infarction: the TACT randomized trial.* JAMA, 2013. **309**(12): p. 1241-50.

191. Araki, S., H. Aono, and K. Murata, *Mobilisation of heavy metals into the urine by CaEDTA: relation to erythrocyte and plasma concentrations and exposure indicators.* Br J Ind Med, 1986. **43**(9): p. 636-41.

192. Flora, G.J., et al., *Therapeutic efficacy of combined meso 2,3-dimercaptosuccinic acid and calcium disodium edetate treatment during acute lead intoxication in rats.* Hum Exp Toxicol, 1995. **14**(5): p. 410-3.

193. Leckie, W.J. and S.L. Tompsett, *The diagnostic and therapeutic use of edathamil calcium disodium (EDTA, versene) in excessive inorganic lead absorption.* Q J Med, 1958. **27**(105): p. 65-82.

194. Hayden, M.R., et al., *Vascular ossification–calcification in metabolic syndrome, type 2 diabetes mellitus, chronic kidney disease, and calciphylaxis–calcific uremic arteriolopathy: the emerging role of sodium thiosulfate.* Cardiovascular diabetology, 2005. **4**(1): p. 4.

195. Bebarta, V.S., et al., *Hydroxocobalamin versus sodium thiosulfate for the treatment of acute cyanide toxicity in a swine (Sus scrofa) model.* Annals of emergency medicine, 2012. **59**(6): p. 532-539.

196. Caravan, P., et al., *Gadolinium (III) chelates as MRI contrast agents: structure, dynamics, and applications.* Chemical reviews, 1999. **99**(9): p. 2293-2352.

197. Brown, M.A., A. Paulenova, and A.V. Gelis, *Aqueous complexation of thorium (IV), uranium (IV), neptunium (IV), plutonium (III/IV), and cerium (III/IV) with DTPA.* Inorganic chemistry, 2012. **51**(14): p. 7741-7748.

198. Flora, S.J. and V. Pachauri, *Chelation in metal intoxication.* Int J Environ Res Public Health, 2010. **7**(7): p. 2745-88.

199. Leggio, L., et al., *Wilson's disease: clinical, genetic and pharmacological findings.* Int J Immunopathol Pharmacol, 2005. **18**(1): p. 7-14.

200. Goldman, M. and J.C. Dacre, *Lewisite: its chemistry, toxicology, and biological effects.* Rev Environ Contam Toxicol, 1989. **110**: p. 75-115.

201. Vilensky, J.A. and K. Redman, *British anti-Lewisite (dimercaprol): an amazing history.* Ann Emerg Med, 2003. **41**(3): p. 378-83.

202. Smith, D. and B.J. Strupp, *The scientific basis for chelation: animal studies and lead chelation.* J Med Toxicol, 2013. **9**(4): p. 326-38.

203. Graziano, J.H., *Role of 2,3-dimercaptosuccinic acid in the treatment of heavy metal poisoning.* Med Toxicol, 1986. **1**(3): p. 155-62.

204. Archbold, G.P., R.M. McGuckin, and N.A. Campbell, *Dimercaptosuccinic acid loading test for assessing mercury burden in healthy individuals.* Ann Clin Biochem, 2004. **41**(Pt 3): p. 233-6.

205. Guha Mazumder, D.N., et al., *Randomized placebo-controlled trial of 2,3-dimercapto-1-propanesulfonate (DMPS) in therapy of chronic arsenicosis due to drinking arsenic-contaminated water.* J Toxicol Clin Toxicol, 2001. **39**(7): p. 665-74.

206. Rencova, J., et al., *Decorporation of polonium from rats by new chelating agents.* Radiation protection dosimetry, 1994. **53**(1-4): p. 311-313.

207. Peterson, R.G. and B.H. Rumack, *D-penicillamine therapy of acute arsenic poisoning.* J Pediatr, 1977. **91**(4): p. 661-6.

208. Rousseaux, C.G. and L.G. MacNabb, *Oral administration of D-penicillamine causes neonatal mortality without morphological defects in CD-1 mice.* J Appl Toxicol, 1992. **12**(1): p. 35-8.

209. Hoffbrand, A.V., A. Cohen, and C. Hershko, *Role of deferiprone in chelation therapy for transfusional iron overload.* Blood, 2003. **102**(1): p. 17-24.

210. Wu, H., et al., *Iron toxicity in mice with collagenase-induced intracerebral hemorrhage.* J Cereb Blood Flow Metab, 2011. **31**(5): p. 1243-50.

211. Lamas, G.A., et al., *Effect of disodium EDTA chelation regimen on cardiovascular events in patients with previous myocardial infarction: the TACT randomized trial.* Jama, 2013. **309**(12): p. 1241-1250.

212. Clarke, N.E., Sr., *Atherosclerosis, occlusive vascular disease and EDTA.* Am J Cardiol, 1960. **6**: p. 233-6.

213. BECHTEL, J.T., J.E. WHITE, and E.H. ESTES JR, *The electrocardiographic effects of hypocalcemia induced in normal subjects with edathamil disodium.* Circulation, 1956. **13**(6): p. 837-842.

214. BESSMAN, S.P. and N.J. DOORENBOS, *Chelation.* Annals of internal medicine, 1957. **47**(5): p. 1036-1041.

215. Szekely, P. and N. Wynne, *Effects of calcium chelation on digitalis-induced cardiac arrhythmias.* British heart journal, 1963. **25**(5): p. 589.

216. Wilder, L.W., et al., *Mobilization of atherosclerotic plaque calcium with EDTA utilizing the isolation-perfusion principle.* Surgery, 1962. **52**(5): p. 793-795.

217. Boyle, A., et al. *Chelation therapy in circulatory and sclerosing diseases*. in *Federation proceedings*. 1961.

218. Olszewer, E., F.C. Sabbag, and J.P. Carter, *A pilot double-blind study of sodium-magnesium EDTA in peripheral vascular disease.* J Natl Med Assoc, 1990. **82**(3): p. 173-7.

219. McDonagh, E., C. Rudolph, and E. Cheraskin, *An oculocerebrovasculometric analysis of the improvement in arterial stenosis following EDTA chelation therapy.* J Holistic Med, 1982. **4**(1): p. 21-23.

220. Hancke, C. and K. Flytlie, *[Manipulation with EDTA].* Ugeskr Laeger, 1992. **154**(32): p. 2213-5.

221. Green, S. and W. Sampson, *EDTA chelation therapy for atherosclerosis and degenerative diseases: implausibility and paradoxical oxidant effects.* SCIENTIFIC REVIEW OF ALTERNATIVE MEDICINE AND ABERRANT MEDICAL PRACTICES, 2002. **6**(1): p. 17-22.

222. Guldager, B., et al., *EDTA treatment of intermittent claudication--a double-blind, placebo-controlled study.* J Intern Med, 1992. **231**(3): p. 261-7.

223. van Rij, A.M., et al., *Chelation therapy for intermittent claudication. A double-blind, randomized, controlled trial.* Circulation, 1994. **90**(3): p. 1194-9.

224. Knudtson, M.L., et al., *Chelation therapy for ischemic heart disease: a randomized controlled trial.* JAMA, 2002. **287**(4): p. 481-6.

225. Escolar, E., et al., *The effect of an EDTA-based chelation regimen on patients with diabetes mellitus and prior myocardial infarction in the Trial to Assess Chelation Therapy (TACT).* Circ Cardiovasc Qual Outcomes, 2014. **7**(1): p. 15-24.

226. Avila, M.D., E. Escolar, and G.A. Lamas, *Chelation therapy after the trial to assess chelation therapy: results of a unique trial.* Curr Opin Cardiol, 2014. **29**(5): p. 481-8.

227. Gupta, A.S., *Nanomedicine approaches in vascular disease: a review.* Nanomedicine: Nanotechnology, Biology and Medicine, 2011. **7**(6): p. 763-779.

228. Smith, B.R. and S.S. Gambhir, *Nanomaterials for in vivo imaging.* Chemical reviews, 2017. **117**(3): p. 901-986.

229. de La Zerda, A. and S.S. Gambhir, *Drug delivery: keeping tabs on nanocarriers.* Nature nanotechnology, 2007. **2**(12): p. 745.

230. Wilczewska, A.Z., et al., *Nanoparticles as drug delivery systems.* Pharmacological reports, 2012. **64**(5): p. 1020-1037.

231. Ding, B.-S., et al., *Advanced drug delivery systems that target the vascular endothelium.* Molecular interventions, 2006. **6**(2): p. 98.

232. Flores, A.M., et al., *Nanoparticle therapy for vascular diseases.* Arteriosclerosis, thrombosis, and vascular biology, 2019. **39**(4): p. 635-646.

233. Owens III, D.E. and N.A. Peppas, *Opsonization, biodistribution, and pharmacokinetics of polymeric nanoparticles.* International journal of pharmaceutics, 2006. **307**(1): p. 93-102.

234. Sahoo, S.K. and V. Labhasetwar, *Nanotech approaches to drug delivery and imaging.* Drug discovery today, 2003. **8**(24): p. 1112-1120.

235. Suk, J.S., et al., *PEGylation as a strategy for improving nanoparticle-based drug and gene delivery.* Advanced drug delivery reviews, 2016. **99**: p. 28-51.

236. Danhier, F., O. Feron, and V. Préat, *To exploit the tumor microenvironment: passive and active tumor targeting of nanocarriers for anti-cancer drug delivery.* Journal of controlled release, 2010. **148**(2): p. 135-146.

237. Kobayashi, H., R. Watanabe, and P.L. Choyke, *Improving conventional enhanced permeability and retention (EPR) effects; what is the appropriate target?* Theranostics, 2014. **4**(1): p. 81.

238. Lombardo, D., M.A. Kiselev, and M.T. Caccamo, *Smart nanoparticles for drug delivery application: development of versatile nanocarrier platforms in biotechnology and nanomedicine.* Journal of Nanomaterials, 2019. **2019**.

239. D Friedman, A., S. E Claypool, and R. Liu, *The smart targeting of nanoparticles.* Current pharmaceutical design, 2013. **19**(35): p. 6315-6329.

240. Elzoghby, A.O., W.M. Samy, and N.A. Elgindy, *Albumin-based nanoparticles as potential controlled release drug delivery systems.* Journal of controlled release, 2012. **157**(2): p. 168-182.

241. Geny, B., et al., *Safety and efficacy of a new transpulmonary echo contrast agent in echocardiographic studies in patients.* Journal of the American College of Cardiology, 1993. **22**(4): p. 1193-1198.

242. Ibrahim, N.K., et al., *Phase I and pharmacokinetic study of ABI-007, a Cremophor-free, protein-stabilized, nanoparticle formulation of paclitaxel.* Clinical Cancer Research, 2002. **8**(5): p. 1038-1044.

243. Mansour, H.M., et al., *Materials for pharmaceutical dosage forms: molecular pharmaceutics and controlled release drug delivery aspects.* International journal of molecular sciences, 2010. **11**(9): p. 3298-3322.

244. Guldager, B., et al., *Effects of intravenous EDTA treatment on serum parathyroid hormone (1-84) and biochemical markers of bone turnover.* Dan Med Bull, 1993. **40**(5): p. 627-30.

245. Sinha, A., et al., *Nanoparticle targeting to diseased vasculature for imaging and therapy.* Nanomedicine, 2014. **10**(5): p. 1003-12.

246. Nosoudi, N., et al., *Prevention of abdominal aortic aneurysm progression by targeted inhibition of matrix metalloproteinase activity with batimastat-loaded nanoparticles.* Circ Res, 2015. **117**(11): p. e80-9.

247. Nosoudi, N., et al., *Systemic Delivery of Nanoparticles Loaded with Pentagalloyl Glucose Protects Elastic Lamina and Prevents Abdominal Aortic Aneurysm in Rats.* J Cardiovasc Transl Res, 2016. **9**(5-6): p. 445-455.

248. Nosoudi, N., et al., *Reversal of Vascular Calcification and Aneurysms in a Rat Model Using Dual Targeted Therapy with EDTA- and PGG-Loaded Nanoparticles.* Theranostics, 2016. **6**(11): p. 1975-1987.

249. Parasaram, V., et al., *Targeted drug delivery to emphysematous lungs: Inhibition of MMPs by doxycycline loaded nanoparticles.* Pulm Pharmacol Ther, 2016. **39**: p. 64-73.

250. Orlov, S.N., et al., *On the interrelation between calmodulin and EGTA in the regulation of the affinity to Ca2+ and the maximal activity of the erythrocyte-membrane calcium pump.* European journal of biochemistry, 1983. **132**(2): p. 315-319.

251. Gerig, J.T., et al., *Calcium complexation with a highly calcium selective chelator: crystal structure of Ca (CaFBAPTA)· 5H2O.* Journal of inorganic biochemistry, 1987. **31**(2): p. 113-121.

252. Wie, M.B., et al., *BAPTA/AM, an intracellular calcium chelator, induces delayed necrosis by lipoxygenase-mediated free radicals in mouse cortical cultures.* Progress in Neuro-Psychopharmacology and Biological Psychiatry, 2001. **25**(8): p. 1641-1659.

253. Tang, Q., et al., *The membrane permeable calcium chelator BAPTA-AM directly blocks human ether a-go-go-related gene potassium channels stably expressed in HEK 293 cells.* Biochemical pharmacology, 2007. **74**(11): p. 1596-1607.

254. Benjamin, E.J., et al., *Heart Disease and Stroke Statistics-2017 Update: A Report From the American Heart Association.* Circulation, 2017. **135**(10): p. e146-e603.

255. Mizobuchi, M., D. Towler, and E. Slatopolsky, *Vascular calcification: the killer of patients with chronic kidney disease.* J Am Soc Nephrol, 2009. **20**(7): p. 1453-64.

256. Leonard, O., J. Spaak, and D. Goldsmith, *Regression of vascular calcification in chronic kidney disease - feasible or fantasy? A review of the clinical evidence.* British Journal of Clinical Pharmacology, 2013. **76**(4): p. 560-572.

257. O'Neill, W.C. and K.A. Lomashvili, *Recent progress in the treatment of vascular calcification.* Kidney Int, 2010. **78**(12): p. 1232-9.

258. Lei, Y., et al., *Efficacy of reversal of aortic calcification by chelating agents.* Calcif Tissue Int, 2013. **93**(5): p. 426-35.

259. Lei, Y., N. Nosoudi, and N. Vyavahare, *Targeted chelation therapy with EDTA-loaded albumin nanoparticles regresses arterial calcification without causing systemic side effects.* Journal of Controlled Release, 2014. **196**: p. 79-86.

260. Shobeiri, N., M.A. Adams, and R.M. Holden, *Vascular calcification in animal models of CKD: A review.* Am J Nephrol, 2010. **31**(6): p. 471-81.

261. Diwan, V., et al., *Adenine-induced chronic kidney and cardiovascular damage in rats.* J Pharmacol Toxicol Methods, 2013. **68**(2): p. 197-207.

262. Jia, T., et al., *A novel model of adenine-induced tubulointerstitial nephropathy in mice.* BMC Nephrol, 2013. **14**: p. 116.

263. Weissleder, R., M. Nahrendorf, and M.J. Pittet, *Imaging macrophages with nanoparticles.* Nature Materials, 2014. **13**(2): p. 125-138.

264. Nie, S.M., *Understanding and overcoming major barriers in cancer nanomedicine.* Nanomedicine, 2010. **5**(4): p. 523-528.

265. Alexis, F., et al., *Factors affecting the clearance and biodistribution of polymeric nanoparticles.* Molecular Pharmaceutics, 2008. **5**(4): p. 505-515.

266. Guldager, B., et al., *Effects of Intravenous Edta Treatment on Serum Parathyroid-Hormone (1-84) and Biochemical Markers of Bone Turnover.* Danish Medical Bulletin, 1993. **40**(5): p. 627-630.

267. Holland, J.F., E. Danielson, and A. Sahagianedwards, *Use of Ethylene Diamine Tetra Acetic Acid in Hypercalcemic Patients.* Proceedings of the Society for Experimental Biology and Medicine, 1953. **84**(2): p. 359-364.

268. Chung, A.W., et al., *Matrix metalloproteinase-2 and -9 exacerbate arterial stiffening and angiogenesis in diabetes and chronic kidney disease.* Cardiovasc Res, 2009. **84**(3): p. 494-504.

269. Gendron, R., et al., *Inhibition of the activities of matrix metalloproteinases 2, 8, and 9 by chlorhexidine.* Clinical and Diagnostic Laboratory Immunology, 1999. **6**(3): p. 437-439.

270. Lowrey, G.E., et al., *MMP-9 protein level does not reflect overall MMP activity in the airways of patients with COPD.* Respiratory Medicine, 2008. **102**(6): p. 845-851.

271. Proudfoot, D., et al., *The role of apoptosis in the initiation of vascular calcification.* Z Kardiol, 2001. **90 Suppl 3**: p. 43-6.

272. Favreau, J.T., et al., *Murine ultrasound imaging for circumferential strain analyses in the angiotensin II abdominal aortic aneurysm model.* J Vasc Surg, 2012. **56**(2): p. 462-9.

273. Lei, Y., et al., *Hydroxyapatite and calcified elastin induce osteoblast-like differentiation in rat aortic smooth muscle cells.* Exp Cell Res, 2014. **323**(1): p. 198-208.

274. Nahar-Gohad, P., et al., *Rat aortic smooth muscle cells cultured on hydroxyapatite differentiate into osteoblast-like cells via BMP-2-SMAD-5 pathway.* Calcif Tissue Int, 2015. **96**(4): p. 359-69.

275. Reynolds, J.L., et al., *Human vascular smooth muscle cells undergo vesicle-mediated calcification in response to changes in extracellular calcium and phosphate concentrations: a potential mechanism for accelerated vascular calcification in ESRD.* J Am Soc Nephrol, 2004. **15**(11): p. 2857-67.

276. Iyemere, V.P., et al., *Vascular smooth muscle cell phenotypic plasticity and the regulation of vascular calcification.* J Intern Med, 2006. **260**(3): p. 192-210.

277. Ali, B.H., et al., *New model for adenine-induced chronic renal failure in mice, and the effect of gum acacia treatment thereon: comparison with rats.* J Pharmacol Toxicol Methods, 2013. **68**(3): p. 384-93.

278. Rabe, M. and F. Schaefer, *Non-Transgenic Mouse Models of Kidney Disease.* Nephron, 2016. **133**(1): p. 53-61.

279. Santana, A.C., et al., *Thalidomide suppresses inflammation in adenine-induced CKD with uraemia in mice.* Nephrol Dial Transplant, 2013. **28**(5): p. 1140-9.

280. Al Za'abi, M., et al., *Development of a new model for the induction of chronic kidney disease via intraperitoneal adenine administration, and the effect of treatment with gum acacia thereon.* Am J Transl Res, 2015. **7**(1): p. 28-38.

281. Karamched, S.R., et al., *Site-specific chelation therapy with EDTA-loaded albumin nanoparticles reverses arterial calcification in a rat model of chronic kidney disease.* Sci Rep, 2019. **9**(1): p. 2629.

282. Aikawa, E., et al., *Arterial and aortic valve calcification abolished by elastolytic cathepsin S deficiency in chronic renal disease.* Circulation, 2009. **119**(13): p. 1785-94.

283. Ivandic, B.T., et al., *New Dyscalc loci for myocardial cell necrosis and calcification (dystrophic cardiac calcinosis) in mice.* Physiol Genomics, 2001. **6**(3): p. 137-44.

284. Pai, A., et al., *Elastin degradation and vascular smooth muscle cell phenotype change precede cell loss and arterial medial calcification in a uremic mouse model of chronic kidney disease.* Am J Pathol, 2011. **178**(2): p. 764-73.

285. Lau, W.L., et al., *High phosphate feeding promotes mineral and bone abnormalities in mice with chronic kidney disease.* Nephrol Dial Transplant, 2013. **28**(1): p. 62-9.

286. Lomashvili, K.A., et al., *Phosphate-induced vascular calcification: role of pyrophosphate and osteopontin.* J Am Soc Nephrol, 2004. **15**(6): p. 1392-401.

287. Tani, T., et al., *Development of a novel chronic kidney disease mouse model to evaluate the progression of hyperphosphatemia and associated mineral bone disease.* Sci Rep, 2017. **7**(1): p. 2233.

288. Yoshida, T., et al., *Smooth Muscle-Selective Nuclear Factor-kappaB Inhibition Reduces Phosphate-Induced Arterial Medial Calcification in Mice With Chronic Kidney Disease.* J Am Heart Assoc, 2017. **6**(11).

289. Rahman, A., et al., *A novel approach to adenine-induced chronic kidney disease associated anemia in rodents.* PLoS One, 2018. **13**(2): p. e0192531.

290. Kukida, M., et al., *AT2 receptor stimulation inhibits phosphate-induced vascular calcification.* Kidney Int, 2019. **95**(1): p. 138-148.

291. Wait, J.M., et al., *Detection of aortic arch calcification in apolipoprotein E-null mice using carbon nanotube-based micro-CT system.* J Am Heart Assoc, 2013. **2**(1): p. e003358.

292. Wang, J.H., et al., *The omega-3 polyunsaturated fatty acid, eicosapentaenoic acid, attenuates abdominal aortic aneurysm development via suppression of tissue remodeling.* PLoS One, 2014. **9**(5): p. e96286.

293. Awan, Z., et al., *The LDLR deficient mouse as a model for aortic calcification and quantification by micro-computed tomography.* Atherosclerosis, 2011. **219**(2): p. 455-62.

294. Hsu, J.J., et al., *Effects of teriparatide on morphology of aortic calcification in aged hyperlipidemic mice.* Am J Physiol Heart Circ Physiol, 2018. **314**(6): p. H1203-H1213.

295. Lee, L., et al., *Aortic and Cardiac Structure and Function Using High-Resolution Echocardiography and Optical Coherence Tomography in a Mouse Model of Marfan Syndrome.* PLoS One, 2016. **11**(11): p. e0164778.

296. Hartley, C.J., et al., *Noninvasive determination of pulse-wave velocity in mice.* Am J Physiol, 1997. **273**(1 Pt 2): p. H494-500.

297. Donato, A.J., et al., *Life-long caloric restriction reduces oxidative stress and preserves nitric oxide bioavailability and function in arteries of old mice.* Aging Cell, 2013. **12**(5): p. 772-83.

298. Jung, S.M., et al., *Increased tissue transglutaminase activity contributes to central vascular stiffness in eNOS knockout mice.* Am J Physiol Heart Circ Physiol, 2013. **305**(6): p. H803-10.

299. Trachet, B., et al., *Performance comparison of ultrasound-based methods to assess aortic diameter and stiffness in normal and aneurysmal mice.* PLoS One, 2015. **10**(5): p. e0129007.

300. Mitchell, G.F., et al., *Comparison of techniques for measuring pulse-wave velocity in the rat.* J Appl Physiol (1985), 1997. **82**(1): p. 203-10.

301. Katz, P.S., et al., *Coronary arterioles in type 2 diabetic (db/db) mice undergo a distinct pattern of remodeling associated with decreased vessel stiffness.* Basic Res Cardiol, 2011. **106**(6): p. 1123-34.

302. Di Lascio, N., et al., *Non-invasive assessment of pulse wave velocity in mice by means of ultrasound images.* Atherosclerosis, 2014. **237**(1): p. 31-7.

303. Ketteler, M. and C. Giachelli, *Novel insights into vascular calcification.* Kidney International, 2006. **70**: p. S5-S9.

304. Hruska, K.A., S. Mathew, and G. Saab, *Bone morphogenetic proteins in vascular calcification.* Circulation research, 2005. **97**(2): p. 105-114.

305. Shanahan, C.M., et al., *Medial localization of mineralization-regulating proteins in association with Monckeberg's sclerosis: evidence for smooth muscle cell–mediated vascular calcification.* Circulation, 1999. **100**(21): p. 2168-2176.

306. Byon, C.H., et al., *Oxidative stress induces vascular calcification through modulation of the osteogenic transcription factor Runx2 by AKT signaling.* Journal of Biological Chemistry, 2008. **283**(22): p. 15319-15327.

307. Collett, G.D., et al., *Axl/phosphatidylinositol 3-kinase signaling inhibits mineral deposition by vascular smooth muscle cells.* Circulation research, 2007. **100**(4): p. 502-509.

308. Ewence, A.E., et al., *Calcium phosphate crystals induce cell death in human vascular smooth muscle cells: a potential mechanism in atherosclerotic plaque destabilization.* Circulation research, 2008. **103**(5): p. e28-e34.

309. Akiyoshi, T., et al., *A novel organ culture model of aorta for vascular calcification.* Atherosclerosis, 2016. **244**: p. 51-8.

310. Lee, K., et al., *APE1/Ref-1 inhibits phosphate-induced calcification and osteoblastic phenotype changes in vascular smooth muscle cells.* International journal of molecular sciences, 2017. **18**(10): p. 2053.

311. Wang, P., et al., *Spironolactone dose-dependently alleviates the calcification of aortic rings cultured in hyperphosphatemic medium with or without hyperglycemia by suppressing phenotypic transition of VSMCs through downregulation of Pit-1.* Molecular medicine reports, 2019. **19**(5): p. 3622-3632.

312. Johnson, K.A., M. Polewski, and R.A. Terkeltaub, *Transglutaminase 2 is central to induction of the arterial calcification program by smooth muscle cells.* Circulation research, 2008. **102**(5): p. 529-537.

313. Andrault, P.-M., et al., *Elastolytic activity of cysteine cathepsins K, S, and V promotes vascular calcification.* Scientific Reports, 2019. **9**(1): p. 9682.

314. Hosaka, N., et al., *Elastin degradation accelerates phosphate-induced mineralization of vascular smooth muscle cells.* Calcified tissue international, 2009. **85**(6): p. 523.

315. Simionescu, A., K. Philips, and N. Vyavahare, *Elastin-derived peptides and TGF-β1 induce osteogenic responses in smooth muscle cells.* Biochemical and biophysical research communications, 2005. **334**(2): p. 524-532.

316. Jono, S., et al., *Phosphate regulation of vascular smooth muscle cell calcification.* Circulation research, 2000. **87**(7): p. e10-e17.

317. Iyemere, V., et al., *Vascular smooth muscle cell phenotypic plasticity and the regulation of vascular calcification.* Journal of internal medicine, 2006. **260**(3): p. 192-210.

318. Proudfoot, D., et al., *The role of apoptosis in the initiation of vascular calcification.* Zeitschrift für Kardiologie, 2001. **90**(3): p. 43-46.

319. Yang, H., G. Curinga, and C.M. Giachelli, *Elevated extracellular calcium levels induce smooth muscle cell matrix mineralization in vitro.* Kidney international, 2004. **66**(6): p. 2293-2299.

320. Becker, A., et al., *A comparative study of clinically well-characterized human atherosclerotic plaques with histological, chemical, and ultrastructural methods.* Journal of inorganic biochemistry, 2004. **98**(12): p. 2032-2038.

321. Contiguglia, S.R., et al., *Nature of soft tissue calcification in uremia.* Kidney international, 1973. **4**(3): p. 229-235.

322. Schlieper, G., et al., *Ultrastructural analysis of vascular calcifications in uremia.* Journal of the American Society of Nephrology, 2010. **21**(4): p. 689-696.

323. Verberckmoes, S., et al., *Uremia-related vascular calcification: more than apatite deposition.* Kidney international, 2007. **71**(4): p. 298-303.

324. Wang, X., et al., *Gold nanoparticles that target degraded elastin improve imaging and rupture prediction in an AngII mediated mouse model of abdominal aortic aneurysm.* THERANOSTICS, 2019. **9**(14): p. 4156-4167.

325. Guzman, R.J., et al., *Tibial artery calcification as a marker of amputation risk in patients with peripheral arterial disease.* Journal of the American College of Cardiology, 2008. **51**(20): p. 1967-1974.

326. Lehto, S., et al., *Medial artery calcification: a neglected harbinger of cardiovascular complications in non–insulin-dependent diabetes mellitus.* Arteriosclerosis, thrombosis, and vascular biology, 1996. **16**(8): p. 978-983.

327. Chen, L.-S., et al., *A new prospect in cancer therapy: targeting cancer stem cells to eradicate cancer.* Chinese journal of cancer, 2012. **31**(12): p. 564.

328. Ji, W., B. Sun, and C. Su, *Targeting microRNAs in cancer gene therapy.* Genes, 2017. **8**(1): p. 21.